NASA TECHNICAL NOTE

NASA TN D-8335

INVESTIGATION OF VERY LOW BLOCKAGE RATIO BOATTAIL MODELS IN THE LANGLEY 16-FOOT TRANSONIC TUNNEL

David E. Reubush

Langley Research Center
Hampton, Va. 23665

NATIONAL AERONAUTICS AND SPACE ADMINISTRATION • WASHINGTON, D. C. • NOVEMBER 1976

1. Report No. NASA TN D-8335	2. Government Accession No.	3. Recipient's Catalog No.
4. Title and Subtitle INVESTIGATION OF VERY LOW BLOCKAGE RATIO BOATTAIL MODELS IN THE LANGLEY 16-FOOT TRANSONIC TUNNEL		5. Report Date November 1976 6. Performing Organization Code
7. Author(s) David E. Reubush		8. Performing Organization Report No. L-11063
9. Performing Organization Name and Address NASA Langley Research Center Hampton, VA 23665		10. Work Unit No. 505-04-11-01 11. Contract or Grant No.
12. Sponsoring Agency Name and Address National Aeronautics and Space Administration Washington, DC 20546		13. Type of Report and Period Covered Technical Note 14. Sponsoring Agency Code
15. Supplementary Notes		

16. Abstract

An investigation at an angle of attack of 0° has been conducted in the Langley 16-foot transonic tunnel at Mach numbers from 0.4 to 1.05 to determine the limits in Mach number at which valid boattail pressure drag data may be obtained with very low blockage (0.0027 percent) ratio bodies. The results of this investigation indicate that extreme care must be exercised when examining any data taken at subsonic Mach numbers very near 1.0 (e.g., above $M = 0.96$) and lower than the supersonic Mach number at which shock reflections miss the model. Boattail pressure coefficient distributions will generally not indicate any error, but when integrated boattail pressure drag data are plotted as a function of Mach number, data which may be in error can generally be identified.

17. Key Words (Suggested by Author(s)) Boattail drag Wind-tunnel testing techniques Low blockage ratio models	18. Distribution Statement Unclassified – Unlimited Subject Category 02		
19. Security Classif. (of this report) Unclassified	20. Security Classif. (of this page) Unclassified	21. No. of Pages 64	22. Price* $4.25

*For sale by the National Technical Information Service, Springfield, Virginia 22161

INVESTIGATION OF VERY LOW BLOCKAGE RATIO BOATTAIL MODELS IN THE LANGLEY 16-FOOT TRANSONIC TUNNEL

David E. Reubush
Langley Research Center

SUMMARY

An investigation at an angle of attack of 0° has been conducted in the Langley 16-foot transonic tunnel at Mach numbers from 0.4 to 1.05 to determine the limits in Mach number at which valid boattail pressure drag data may be obtained with very low blockage (0.0027) ratio bodies. The results of this investigation indicate that extreme care must be exercised when examining any data taken at subsonic Mach numbers very near 1.0 (e.g., above $M = 0.96$) and lower than the supersonic Mach number at which shock reflections miss the model. Boattail pressure coefficient distributions will generally not indicate any error, but when integrated boattail pressure drag data are plotted as a function of Mach number, data which may be in error can generally be identified.

INTRODUCTION

Even with slotted or porous wall wind tunnels, the difficulties in obtaining valid wind-tunnel data near a Mach number of 1.0 have long been known. At Mach numbers very slightly less than 1.0, although the models used may have relatively small blockage, regions of sonic flow will extend to the wind-tunnel walls. The shape of the sonic regions is changed by the interaction with the walls and the resulting data are then in error. At Mach numbers slightly greater than 1.0, the model bow shock is reflected back from the walls and impinges on the model, again resulting in invalid data. An investigation was recently conducted in the Langley 0.3-meter transonic cryogenic tunnel to determine the effects of Reynolds number on boattail pressure drag (ref. 1). In order to accomplish the objectives of this investigation, six small models (2.54 cm in diameter) with extensive boattail pressure instrumentation were constructed. With these small models available, an investigation was then initiated in the Langley 16-foot transonic tunnel to determine the practical testing limit for Mach number (near 1.0) at which valid boattail pressure data could be obtained since the models would have an extremely low blockage ratio (ratio of model cross-sectional area to tunnel test section cross-sectional area) in this facility. In addition, a facility-to-facility comparison between the 0.3-meter transonic cryogenic

tunnel and the 16-foot transonic tunnel could be made. Also, two of the small models were scale models of two large models which had been previously tested in the 16-foot transonic tunnel (refs. 2 and 3), and an additional data comparison of the effect of model size in the same facility would be possible.

The current investigation used the series of six isolated, sting-mounted, cone-cylinder nacelle models with four different boattail geometries (ref. 1). These models were tested in the Langley 16-foot transonic tunnel at 0° angle of attack at Mach numbers from about 0.4 to 1.05. Reynolds number based on the distance from the nose of the model to the start of the boattail varied from about 1.7×10^6 at $M = 0.4$ to 2.9×10^6 at $M = 1.05$ for four of the models and from about 3.4×10^6 at $M = 0.4$ to 5.7×10^6 at $M = 1.05$ for the other two models.

SYMBOLS

A	cross-sectional area
A_m	maximum cross-sectional area of model
A_β	incremental cross-sectional area assigned to boattail static-pressure orifice for drag integration
$C_{D,\beta}$	boattail pressure drag coefficient (see Data Reduction section)
C_p	static-pressure coefficient, $\frac{p - p_\infty}{q}$
d_m	maximum diameter of model
d_s	sting diameter
L	length of model from nose to start of boattail (characteristic length)
l	length of boattail
M	free-stream Mach number
p	local static pressure on model
p_∞	free-stream static pressure

q	free-stream dynamic pressure
R	Reynolds number (based on length from nose to start of boattail)
x	axial distance from start of boattail, positive aft
y	radial distance from center line of model
ϕ	meridian angle about model axis, clockwise positive facing upstream, 0° at top of model

APPARATUS AND PROCEDURE

Wind Tunnel

This investigation was conducted in the Langley 16-foot transonic tunnel, which is a single-return, continuous-flow, atmospheric tunnel. The test section is a regular octagon in cross section with slots at the corners of the octagon. The tunnel speed can be varied continuously from a Mach number of 0.20 to 1.30. Further description of the Langley 16-foot transonic tunnel can be found in references 4 to 6.

Models and Support System

A generalized sketch of the boattailed cone-cylinder nacelle models used in this investigation is shown in figure 1. Figure 2 is a photograph of all six models. There were four short models of differing boattail geometry with a length of 20.32 cm from the nose to the start of the boattail (characteristic length); there were two long models with a length from the nose to the start of the boattail of 40.64 cm. The boattail geometry of the two long models duplicated the boattail geometry of two of the short models. Details of the geometry of the four boattails are shown in figure 3. The four boattail geometries were a circular arc with a ratio of length to maximum diameter or fineness ratio l/d_m of 0.8 (both short and long models), circular arc with a fineness ratio of 1.77, circular-arc—conic with a fineness ratio of 0.96 (both short and long models), and contoured with a fineness ratio of 0.95. The two circular-arc boattails are scale models of two boattails which have been tested in the Langley 16-foot transonic tunnel (refs. 2 and 3).

The models were all sting mounted with the sting simulating the geometry of a jet exhaust plume for a nozzle operating at its design point. (See ref. 3.) The two circular-arc boattails and the circular-arc—conic boattail had ratios of sting diameter to maximum diameter of 0.50, whereas the contoured nozzle had a ratio of sting diameter to maximum diameter of 0.544. The length of the constant-diameter portion of the stings

was such that, based on the data contained in reference 7, there should be no effect of the tunnel support sting flare on the boattail pressure coefficients. In addition, the sum of the boattail and sting lengths (before the flare) was constant so that the noses of all four of the short models were at the same tunnel station. The noses of the two long models were at the same tunnel station, but this station was not the same as that for the short models. (The start of the boattail was at the same tunnel station for all six models.)

The models were constructed of cast aluminum with stainless-steel pressure tubes cast as an integral part of each model. The tubes were placed in the sand mold in the proper position, the aluminum was poured, and the model was machined to the proper contours.

Figure 4 shows photographs of a typical short model and a typical long model mounted in the Langley 16-foot transonic tunnel. The models had a maximum diameter of 2.54 cm and a resulting tunnel blockage of 0.0027 percent.

Instrumentation and Tests

The six boattails were instrumented with 30 static-pressure orifices in 3 rows of 10 orifices each ($\phi = 0^{\circ}$, 120°, and 240°) at the locations given in table I. These orifices were connected to remotely located 34.47 kPa (5 psi) pressure gages which had an accuracy of ± 0.5 percent of full scale.

All tests were conducted in the Langley 16-foot transonic tunnel at Mach numbers from 0.40 to 1.05 at an angle of attack of 0°. Model attitude was set to account for tunnel upflow (about 0.1° through the Mach number range), but no account was taken of possible sting deflection because it was believed to be insignificant. Boundary-layer transition was natural for all tests to insure a direct comparison with the data from reference 1.

DATA REDUCTION

Model and wind-tunnel data were recorded on magnetic tape and a digital computer was used to compute standard force and pressure coefficients. Pressure drag coefficients were computed from the measured pressures on each boattail. These coefficients, based on the maximum cross-sectional area of the model, were obtained from the pressure data on the boattail portion of the model by assigning an axially projected area to each orifice and computing the coefficients from the following equation:

$$C_{D,\beta} = \frac{1}{qA_m} \sum_{i=1}^{30} (p_i - p_\infty) A_{\beta,i}$$

Accuracy of this step integration scheme was spot-checked by plotting the pressure coefficients as a function of A/A_m and integrating with a planimeter.

DISCUSSION

Boattail Pressure Coefficient Distributions

Boattail pressure coefficient distributions for the six models at the various Mach numbers tested are shown in figures 5 to 10. The significant point to be made about these data is that, even though the data obtained above $M = 1.0$ will later be shown to be in error and some data obtained just below $M = 1.0$ (e.g., above $M = 0.96$) becomes questionable when the integrated boattail pressure drag coefficients are examined, it is impossible to ascertain such errors by looking only at the boattail pressure coefficient distributions. Figure 11 shows typical examples of boattail pressure coefficient distributions for two of the boattails at the Mach numbers tested between about 0.9 and 1.0. (Both the actual data and a fairing through the data are shown since both the $\phi = 0^\circ$ and $\phi = 120^\circ$ rows of pressures are included in the distributions.) Even when boattail pressure coefficient distributions at successive Mach numbers are plotted, the changes in distributions due to the rearward shock movement with Mach number seem reasonable and no error can readily be ascertained.

Boattail Pressure Drag Coefficients

Boattail pressure drag coefficients as a function of Mach number for the six configurations are shown in figure 12. When these curves are examined, it is immediately apparent that the data above $M = 1.0$ are in error. The integrated drag coefficients are not in a smooth curve with Mach number and appear to be shifting up and down slightly. At Mach numbers below 1.0, there is also some question as to the validity of the data for tests above $M = 0.96$. At about $M = 0.98$, the data depart from a smoothly faired curve for all six configurations, and although the data above $M = 0.98$ may generally be faired into a continuation of the lower Mach number curve, this phenomenon leads one to believe that these data at $M = 0.98$ and above are possibly in error. This indication that the onset of transonic wall interference occurs at a Mach number of 0.96 agrees with the results found in reference 8, which are also for low blockage ratio bodies.

It is believed that the phenomenon above $M = 1.0$ is due to the reflected bow shock impinging on the model and would be expected to clear up once a supersonic Mach number is reached at which the reflected shock misses the model. It has been suggested that the phenomenon below $M = 1.0$ is due to a sonic region on the model extending to the wall and its shape being changed through interaction with the wall, but available analytic procedures (e.g., ref. 9) indicate that the sonic region reaches the wall only at Mach numbers greater than 0.99 (for this geometry and blockage ratio).

Comparison of Data

Boattail pressure coefficient distributions.- Boattail pressure coefficient distributions for the $L/d_m = 16.0$, $l/d_m = 0.80$ circular-arc boattail, the $L/d_m = 8.0$ and 16.0, $l/d_m = 0.96$ circular-arc—conic boattails, and the $L/d_m = 8.0$, $l/d_m = 0.95$ contoured boattail obtained in both the Langley 16-foot transonic tunnel (blockage about 0.0027 percent) and the Langley 0.3-meter transonic cryogenic tunnel (ref. 1, blockage about 0.52 percent) are shown in figures 13 to 16 for $M = 0.6$ and 0.9. The other two configurations $\left(L/d_m = 8.0,\ l/d_m = 0.80 \text{ and } 1.77 \text{ circular-arc boattails}\right)$ were not tested at a Reynolds number in the cryogenic tunnel low enough to be sufficiently close to the 16-foot transonic tunnel Reynolds number for a valid comparison. It was shown in reference 1 that although integrated boattail pressure drag coefficients are not sensitive to Reynolds number, the boattail pressure coefficient distributions are sensitive to Reynolds number, and thus while comparisons of pressure drag coefficients are valid at different Reynolds numbers, comparisons of pressure coefficient distributions are not. For those four configurations for which comparisons can be made, only a general trend can be ascertained. The boattail pressure coefficient distributions are generally in reasonable agreement between the two tunnels with the $M = 0.9$ data being in slightly better agreement than the $M = 0.6$ data.

Boattail pressure drag coefficients in the Langley 16-foot transonic tunnel and the Langley 0.3-meter transonic cryogenic tunnel.- Boattail pressure drag coefficients for the data from both the 16-foot tunnel (blockage about 0.0027 percent) and the cryogenic tunnel (ref. 1, blockage about 0.52 percent) and for the large model data from the 16-foot tunnel (ref. 3, blockage of model and support about 0.15 percent) are shown in figure 17. For all six small models, the boattail pressure drag coefficients obtained in both the 16-foot tunnel and the cryogenic tunnel agree quite well at Mach numbers of 0.8 and above. However, the drag levels for the models in the cryogenic tunnel are always lower than those for the models in the 16-foot tunnel at $M = 0.6$ since the pressure coefficients are slightly higher for the cryogenic tunnel than for the 16-foot tunnel at $M = 0.6$. The reason for such a difference between the drag levels is not clear, but possibly may be due to the fact that the cryogenic tunnel has wider slots than the 16-foot tunnel and hence a greater open area. It is not believed that the difference in blockage causes the difference in drag levels because the Mach number is low and the data agree at the higher Mach numbers.

Boattail pressure drag coefficients for two model sizes in the Langley 16-foot transonic tunnel.- For both the large (refs. 2 and 3) and small versions of the two circular-arc boattails $\left(L/d_m = 8.0,\ l/d_m = 0.8 \text{ and } 1.77\right)$ which were tested in the 16-foot tunnel, the results are not the same. The drag coefficients for the $l/d_m = 1.77$ circular-arc boattail which has attached flow at most Mach numbers agree extremely well, whereas

the drag level of the large $\ell/d_m = 0.80$ circular-arc boattail which has separated flow over the rear portion of the boattail (as indicated by the flattening out of the pressure distribution to a constant level) at all Mach numbers tested is somewhat higher than that of the small model. It is believed that this discrepancy for the $\ell/d_m = 0.80$ boattail occurs because boundary-layer transition was fixed at the nose for the large models while it was natural for the small models. The resulting differences in the boundary layer approaching the boattails for the two different size models resulted in changes in the boattail pressure coefficient distribution for the $\ell/d_m = 0.80$ boattail with separated flow, while not for the $\ell/d_m = 1.77$ boattail with attached flow. The sensitivity of the separated-flow boattail to changes in approach boundary layer is not unexpected. Note that for the two large models the drag data above $M = 0.96$ are in error and exhibit a tendency to drop off as $M = 1.0$ is approached. For this blockage ratio in the 16-foot tunnel (0.15 percent), the data in error are easier to detect than for the small blockage ratio models since the effects are larger.

CONCLUSIONS

An investigation at an angle of attack of 0° has been conducted in the Langley 16-foot transonic tunnel at Mach numbers from about 0.4 to 1.05 to determine the limits in Mach number at which valid boattail pressure drag data may be obtained for very low blockage (0.0027 percent) ratio bodies.

First, it was found that extreme care must be exercised when examining any boattail pressure data taken at subsonic Mach numbers greater than about 0.96 and lower than the supersonic Mach number at which shock reflections miss the model. Boattail pressure coefficient distributions will generally not indicate any error, but when integrated boattail pressure drag data are plotted as a function of Mach number, data which may be in error can generally be identified.

Second, comparisons between boattail pressure drag data obtained using both small and large models in the Langley 16-foot transonic tunnel and the data obtained for the small models tested in the Langley 0.3-meter transonic cryogenic tunnel were generally very good.

Langley Research Center
National Aeronautics and Space Administration
Hampton, VA 23665
September 30, 1976

REFERENCES

1. Reubush, David E.; and Putnam, Lawrence E.: An Experimental and Analytical Investigation of the Effect on Isolated Boattail Drag of Varying Reynolds Number up to 130×10^6. NASA TN D-8210, 1976.

2. Reubush, David E.; and Runckel, Jack F.: Effect of Fineness Ratio on the Boattail Drag of Circular-Arc Afterbodies Having Closure Ratios of 0.50 With Jet Exhaust at Mach Numbers up to 1.30. NASA TN D-7192, 1973.

3. Reubush, David E.: Experimental Study of the Effectiveness of Cylindrical Plume Simulators for Predicting Jet-On Boattail Drag at Mach Numbers up to 1.30. NASA TN D-7795, 1974.

4. Ward, Vernon G.; Whitcomb, Charles F.; and Pearson, Merwin D.: Air-Flow and Power Characteristics of the Langley 16-Foot Transonic Tunnel With Slotted Test Section. NACA RM L52E01, 1952.

5. Schaefer, William T., Jr.: Characteristics of Major Active Wind Tunnels at the Langley Research Center. NASA TM X-1130, 1965.

6. Corson, Blake W., Jr.; Runckel, Jack F.; and Igoe, William B.: Calibration of the Langley 16-Foot Transonic Tunnel With Test Section Air Removal. NASA TR R-423, 1974.

7. Cahn, Maurice S.: An Experimental Investigation of Sting-Support Effects on Drag and a Comparison With Jet Effects at Transonic Speeds. NACA Rep. 1353, 1958. (Supersedes NACA RM L56F18a.)

8. Couch, Lana M.; and Brooks, Cuyler W., Jr.: Effect of Blockage Ratio on Drag and Pressure Distributions for Bodies of Revolution at Transonic Speeds. NASA TN D-7331, 1973.

9. Keller, James D.; and South, Jerry C., Jr.: RAXBOD: A Fortran Program for Inviscid Transonic Flow Over Axisymmetric Bodies. NASA TM X-72831, 1976.

TABLE I.- BOATTAIL STATIC-PRESSURE ORIFICE LOCATIONS

Boattail configuration	$\frac{x}{d_m}$ for $\frac{L}{d_m} = 8$ at –			$\frac{x}{d_m}$ for $\frac{L}{d_m} = 16$ at –		
	$\phi = 0^o$	$\phi = 120^o$	$\phi = 240^o$	$\phi = 0^o$	$\phi = 120^o$	$\phi = 240^o$
Circular-arc; $\frac{l}{d_m} = 0.8$	-0.2771	-0.2761	-0.2850	-0.4491	-0.4660	-0.4561
	-.0256	-.0731	-.0700	-.1637	-.2201	-.1552
	.0770	.0256	.0345	-.0600	-.1281	-.0590
	.1765	.1287	.1270	.0337	-.0260	.0390
	.2750	.2257	.2260	.1268	.0744	.1342
	.3679	.3240	.3279	.2279	.1729	.2713
	.4675	.4180	.4200	.3210	.2696	.3718
	.5749	.5166	.5220	.4199	.3679	.4680
	.6698	.6165	.6376	.5231	.4640	.5749
	.7746	.7280	.7400	.6279	.6758	.7304
Circular-arc; $\frac{l}{d_m} = 1.77$	-0.3006	-0.3028	-0.3090			
	-.0086	.2554	-.1088			
	.3515	.5057	-.0113			
	.6314	.7364	.3543			
	.8271	.9091	.5072			
	.9975	1.0652	.8204			
	1.1500	1.2075	.9910			
	1.2776	1.3581	1.3528			
	1.4144	1.4817	1.4846			
	1.5447	1.6202	1.6936			
Circular-arc—conic; $\frac{l}{d_m} = 0.96$	-0.2842	-0.2843	-0.2847	-0.2612	-0.2773	-0.2613
	.0001	-.0352	.0059	.0228	-.0292	.0307
	.1090	.0640	.1044	.1227	.0707	.1246
	.1917	.1577	.2069	.2158	.1705	.2308
	.3000	.2542	.3031	.3107	.2638	.3237
	.4027	.3528	.4453	.4148	.3638	.4648
	.5022	.4499	.5483	.5097	.4607	.5737
	.5991	.5518	.6516	.5967	.5557	.6628
	.6948	.6522	.7494	.7068	.6558	.7706
	.8036	.8488	.9069	.8188	.8678	.9156
Contoured; $\frac{l}{d_m} = 0.95$	-0.2951	-0.2950	-0.3011			
	-.0084	-.0500	-.0021			
	.0925	.0500	.0934			
	.1930	.1485	.1976			
	.2861	.2433	.2913			
	.3759	.3449	.4350			
	.4786	.4417	.5355			
	.5797	.5404	.6335			
	.6840	.6415	.7366			
	.7909	.8425	.8951			

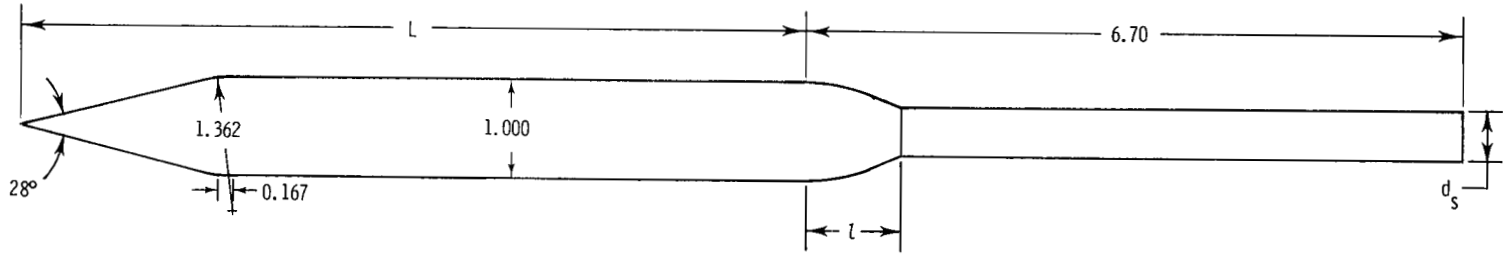

Boattail	l/d_m	L/d_m	d_s/d_m
Circular-arc	0.80	8.00 and 16.00	0.500
Circular-arc	1.77	8.00	.500
Circular-arc—conic		8.00 and 16.00	.500
Contoured		8.00	.544

Figure 1.- Boattailed cone-cylinder nacelle model. All dimensions are nondimensionalized by model maximum diameter (2.54 cm).

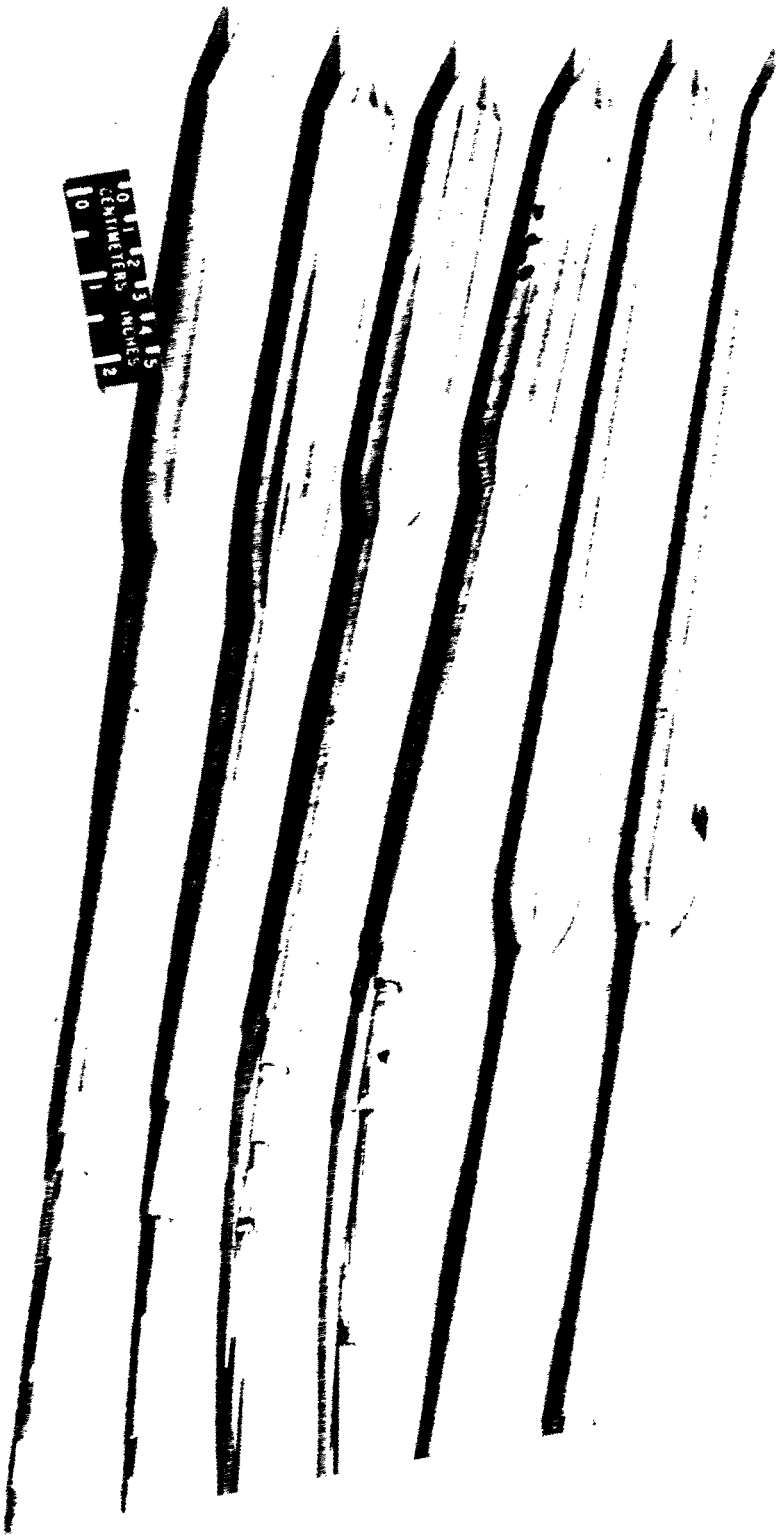

Figure 2.- Six nacelle models used in this investigation.

Circular-arc

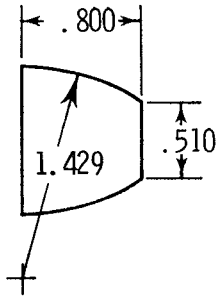

Circular-arc—conic

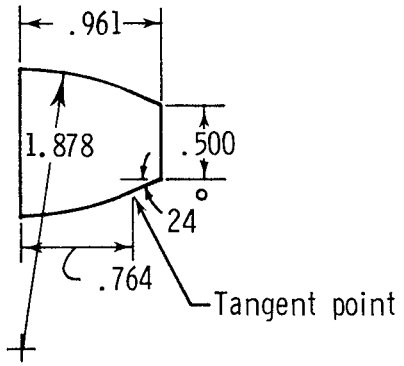

Circular-arc

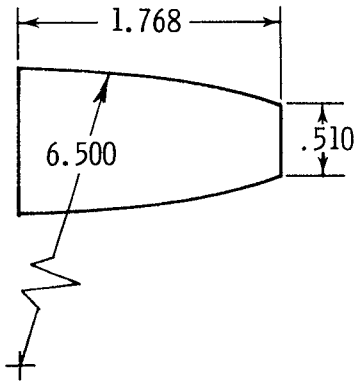

Contoured

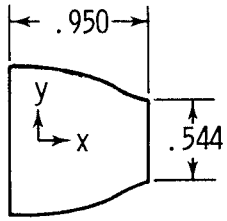

Coordinates for contoured boattail

x/d_m	y/d_m	x/d_m	y/d_m
0.0	0.500	0.640	0.409
.080	.499	.720	.372
.160	.497	.800	.328
.240	.494	.840	.304
.320	.487	.880	.288
.400	.475	.920	.276
.480	.461	.950	.272
.560	.439		

Figure 3.- Details of boattail geometries. All dimensions are nondimensionalized by model maximum diameter (2.54 cm).

L-74-8664

(a) Front view of typical $L/d_m = 8.0$ model.

Figure 4.- Typical model installed in Langley 16-foot transonic tunnel.

L-74-8663

(b) Side view of typical $L/d_m = 8.0$ model.

Figure 4.- Continued.

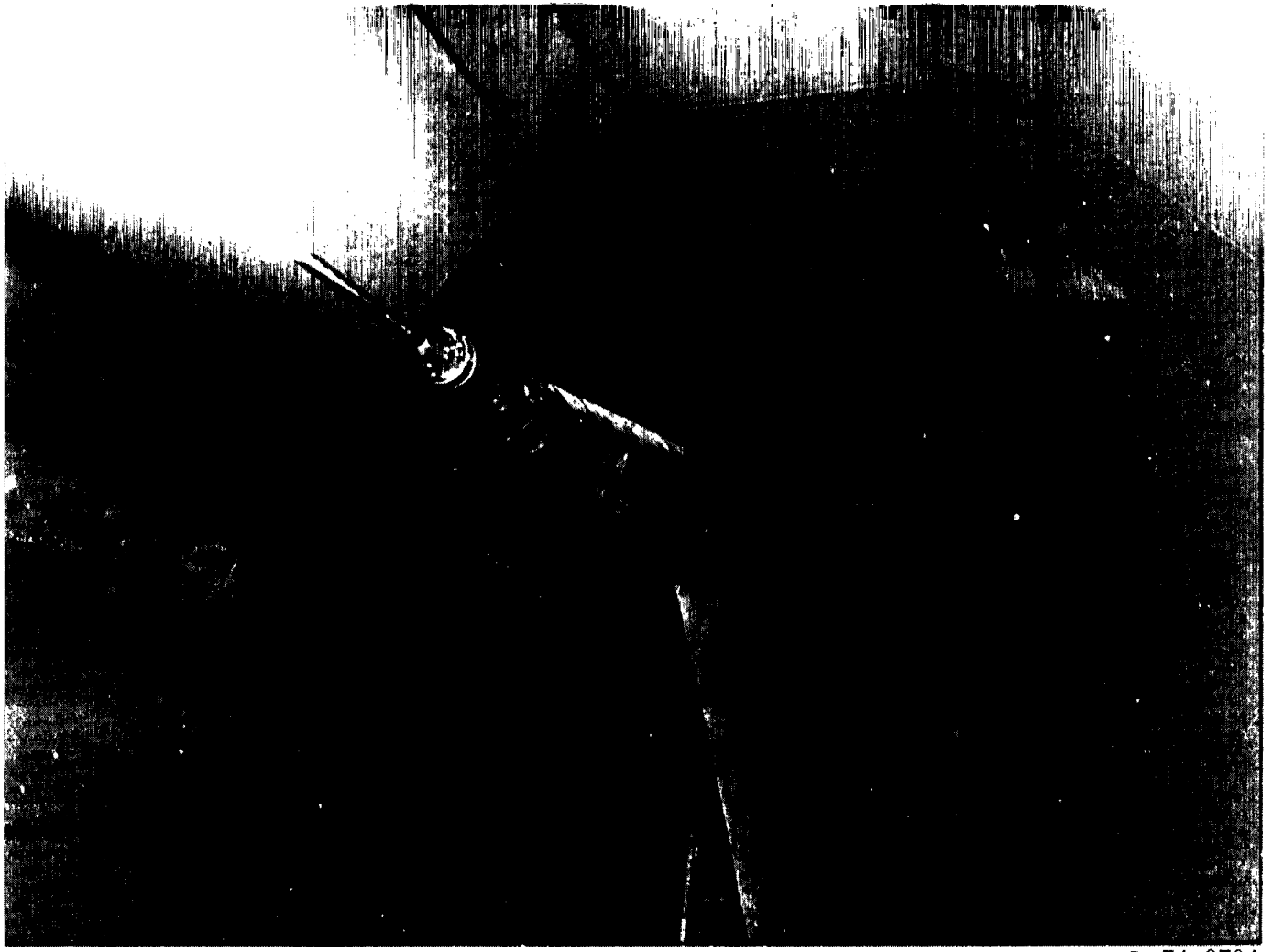

L-74-8704

(c) Front view of typical $L/d_m = 16.0$ model.

Figure 4.- Concluded.

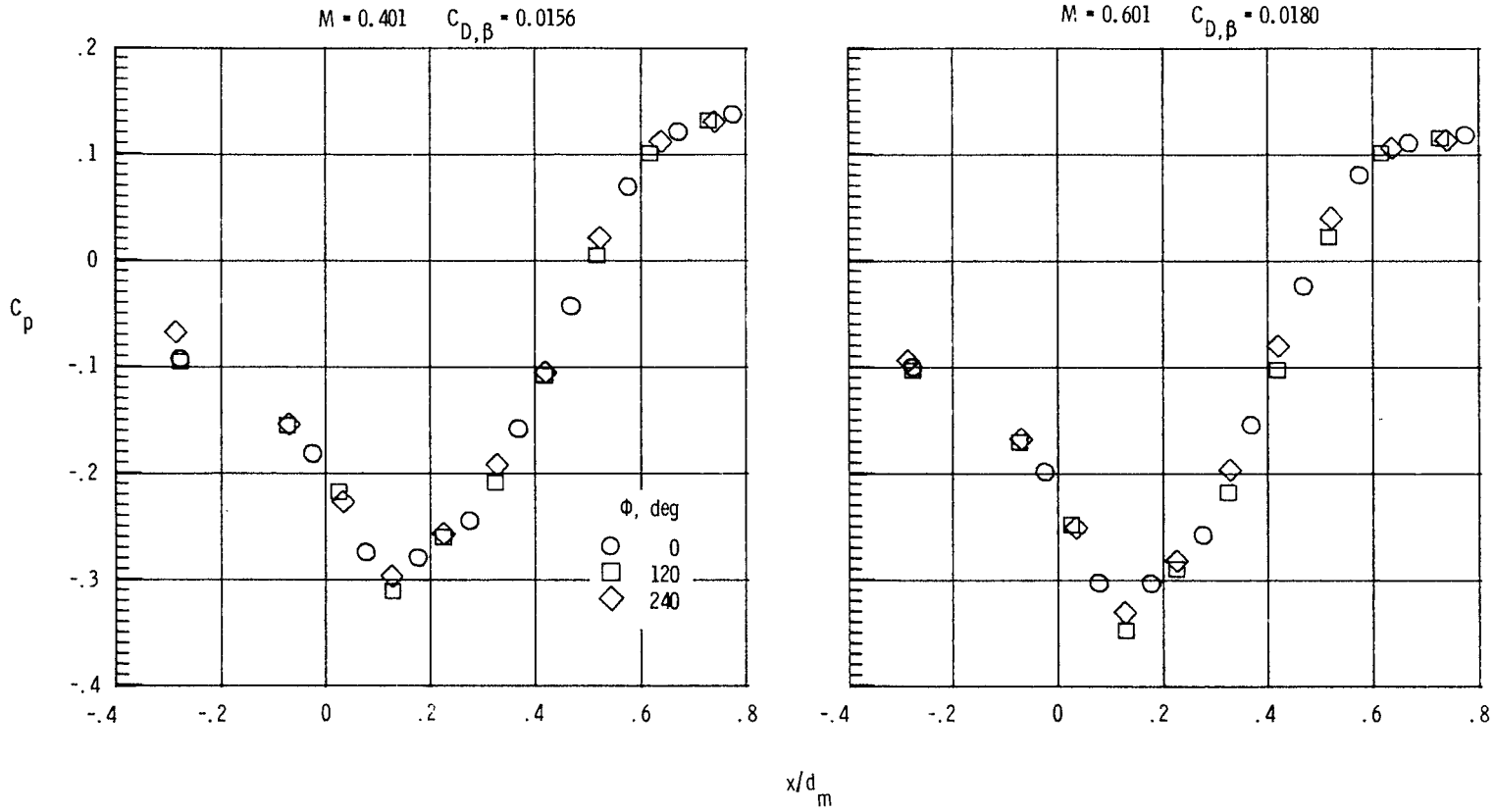

(a) M = 0.4 and 0.6.

Figure 5.- Boattail pressure coefficient distributions for $L/d_m = 8.0$, $l/d_m = 0.80$ circular-arc boattail at 0^o angle of attack at various Mach numbers.

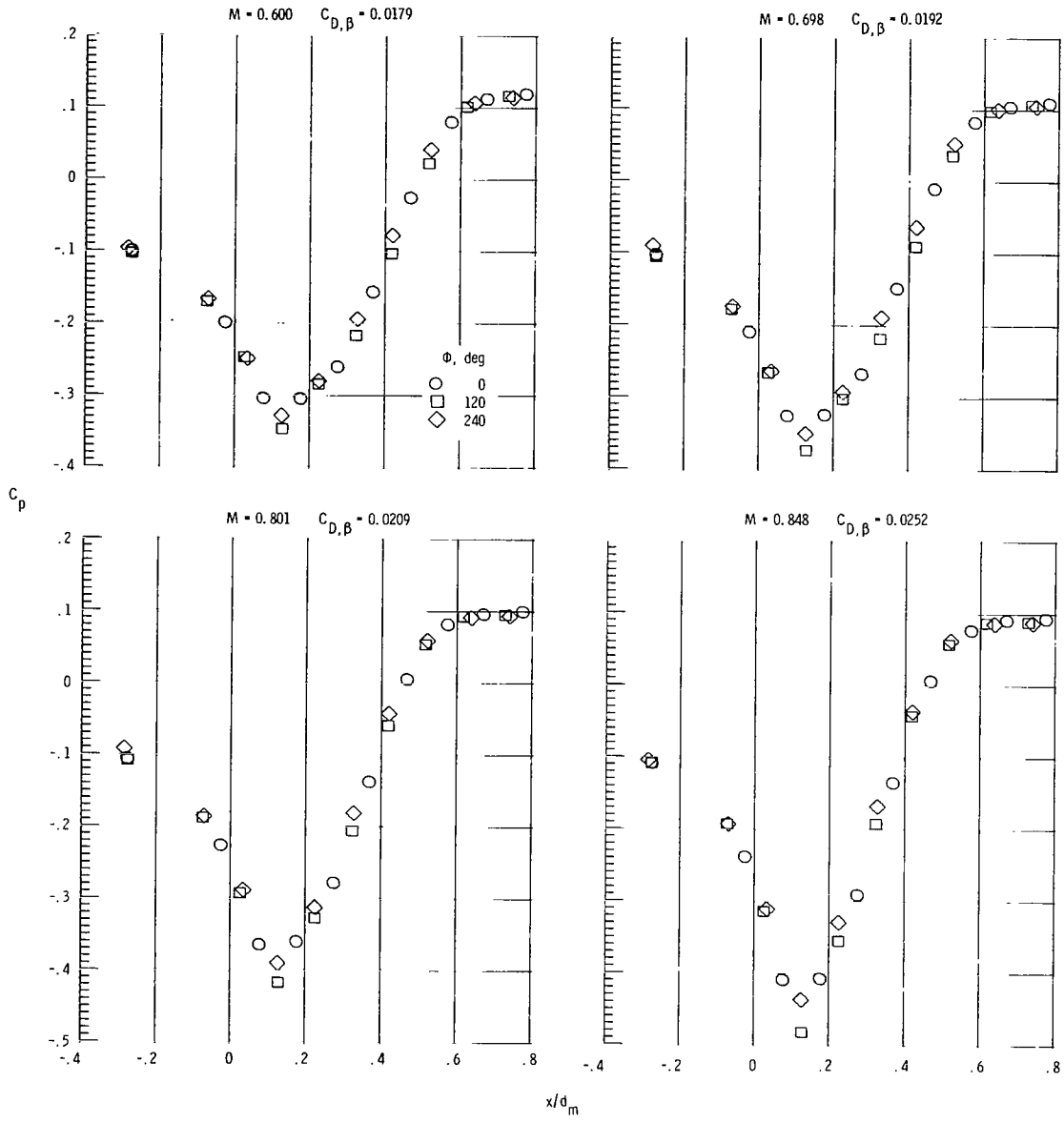

(b) M = 0.6 to 0.85.

Figure 5.- Continued.

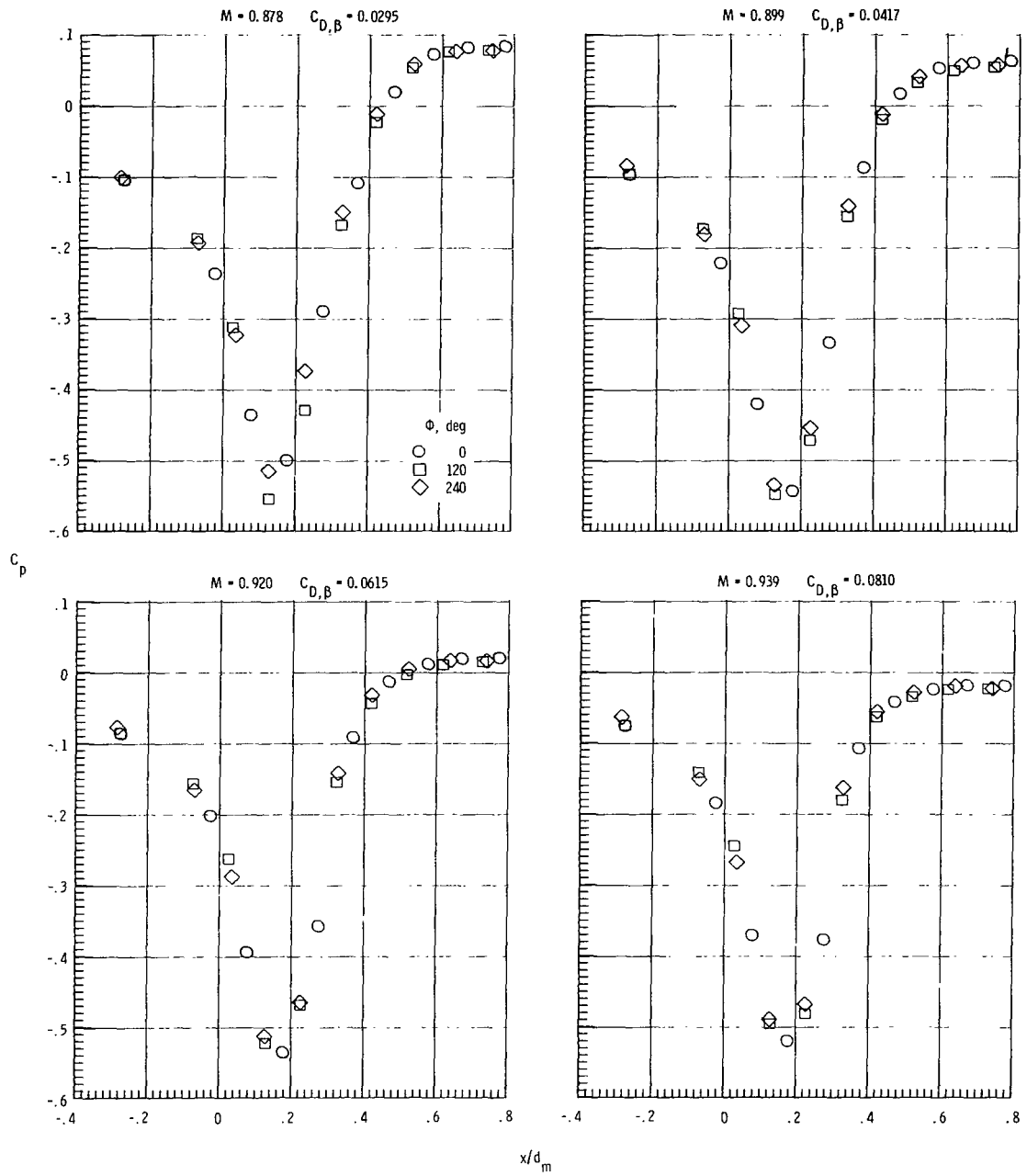

(c) M = 0.88 to 0.94.

Figure 5.- Continued.

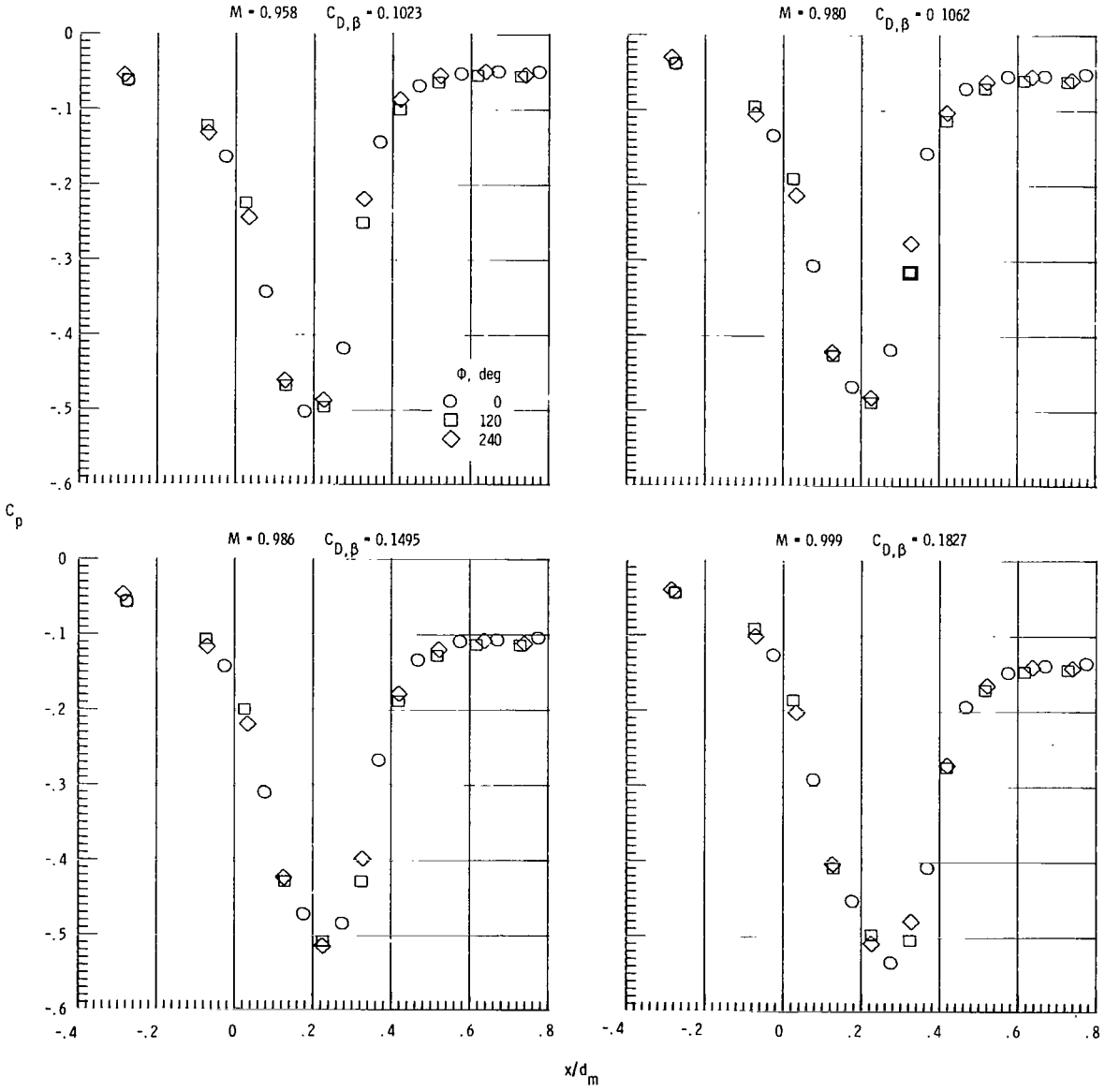

(d) M = 0.96 to 1.00.

Figure 5.- Continued.

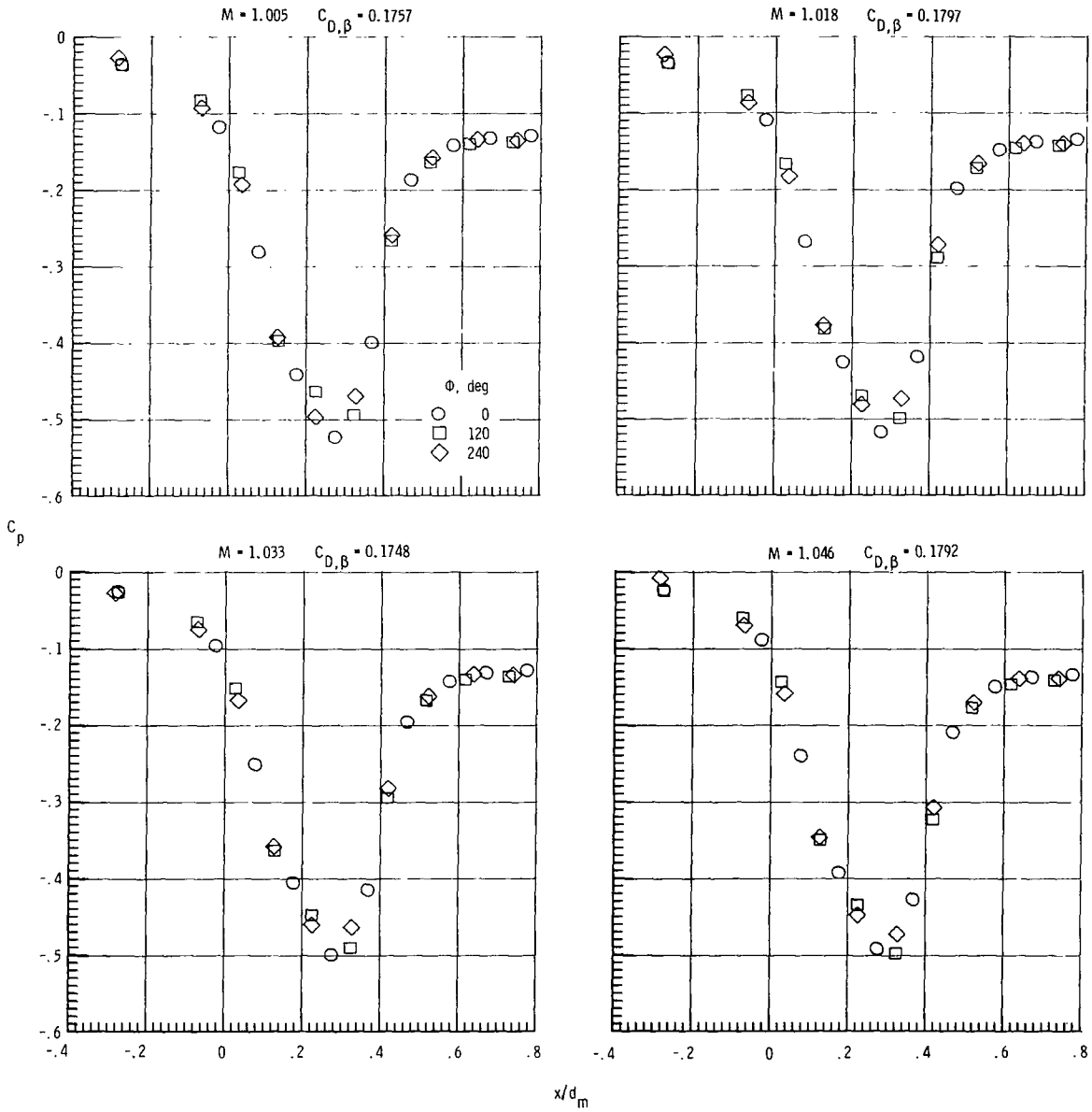

(e) M = 1.01 to 1.05.

Figure 5.- Concluded.

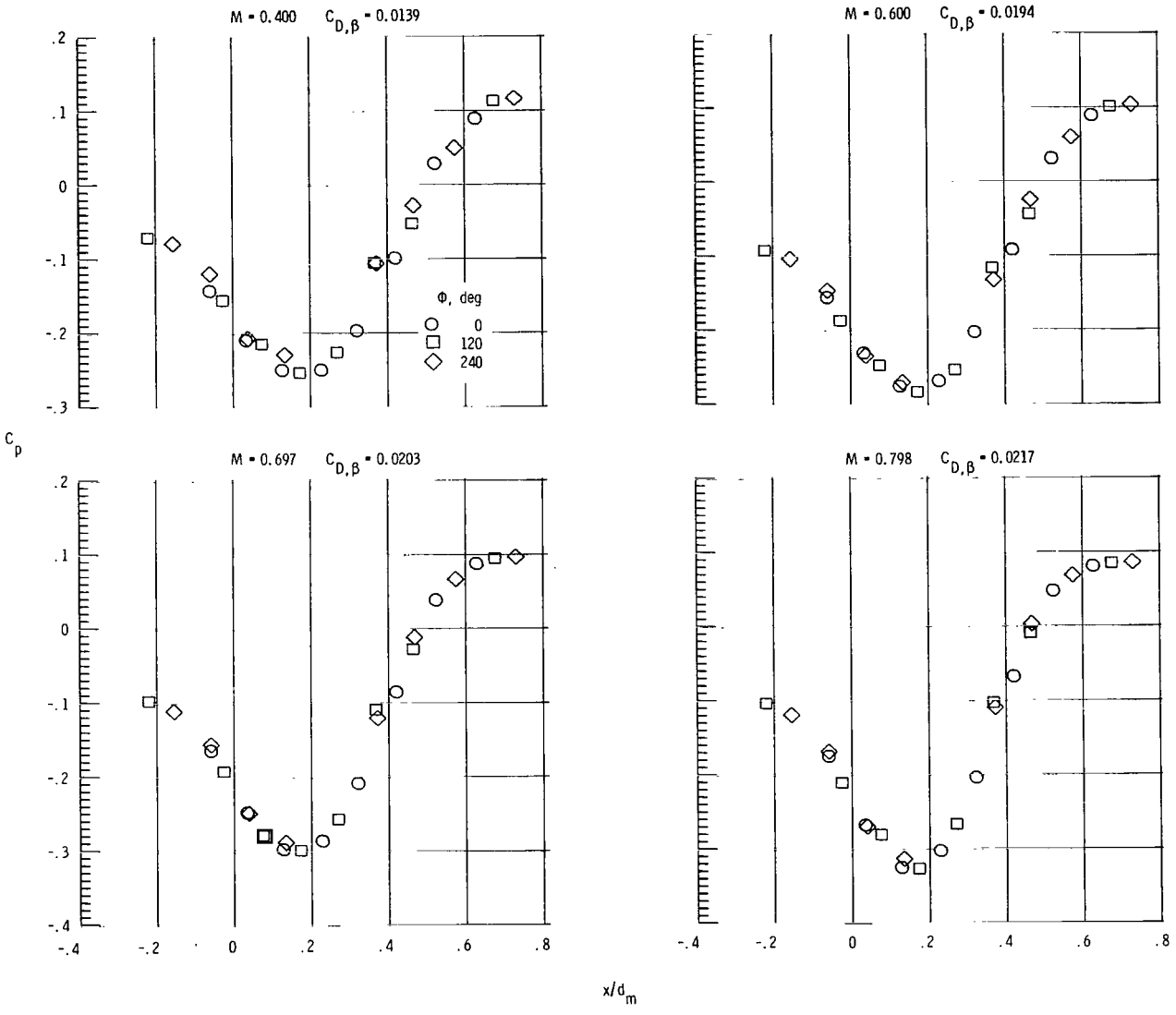

(a) M = 0.4 to 0.8.

Figure 6.- Boattail pressure coefficient distributions for L/d_m = 16.0, l/d_m = 0.80 circular-arc boattail at 0^o angle of attack at various Mach numbers.

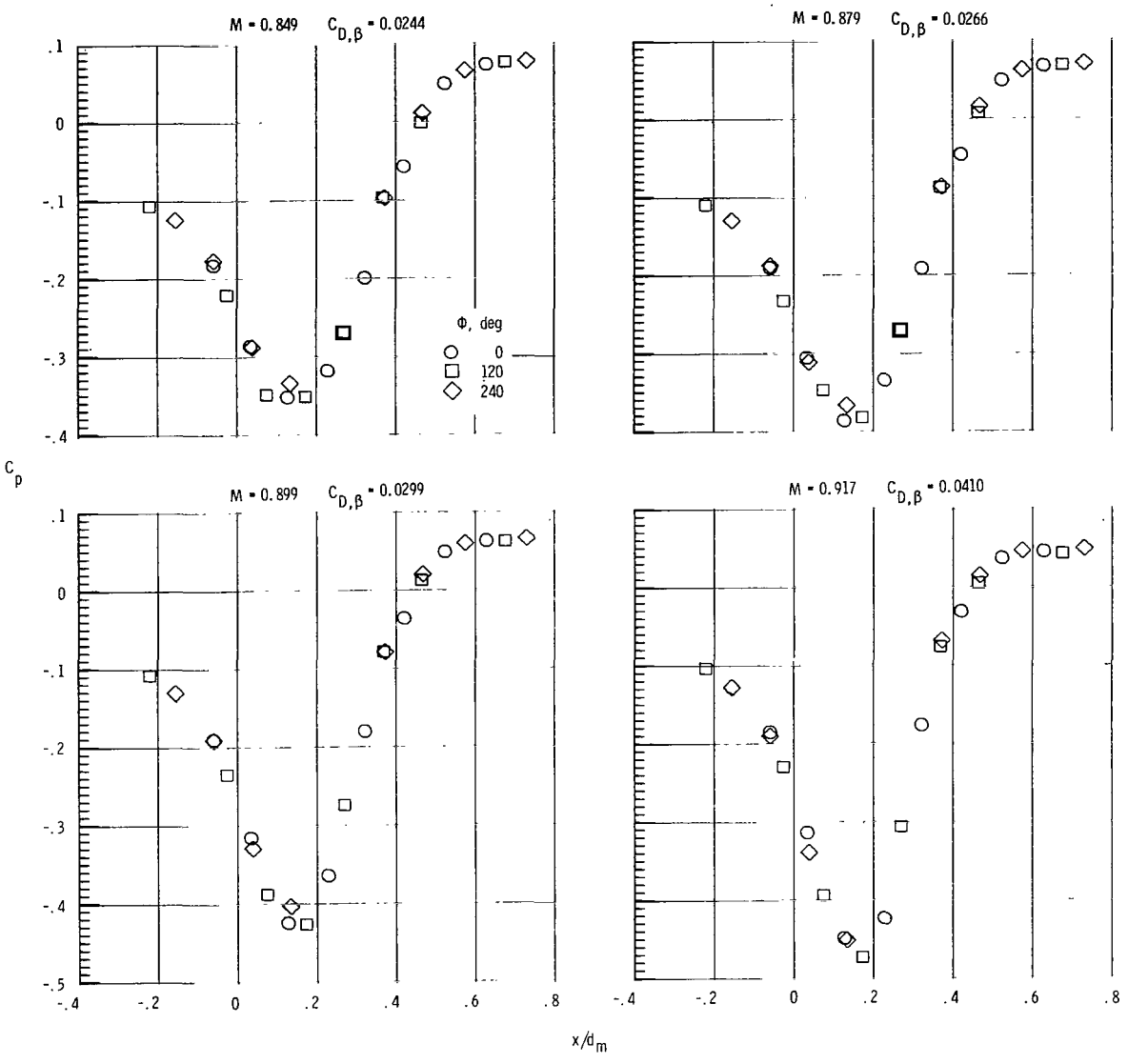

(b) M = 0.85 to 0.92.

Figure 6.- Continued.

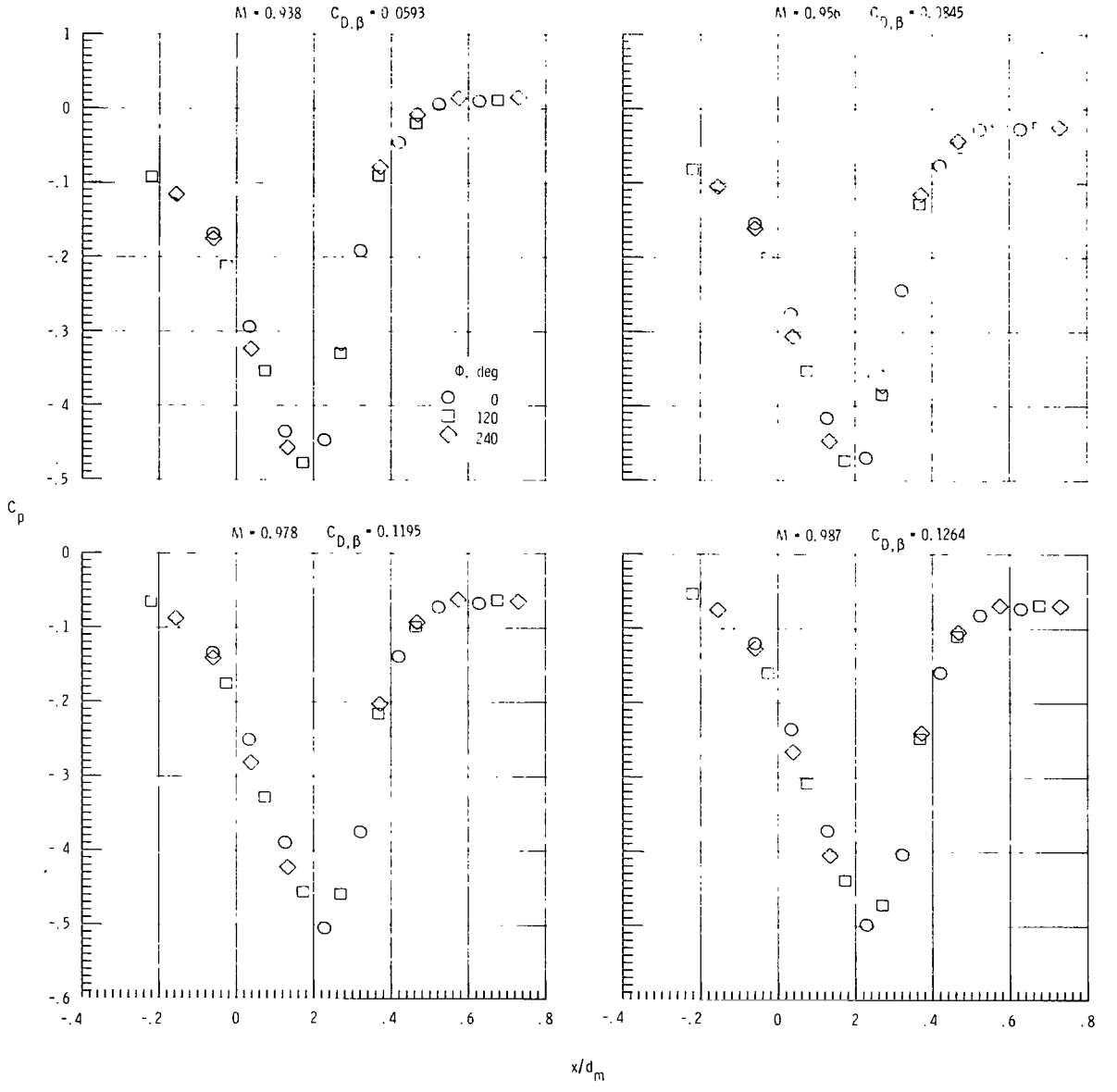

(c) M = 0.94 to 0.99.

Figure 6.- Continued.

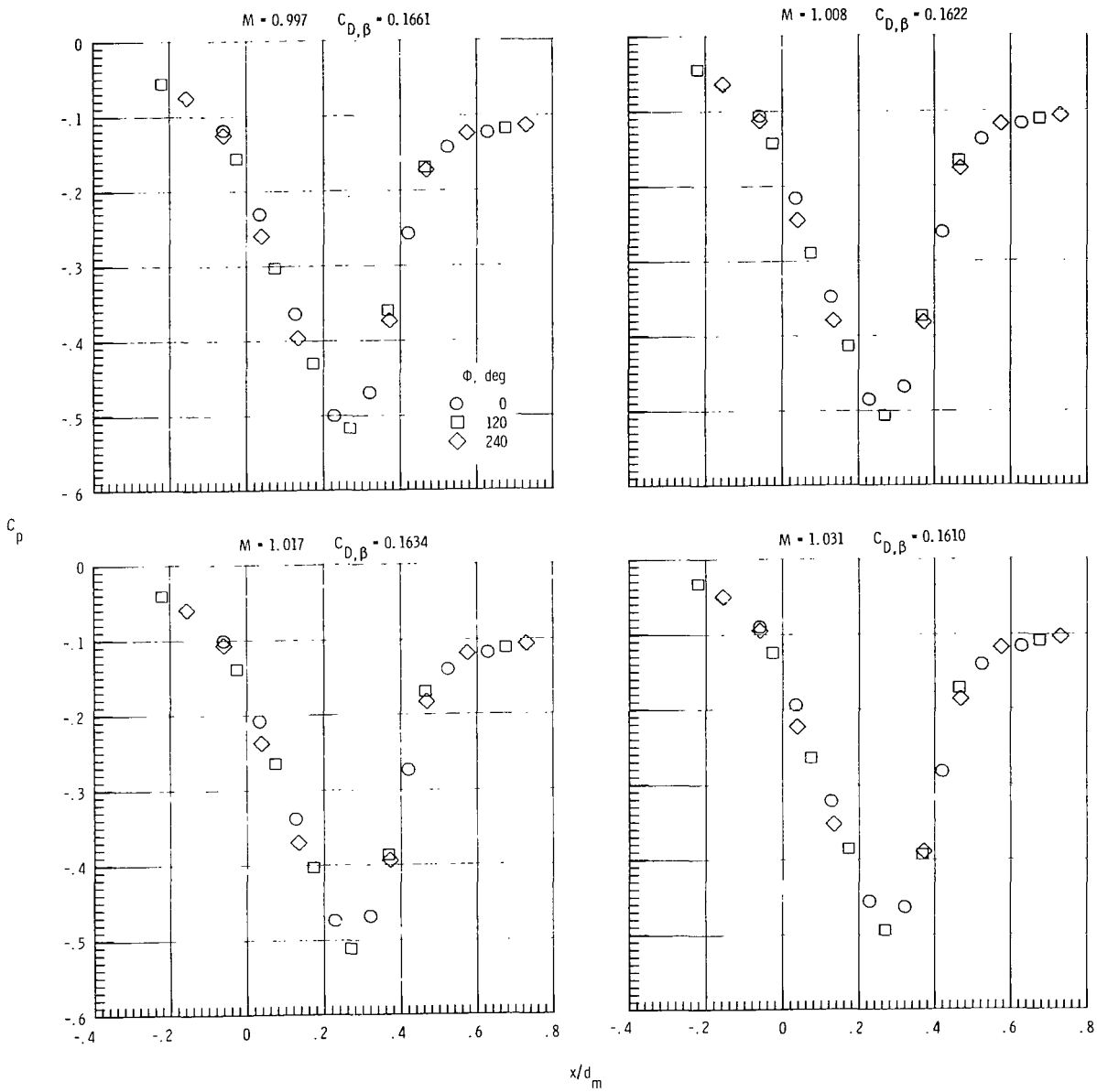

(d) M = 1.00 to 1.03.

Figure 6.- Continued.

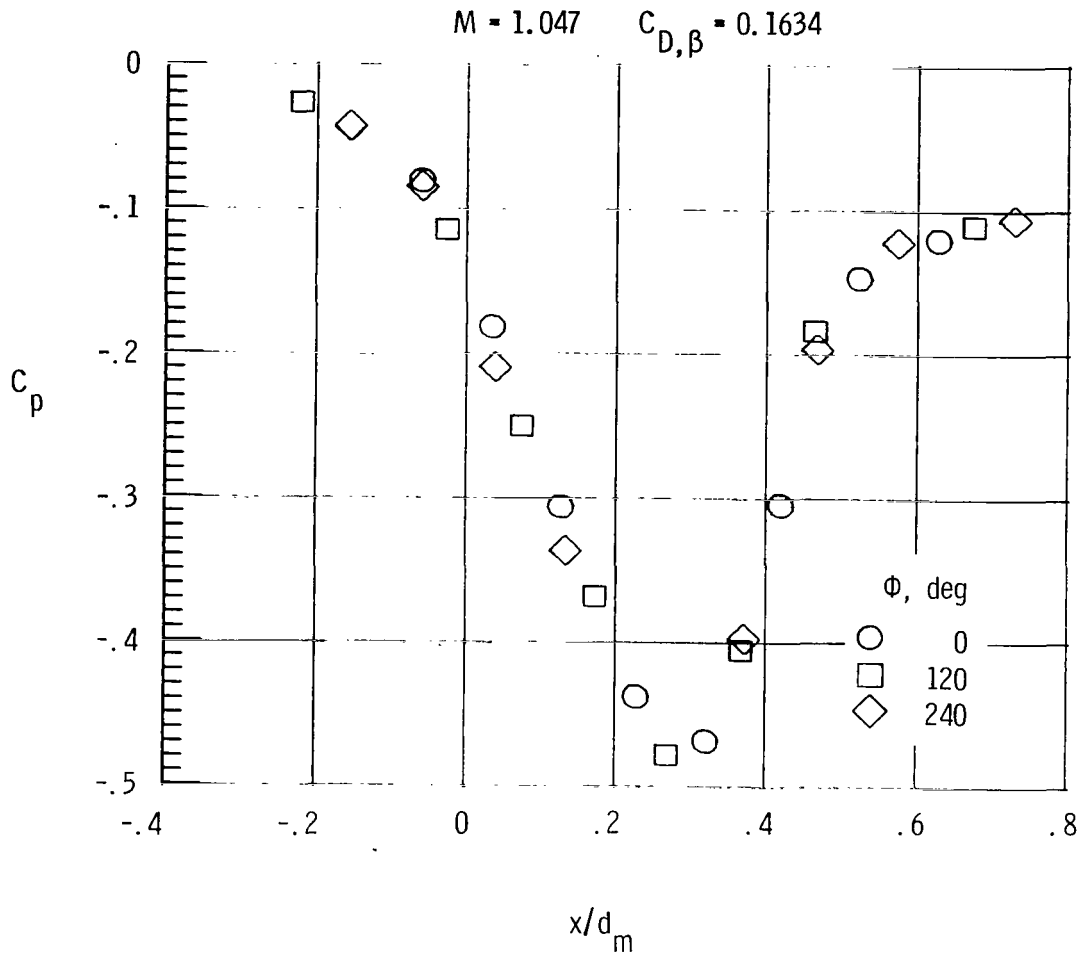

(e) M = 1.05.

Figure 6.- Concluded.

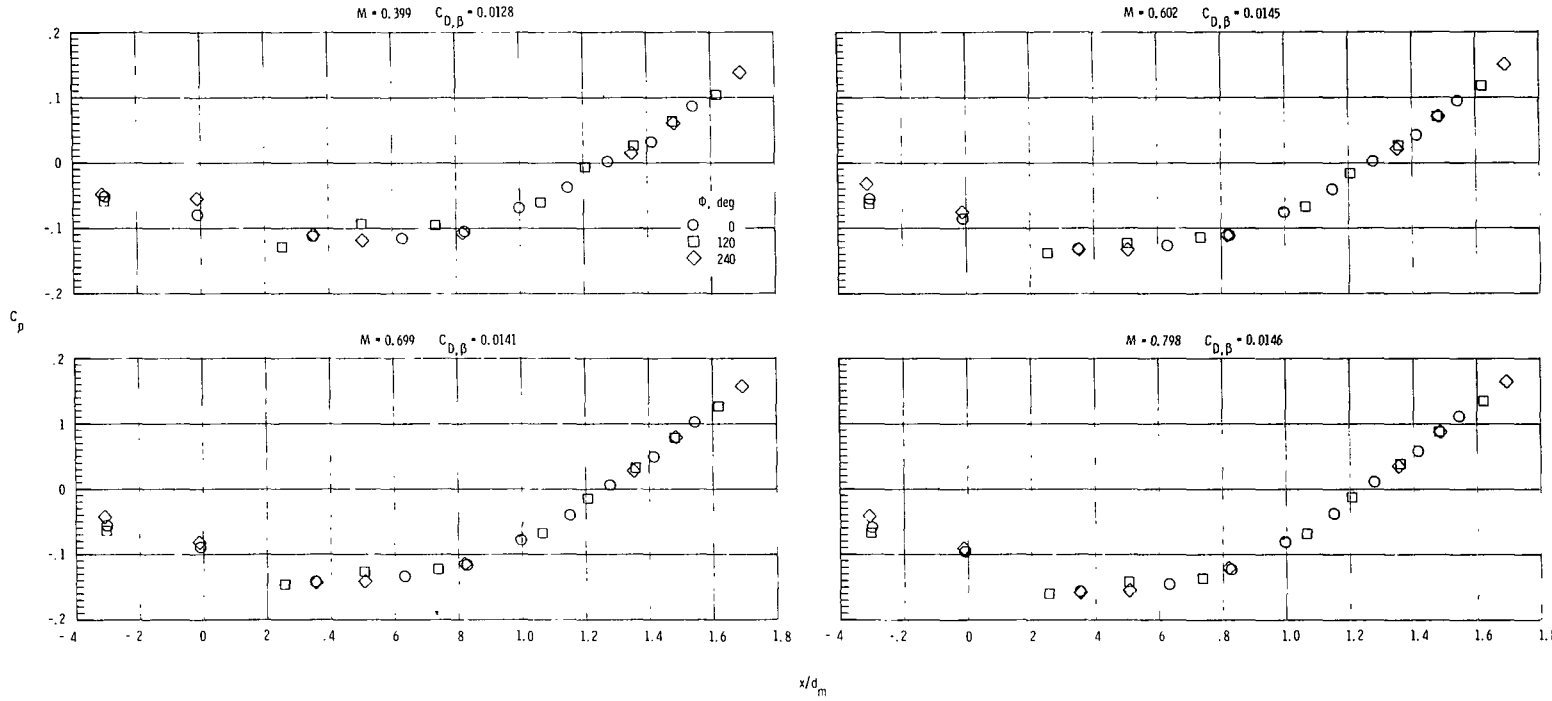

(a) M = 0.4 to 0.8.

Figure 7.- Boattail pressure coefficient distributions for $L/d_m = 8.0$, $l/d_m = 1.77$ circular-arc boattail at 0^o angle of attack at various Mach numbers.

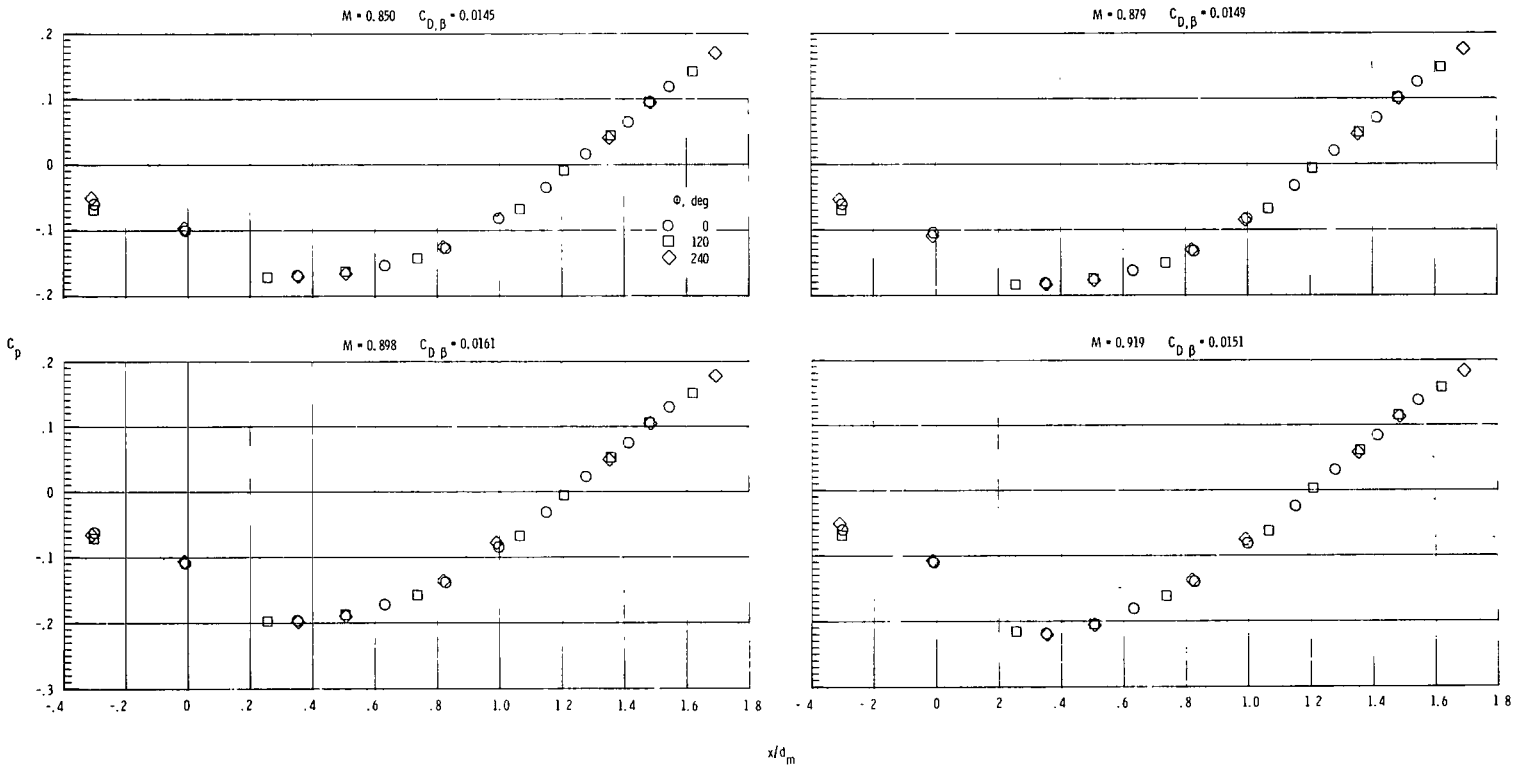

(b) M = 0.85 to 0.92.

Figure 7.- Continued.

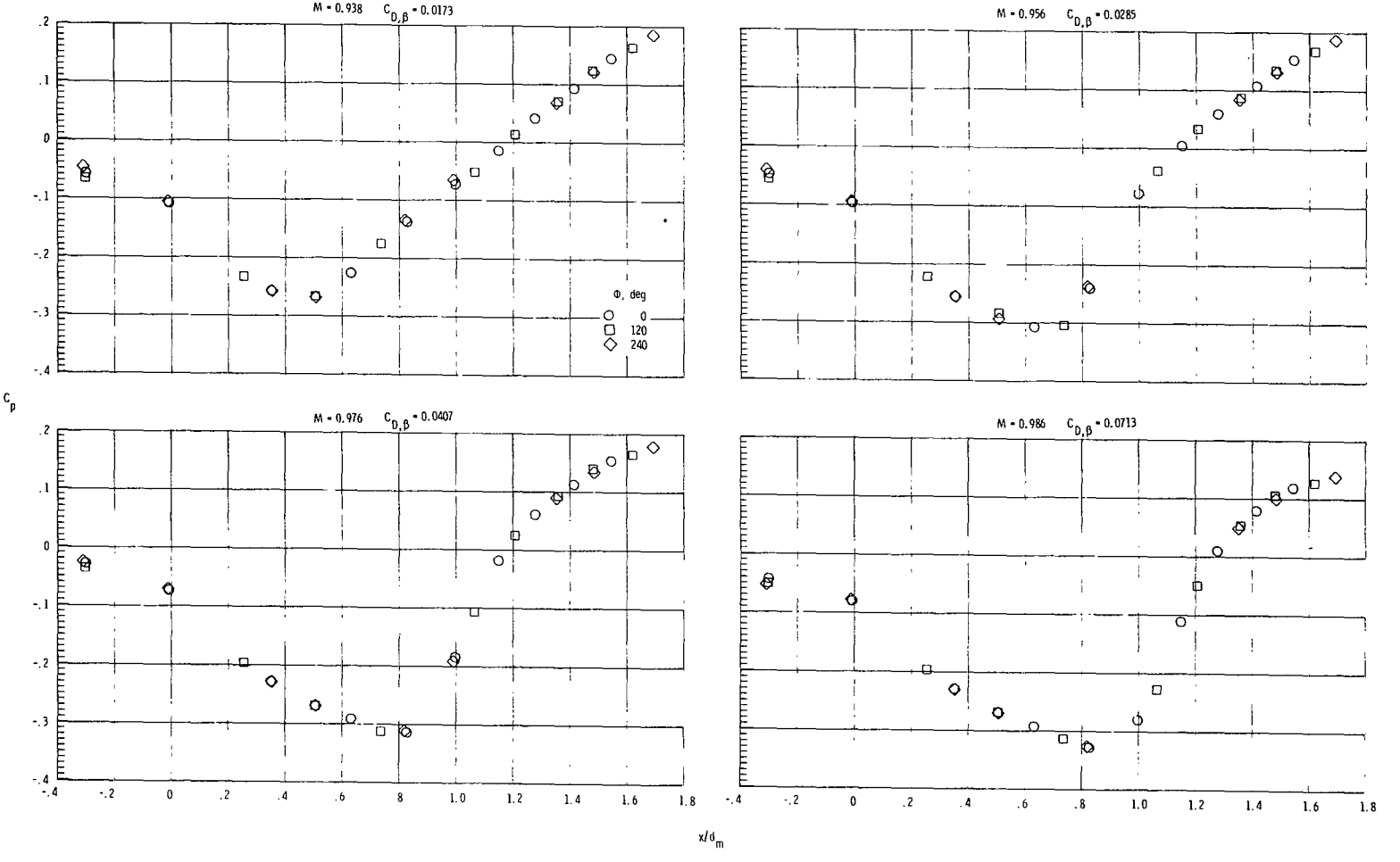

(c) M = 0.94 to 0.99.

Figure 7.- Continued.

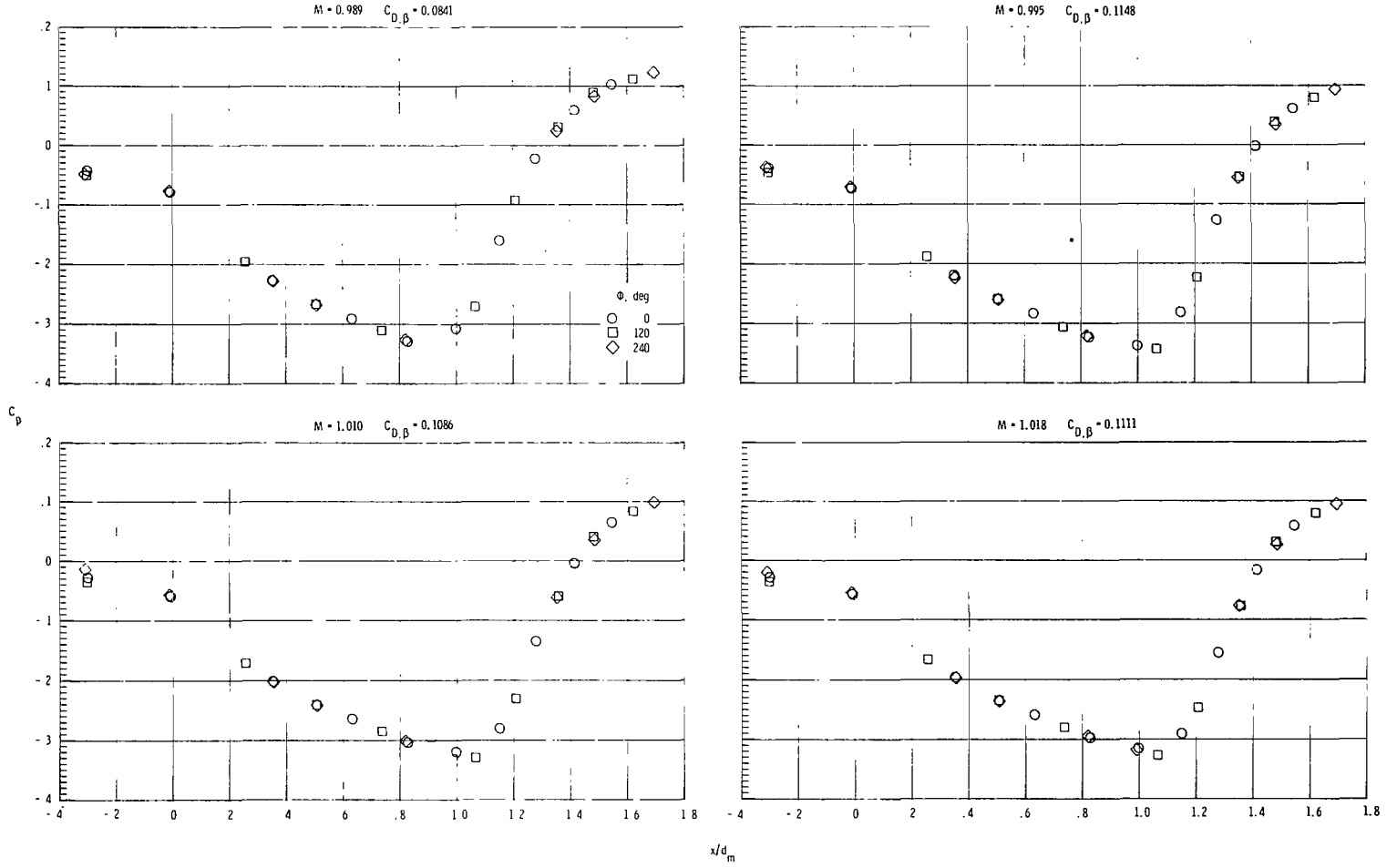

(d) M = 0.99 to 1.02.

Figure 7.- Continued.

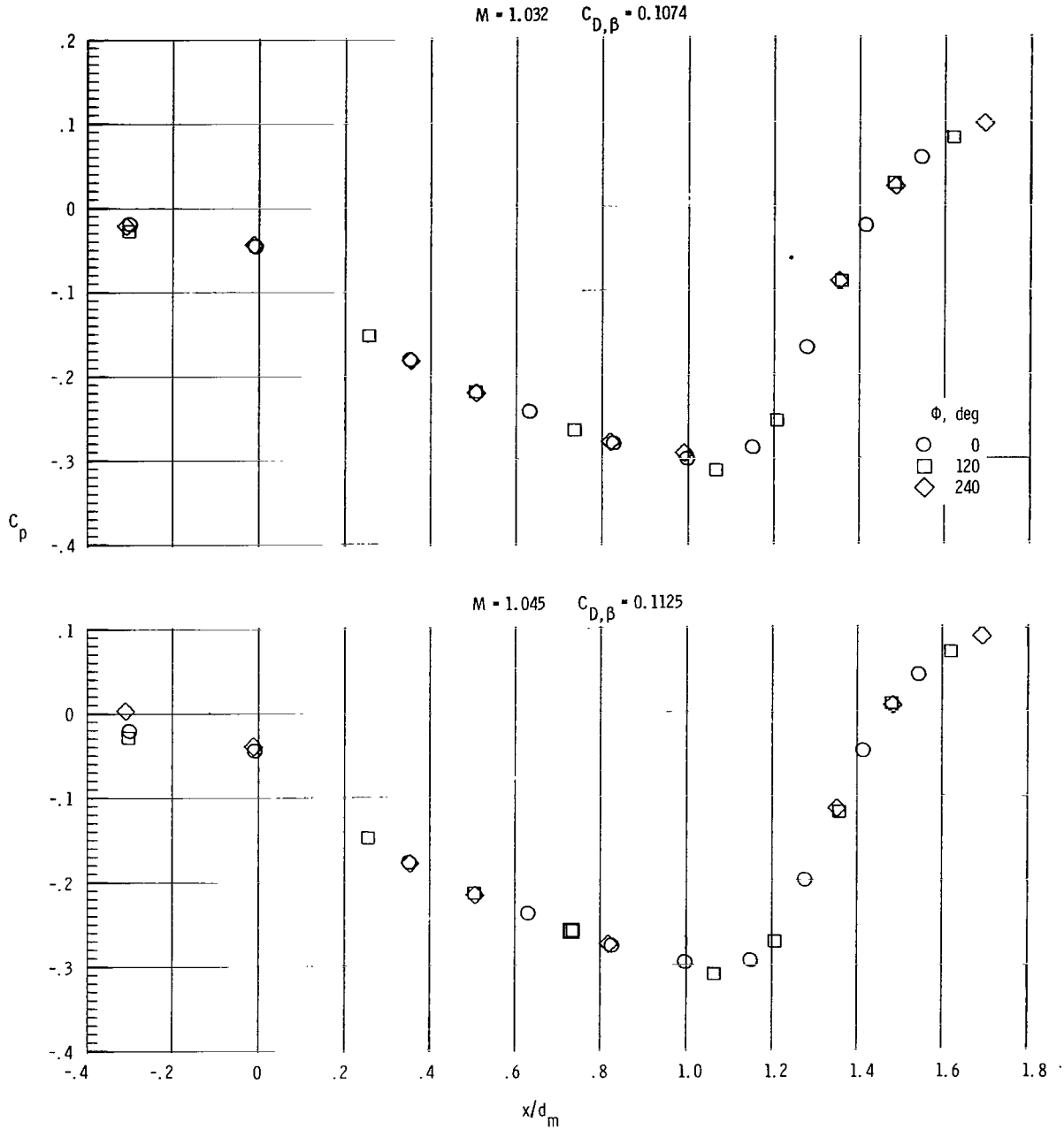

(e) M = 1.03 and 1.05.

Figure 7.- Concluded.

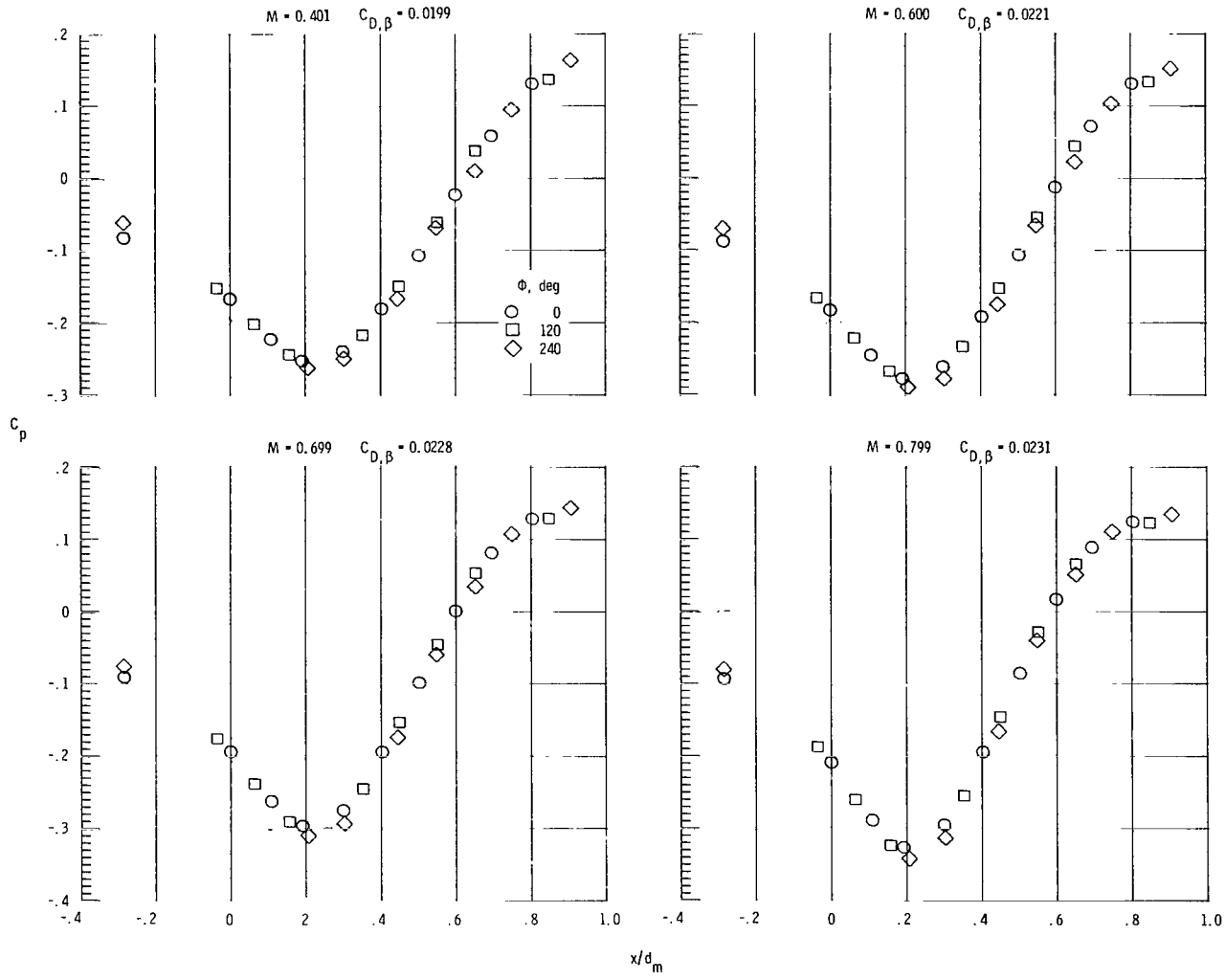

(a) M = 0.4 to 0.8.

Figure 8.- Boattail pressure coefficient distributions for $L/d_m = 8.0$, $l/d_m = 0.96$ circular-arc—conic boattail at 0^o angle of attack at various Mach numbers.

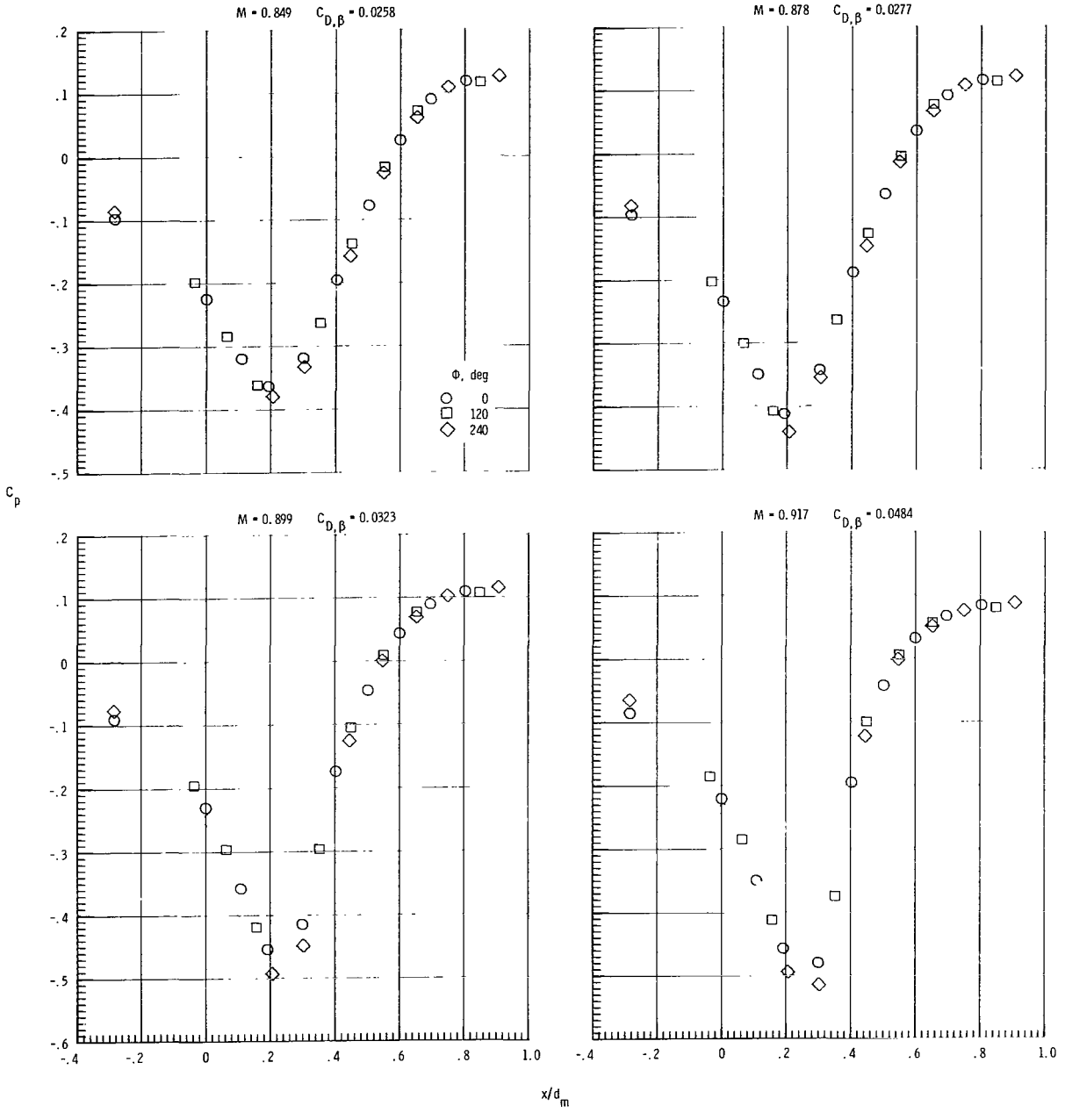

(b) M = 0.85 to 0.92.

Figure 8.- Continued.

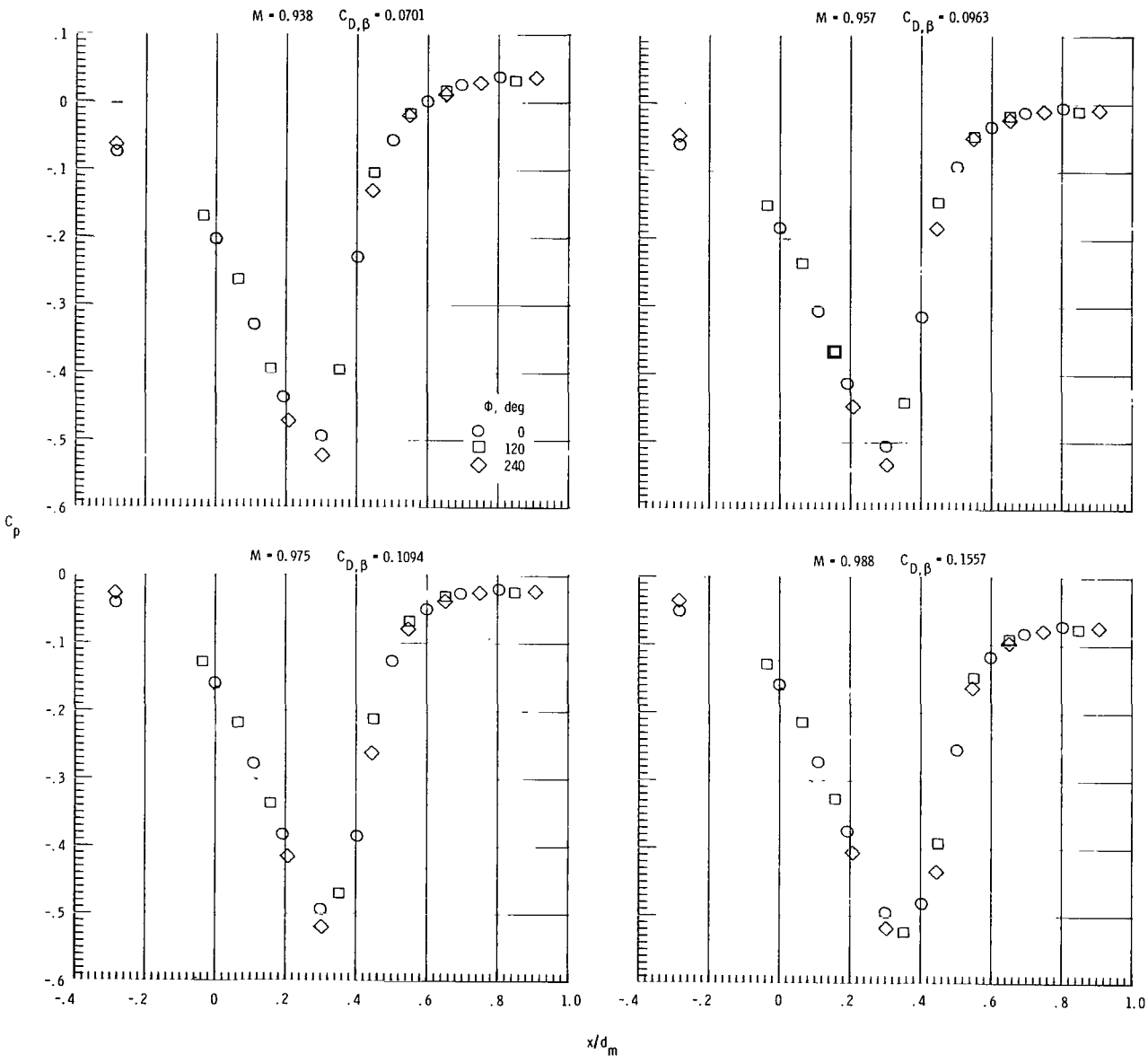

(c) M = 0.94 to 0.99.

Figure 8.- Continued.

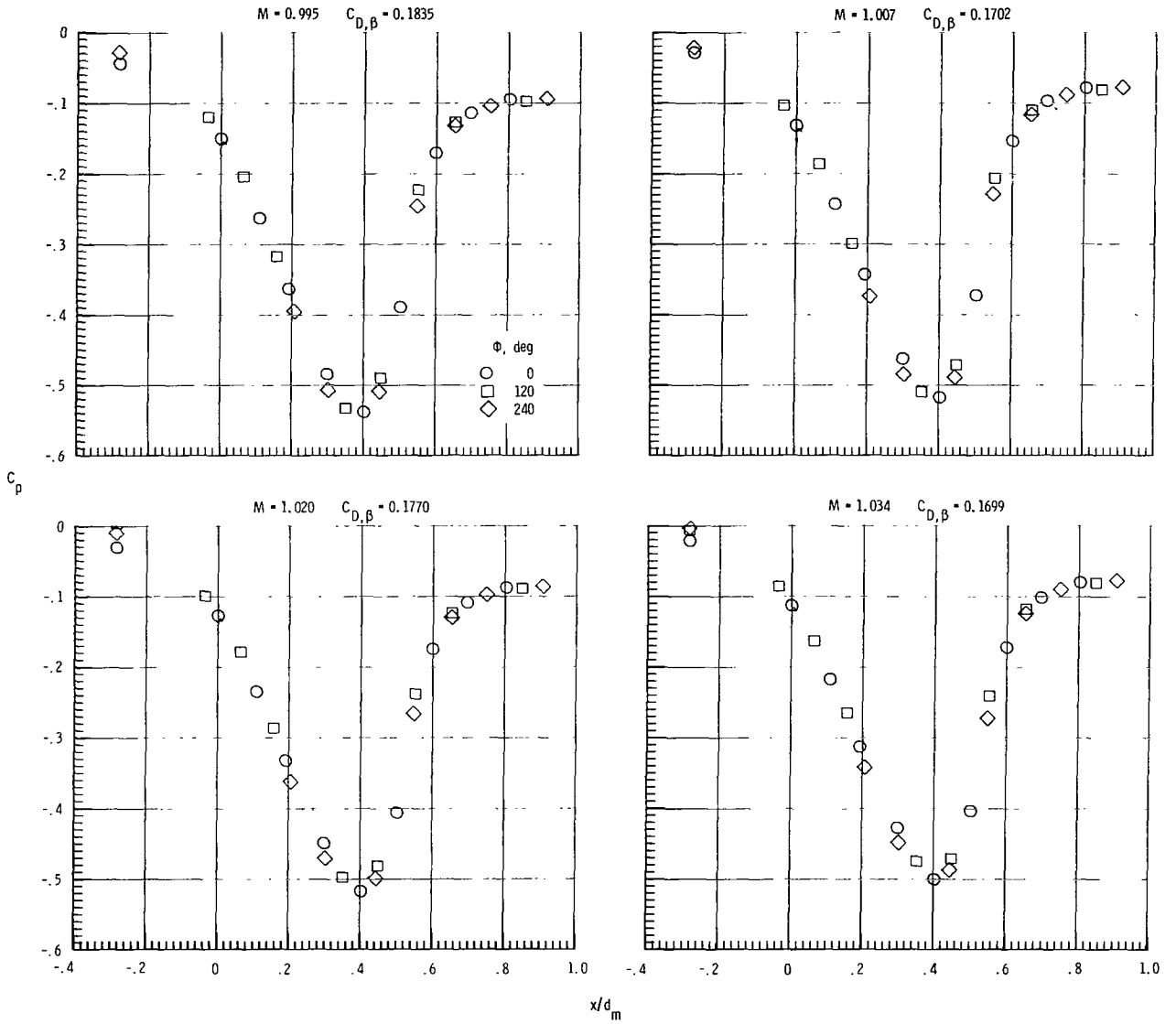

(d) M = 1.00 to 1.03.

Figure 8.- Continued.

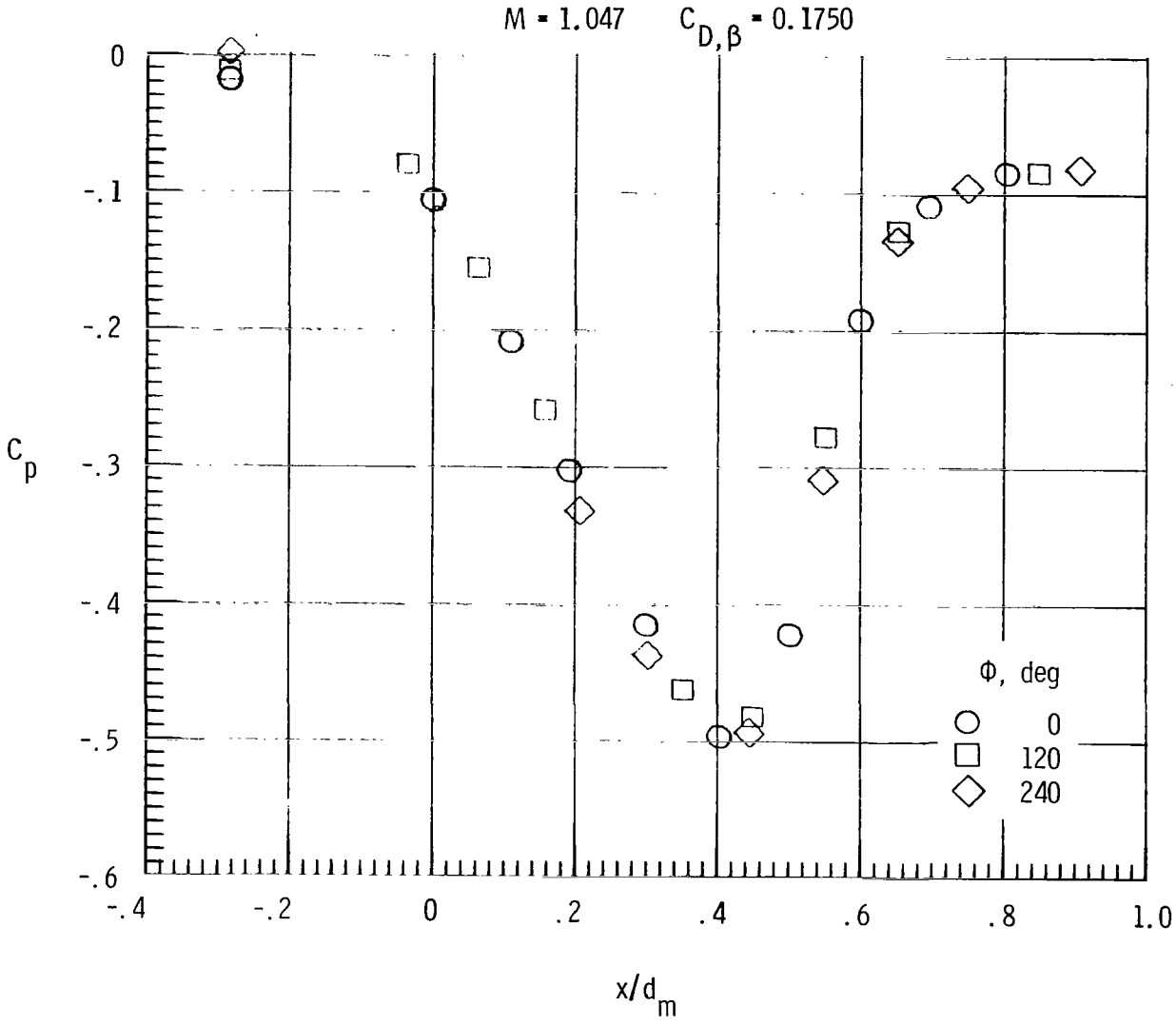

(e) M = 1.05.

Figure 8.- Concluded.

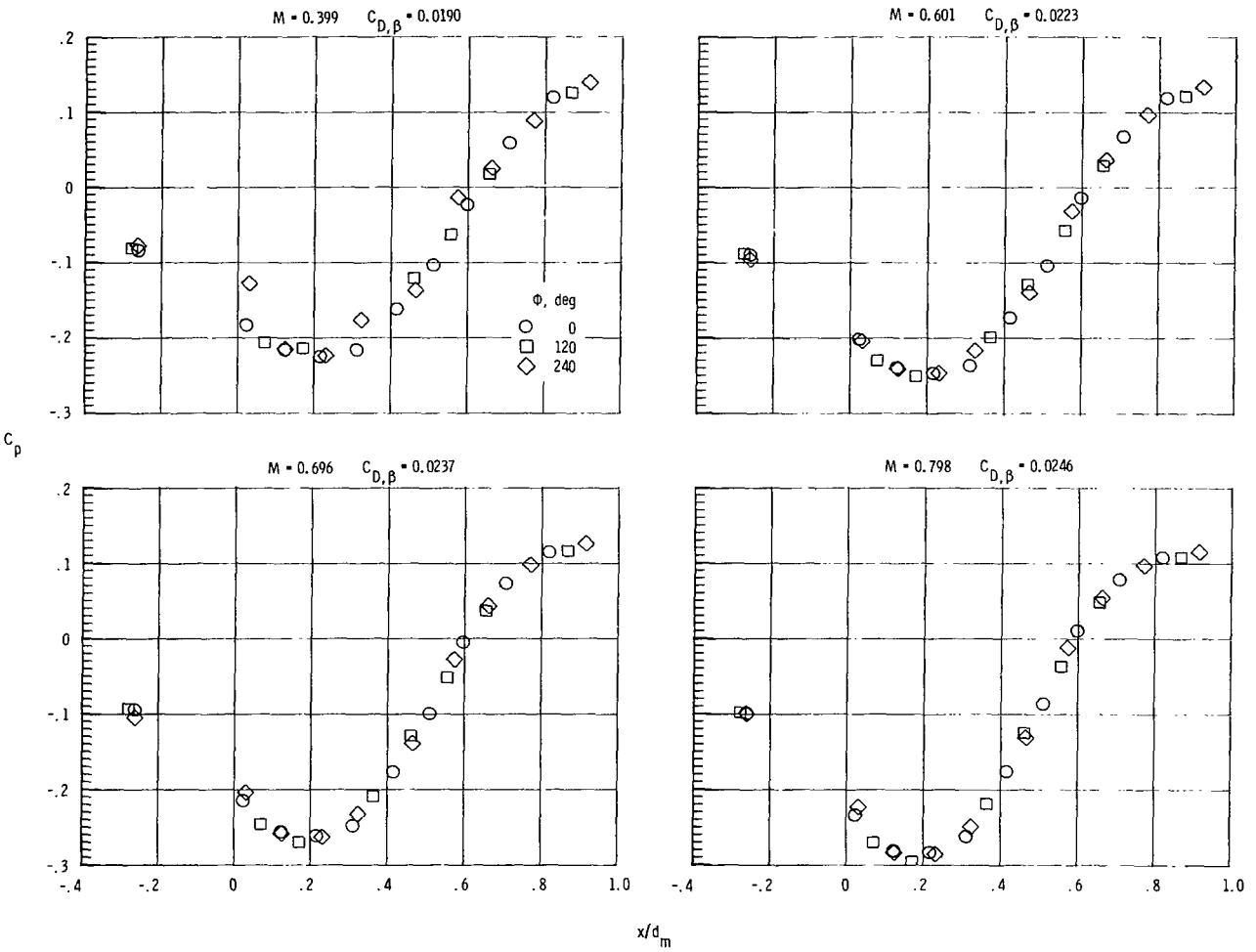

(a) M = 0.4 to 0.8.

Figure 9.- Boattail pressure coefficient distributions for L/d_m = 16.0, l/d_m = 0.96 circular-arc—conic boattail at 0^o angle of attack at various Mach numbers.

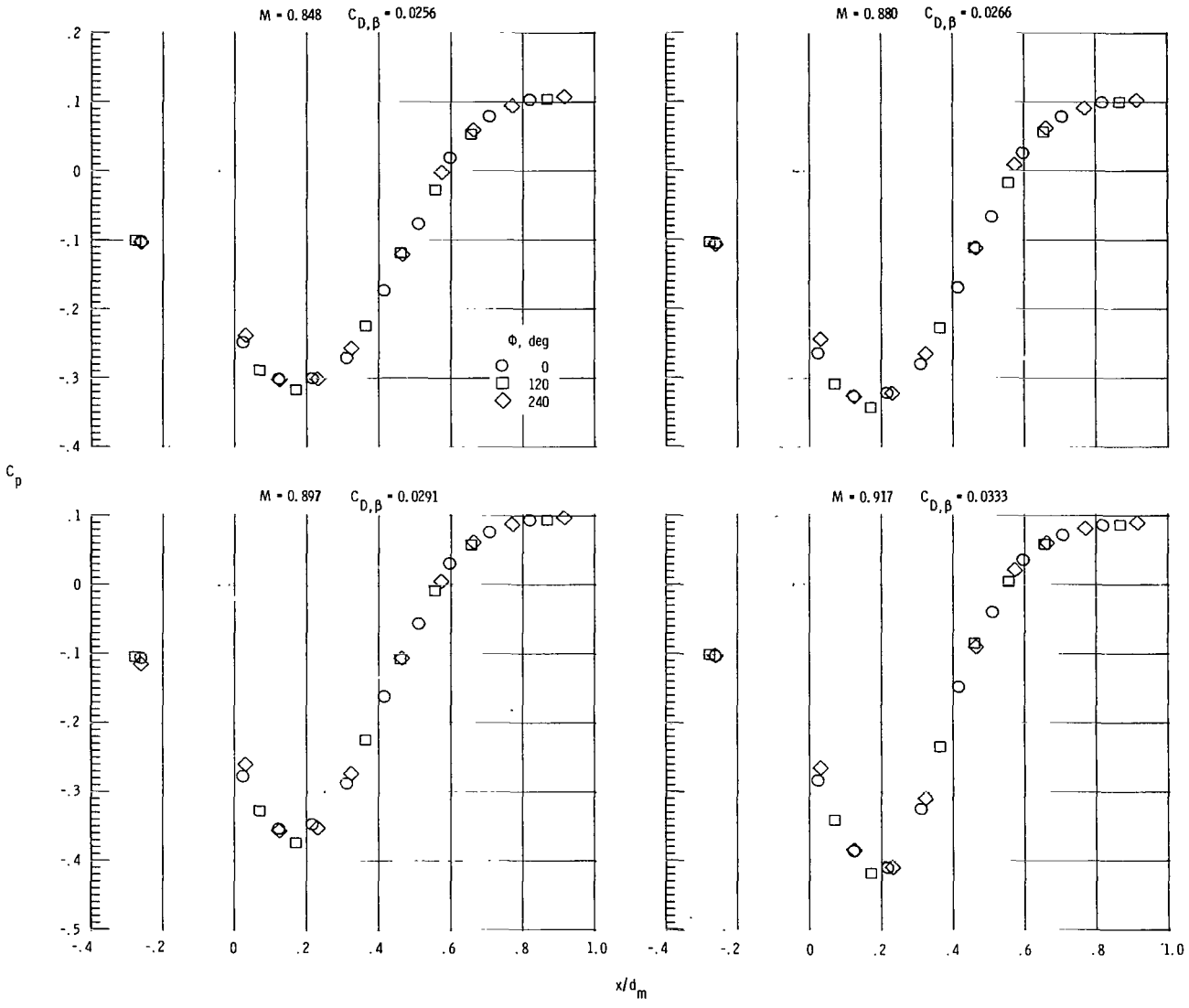

(b) M = 0.85 to 0.92.

Figure 9.- Continued.

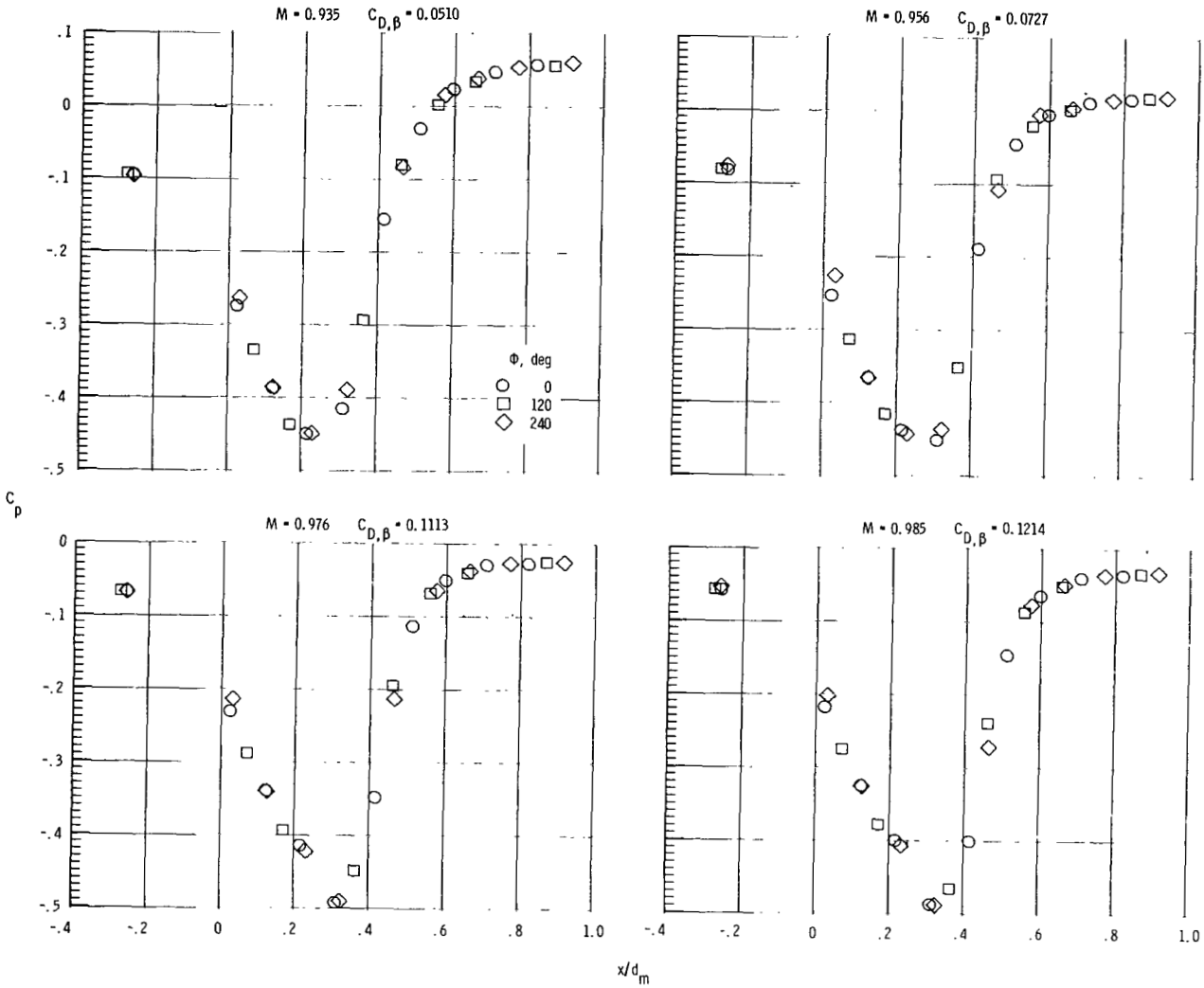

(c) M = 0.94 to 0.99.

Figure 9.- Continued.

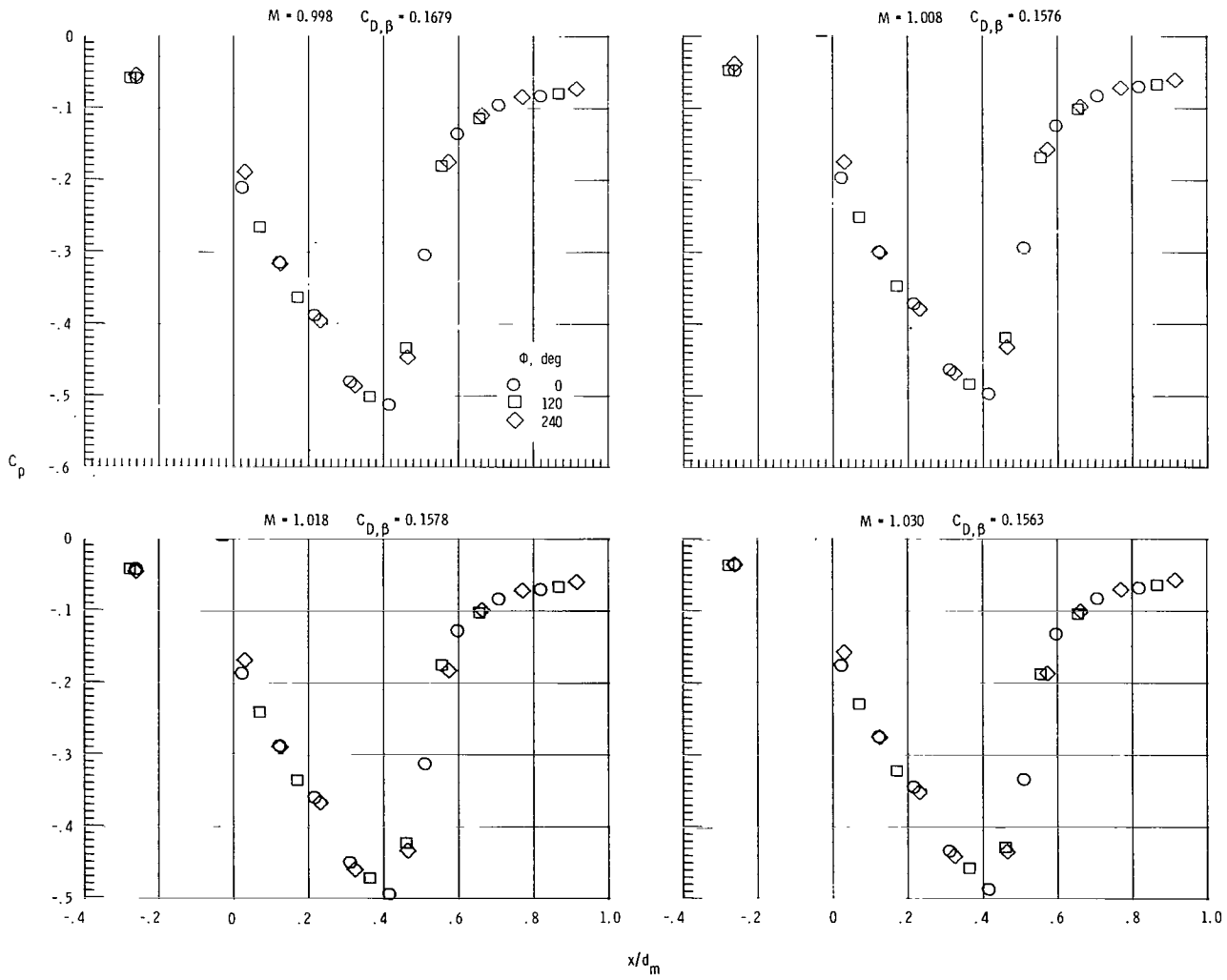

(d) M = 1.00 to 1.03.

Figure 9.- Continued.

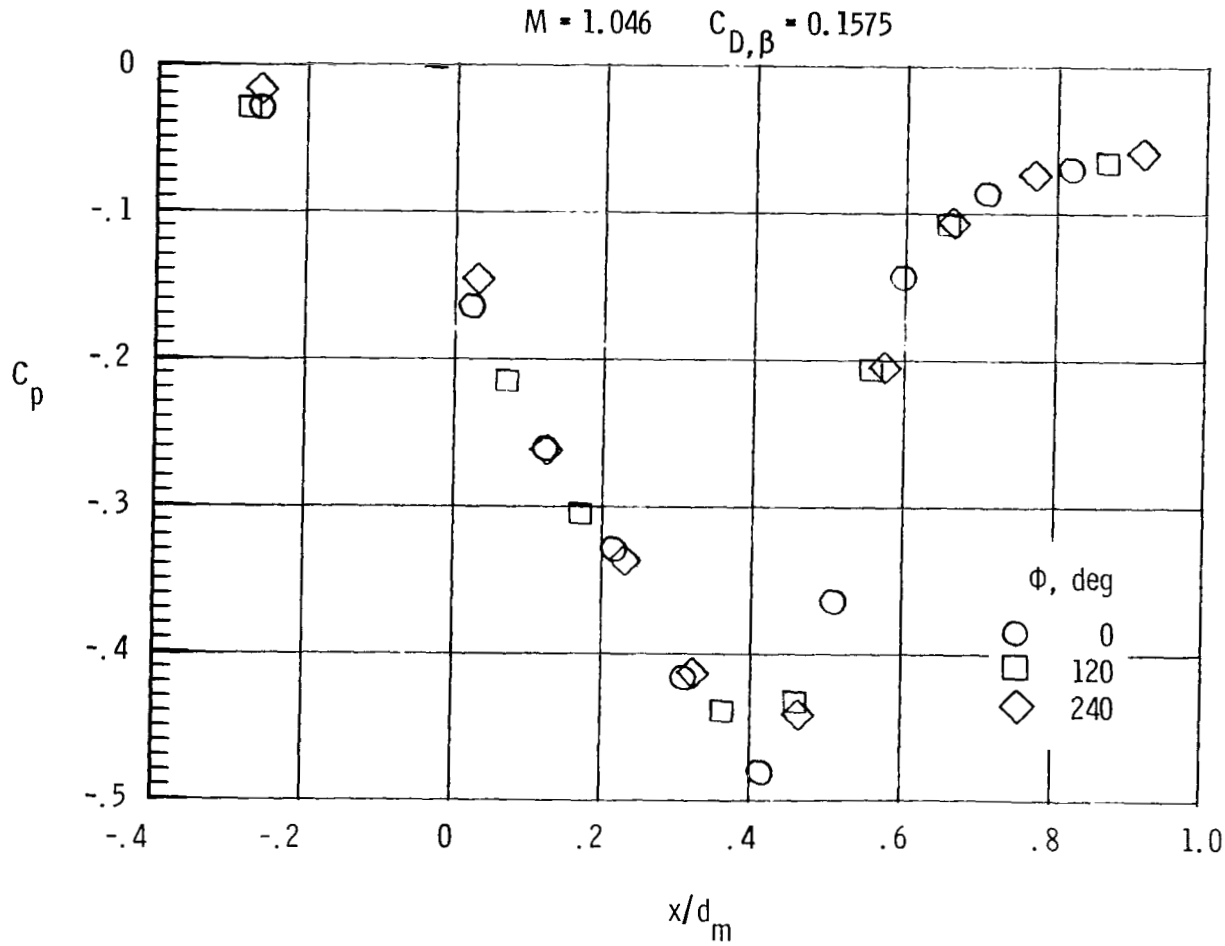

(e) M = 1.05.

Figure 9.- Concluded.

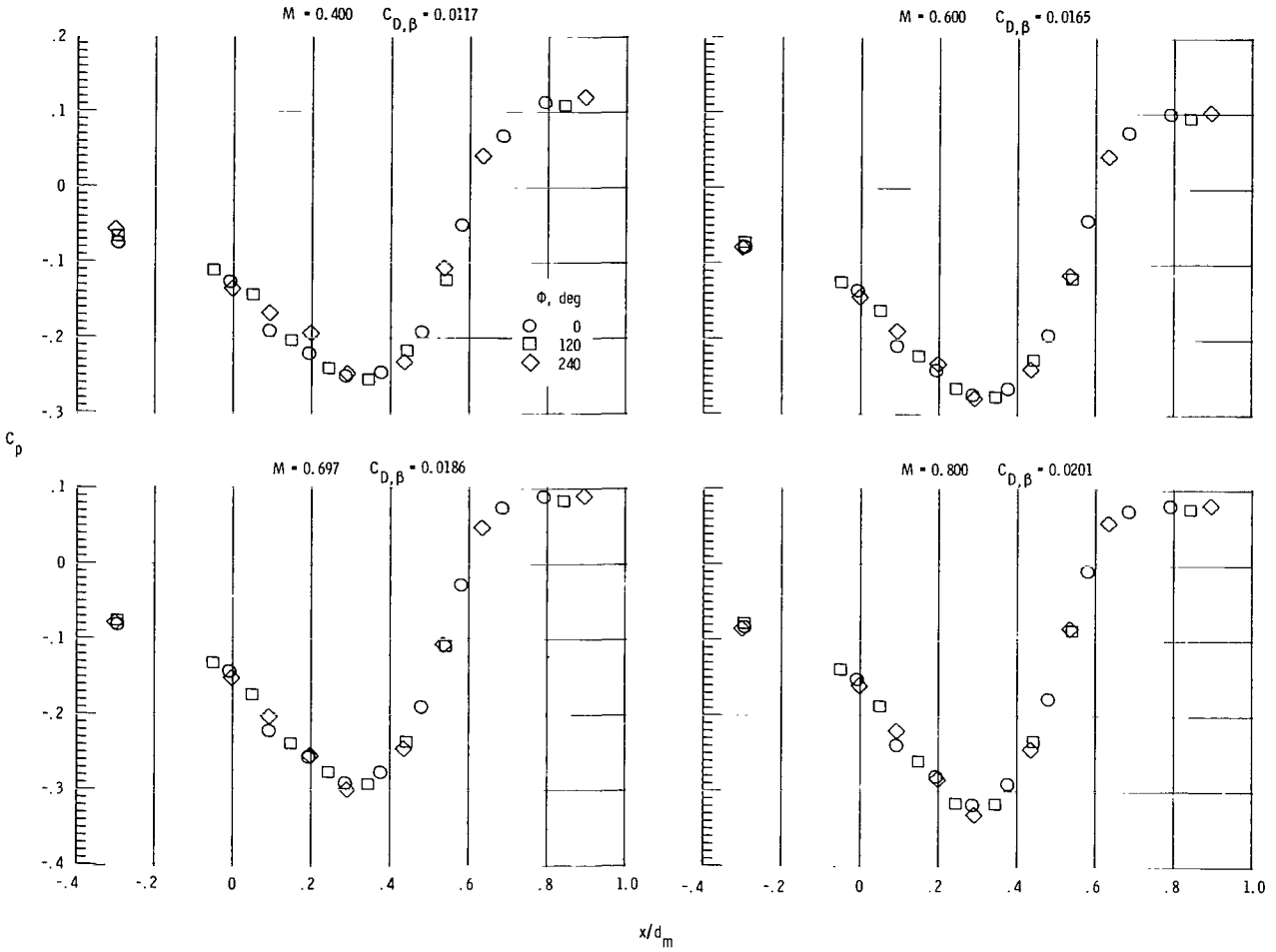

(a) M = 0.4 to 0.8.

Figure 10.- Boattail pressure coefficient distributions for $L/d_m = 8.0$, $l/d_m = 0.95$ contoured boattail at 0^o angle of attack at various Mach numbers.

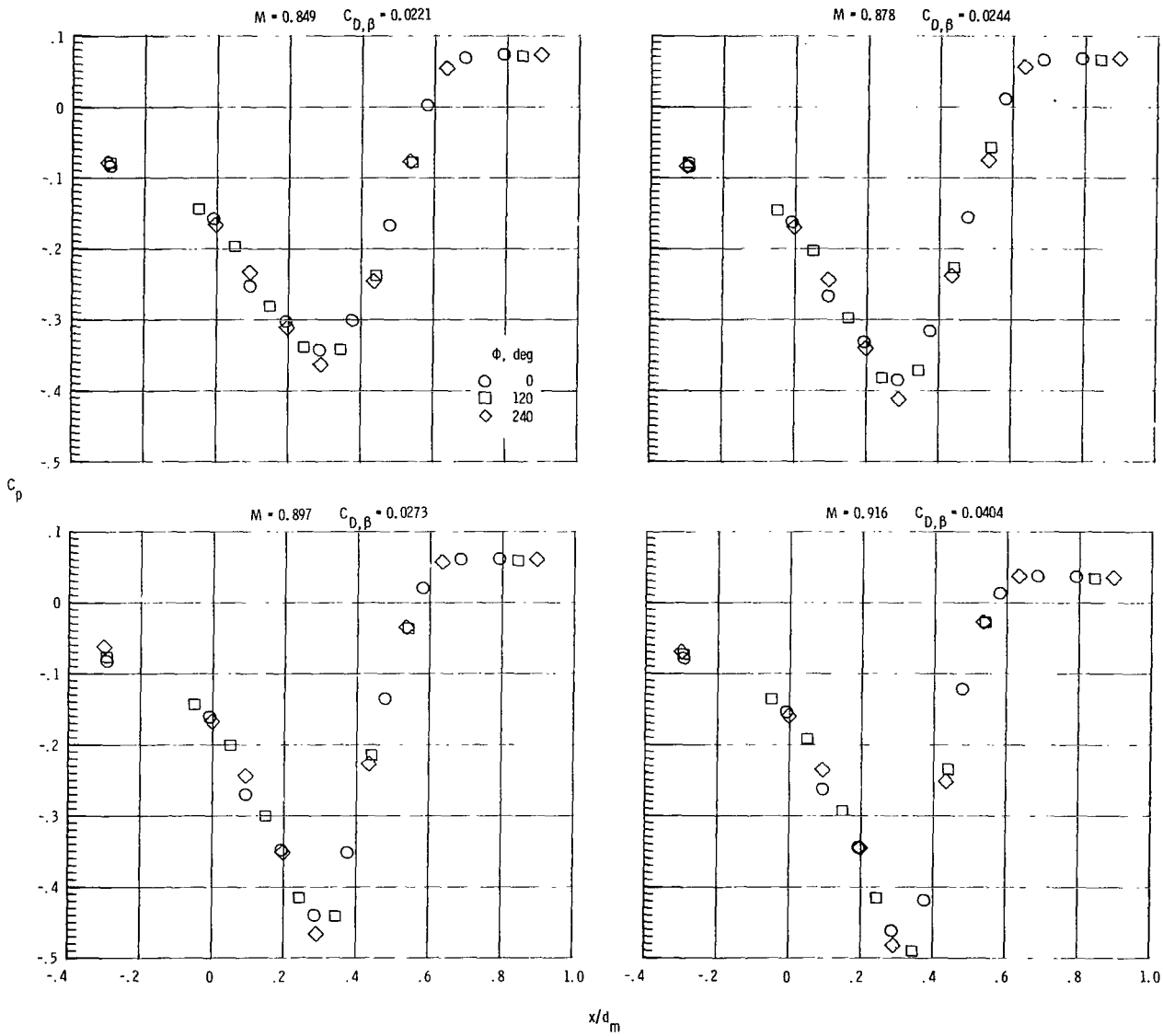

(b) M = 0.85 to 0.92.

Figure 10.- Continued.

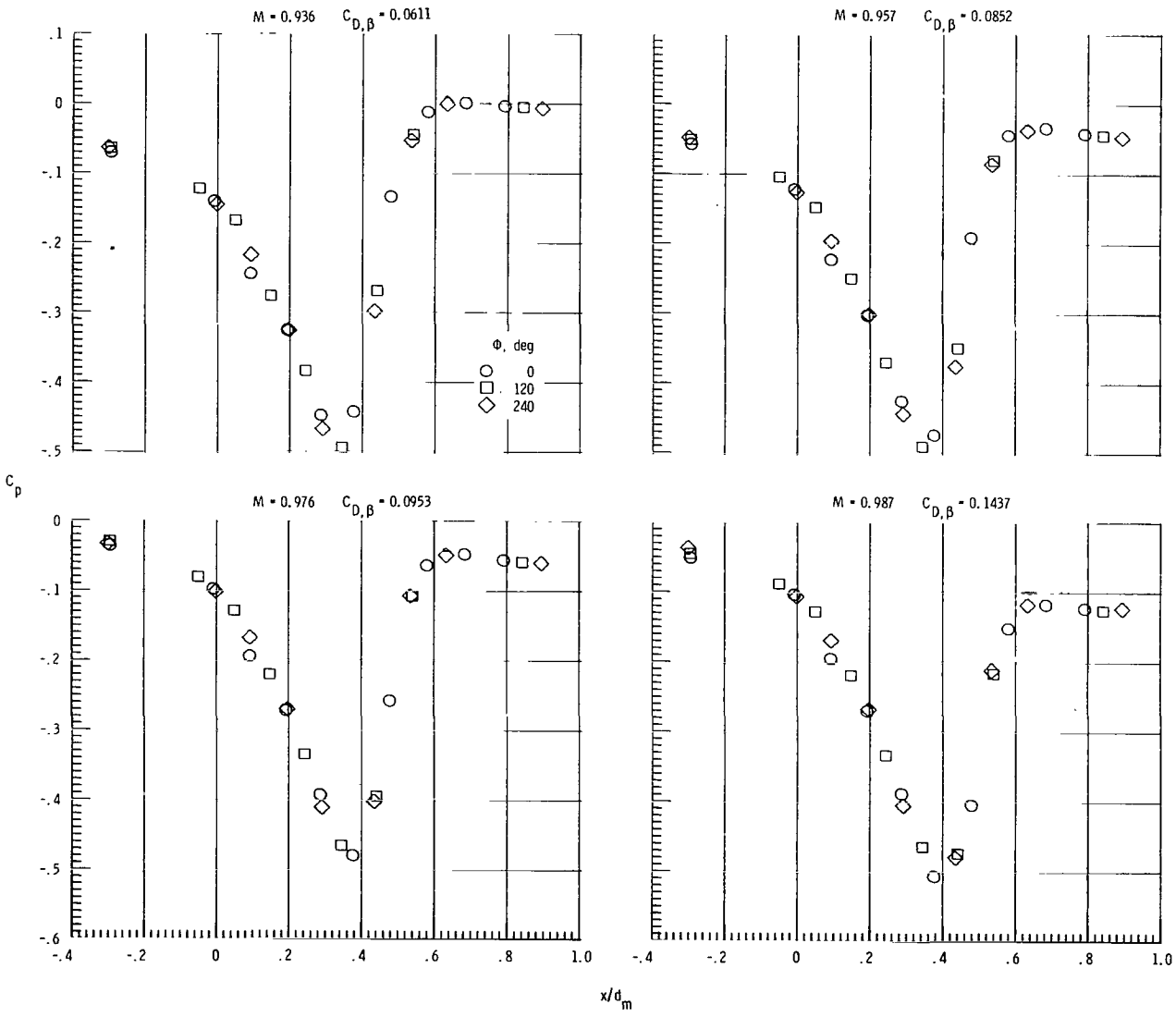

(c) M = 0.94 to 0.99.

Figure 10.- Continued.

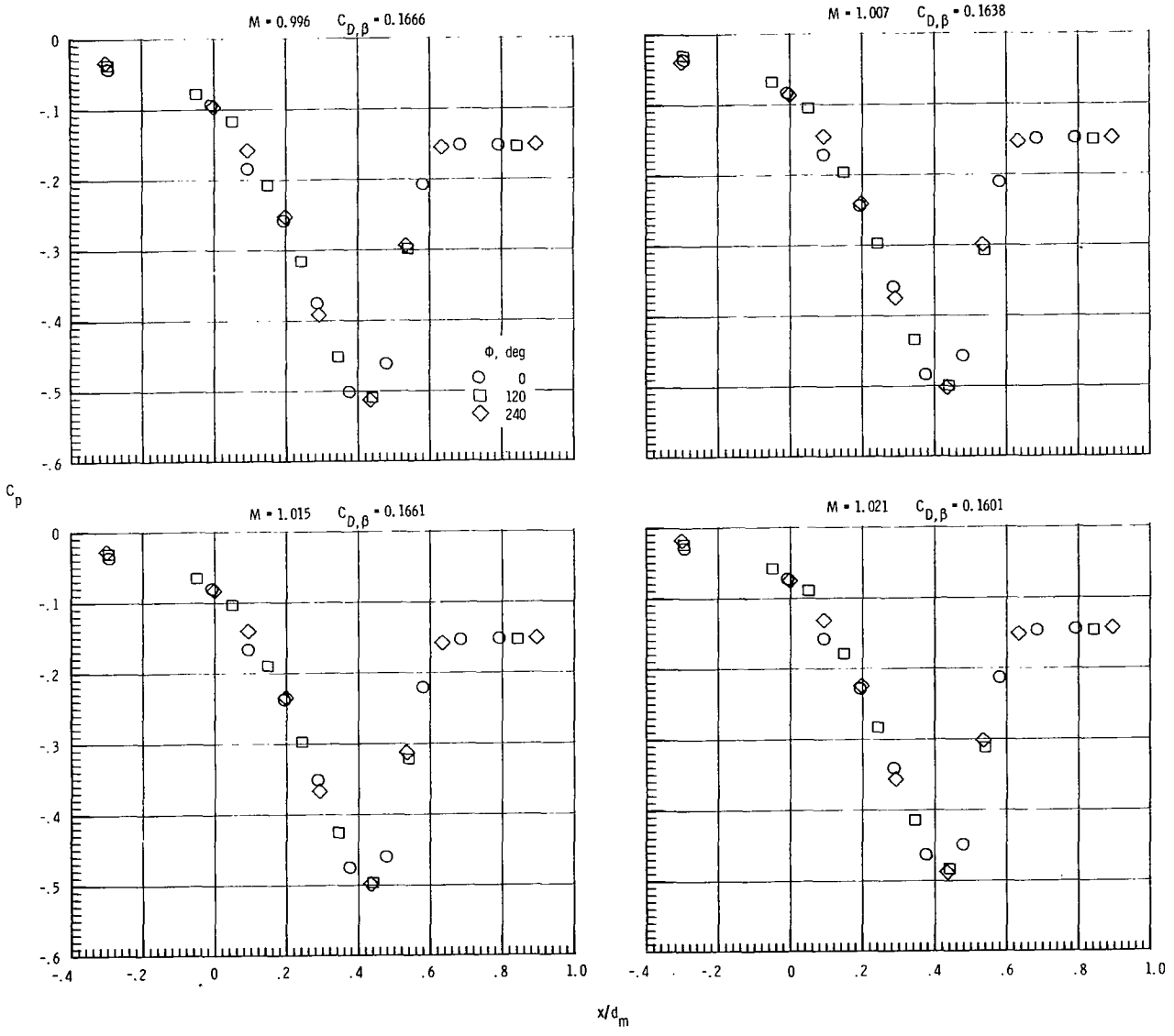

(d) M = 1.00 to 1.02.

Figure 10.- Continued.

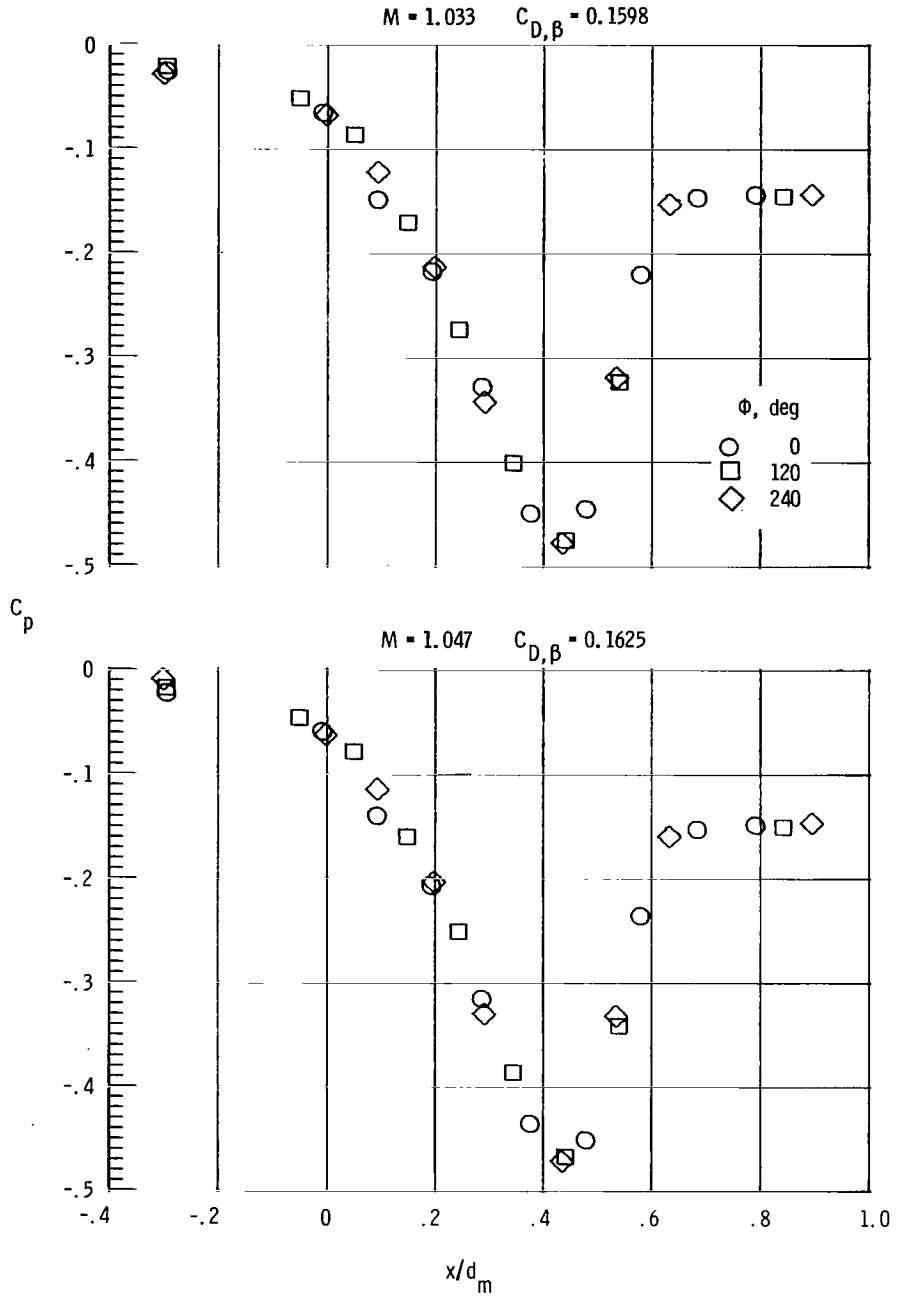

(e) M = 1.03 and 1.05.

Figure 10.- Concluded.

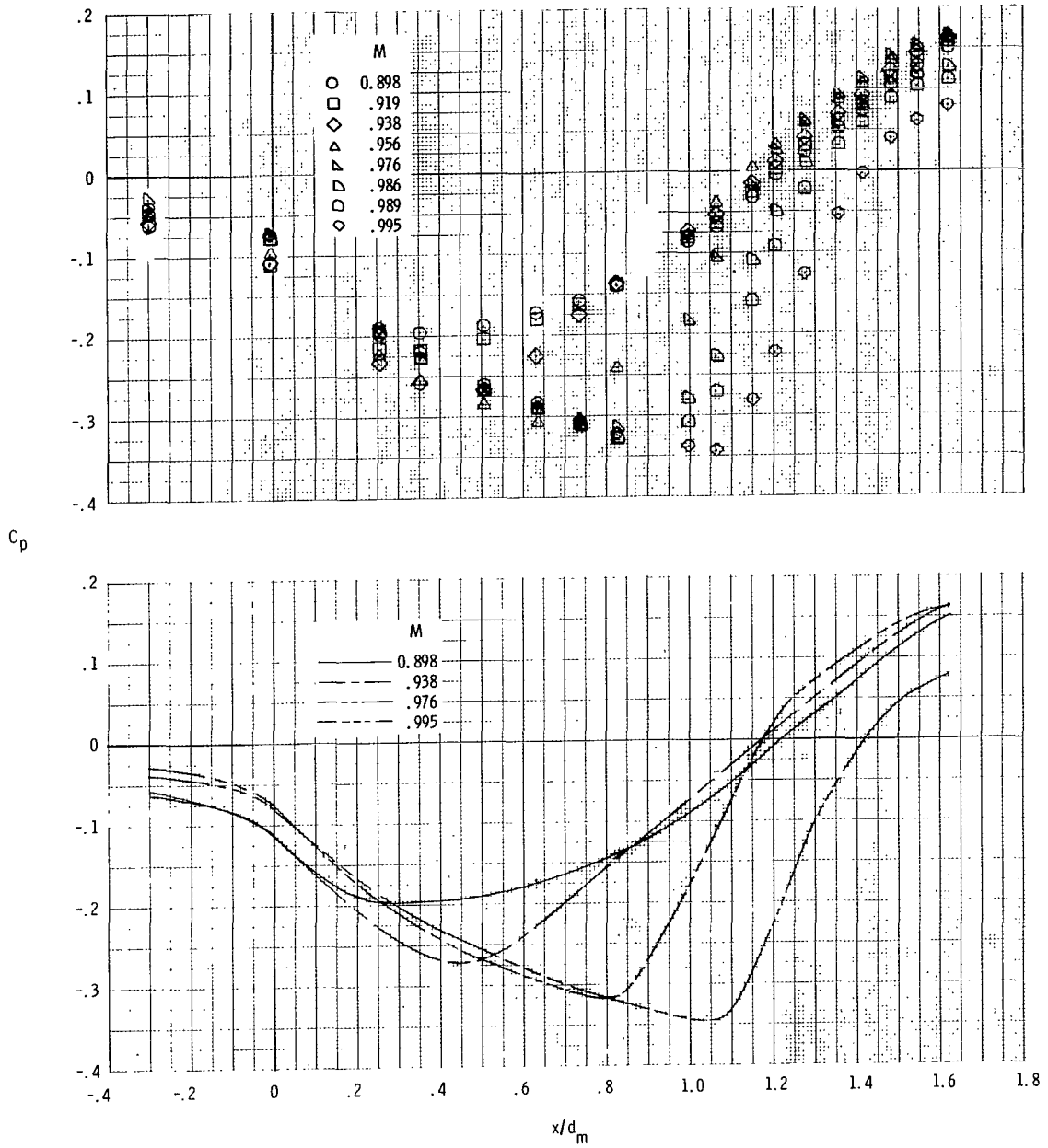

(a) $L/d_m = 8.0$, $\ell/d_m = 1.77$ circular-arc.

Figure 11.- Typical examples of change in boattail pressure coefficient distributions at Mach numbers between about 0.9 and 1.0.

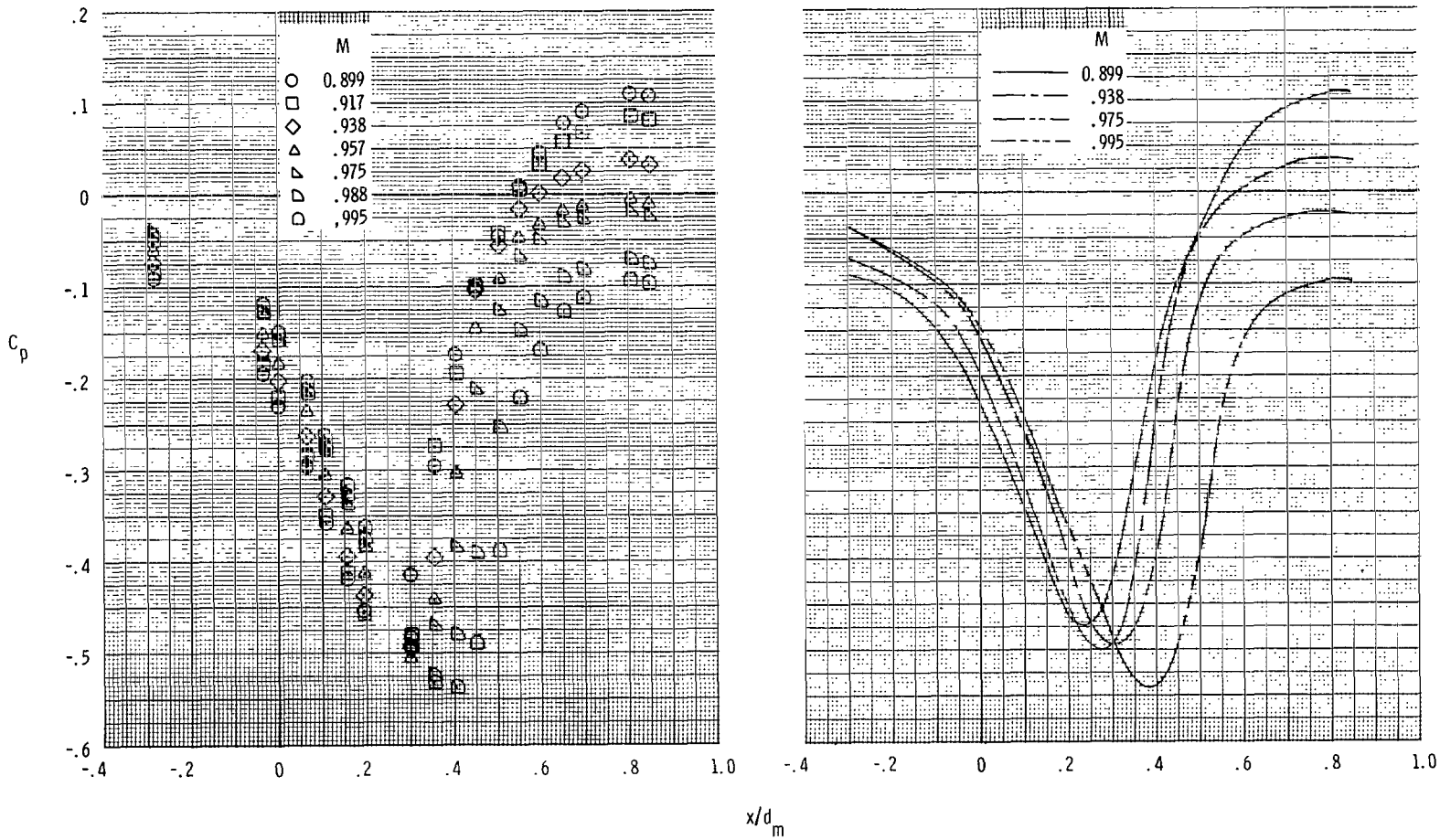

(b) $L/d_m = 8.0$, $l/d_m = 0.96$ circular-arc—conic.

Figure 11.- Concluded.

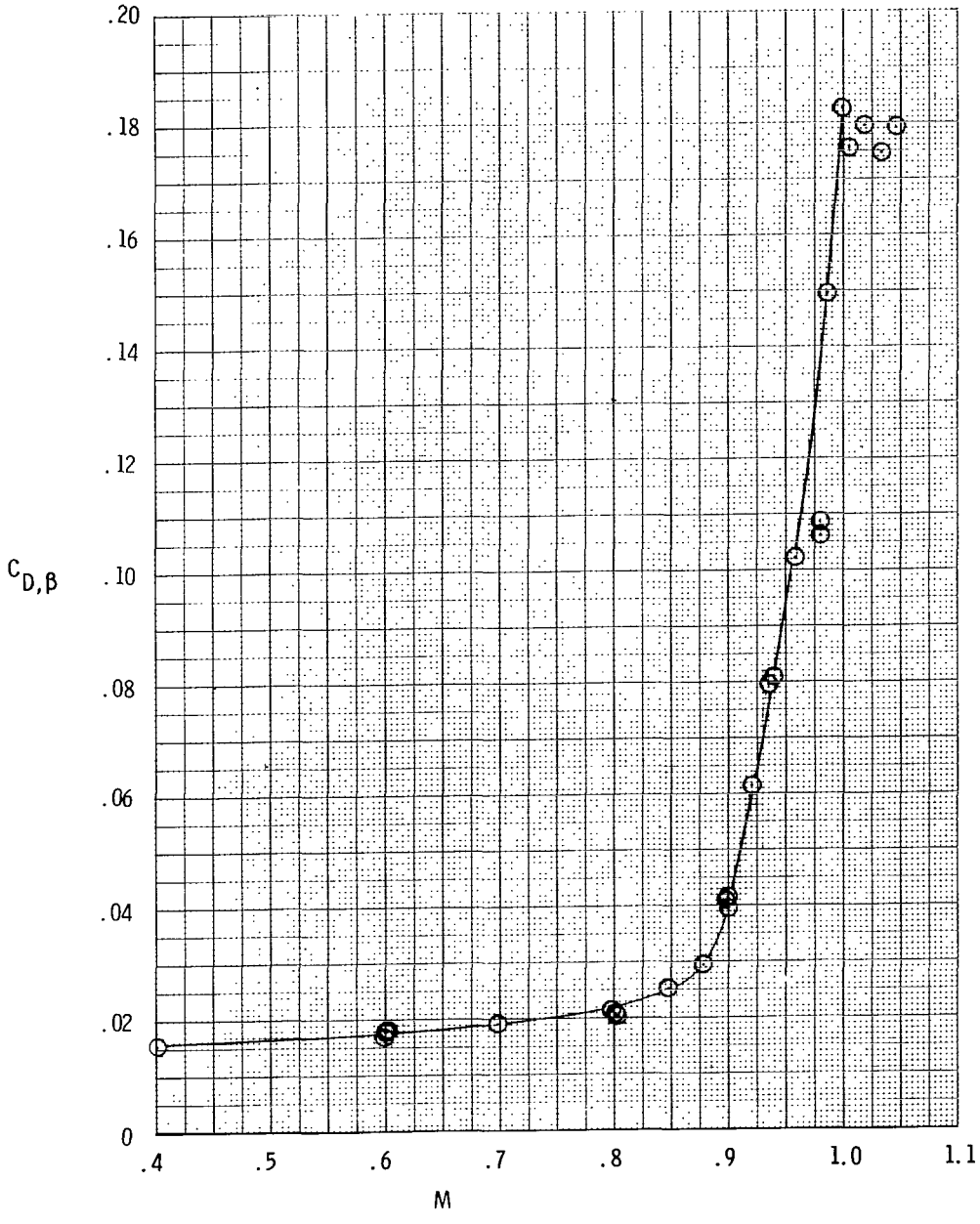

(a) $L/d_m = 8.0$, $l/d_m = 0.80$ circular-arc.

Figure 12.- Effect of Mach number on boattail pressure drag coefficients for the various configurations.

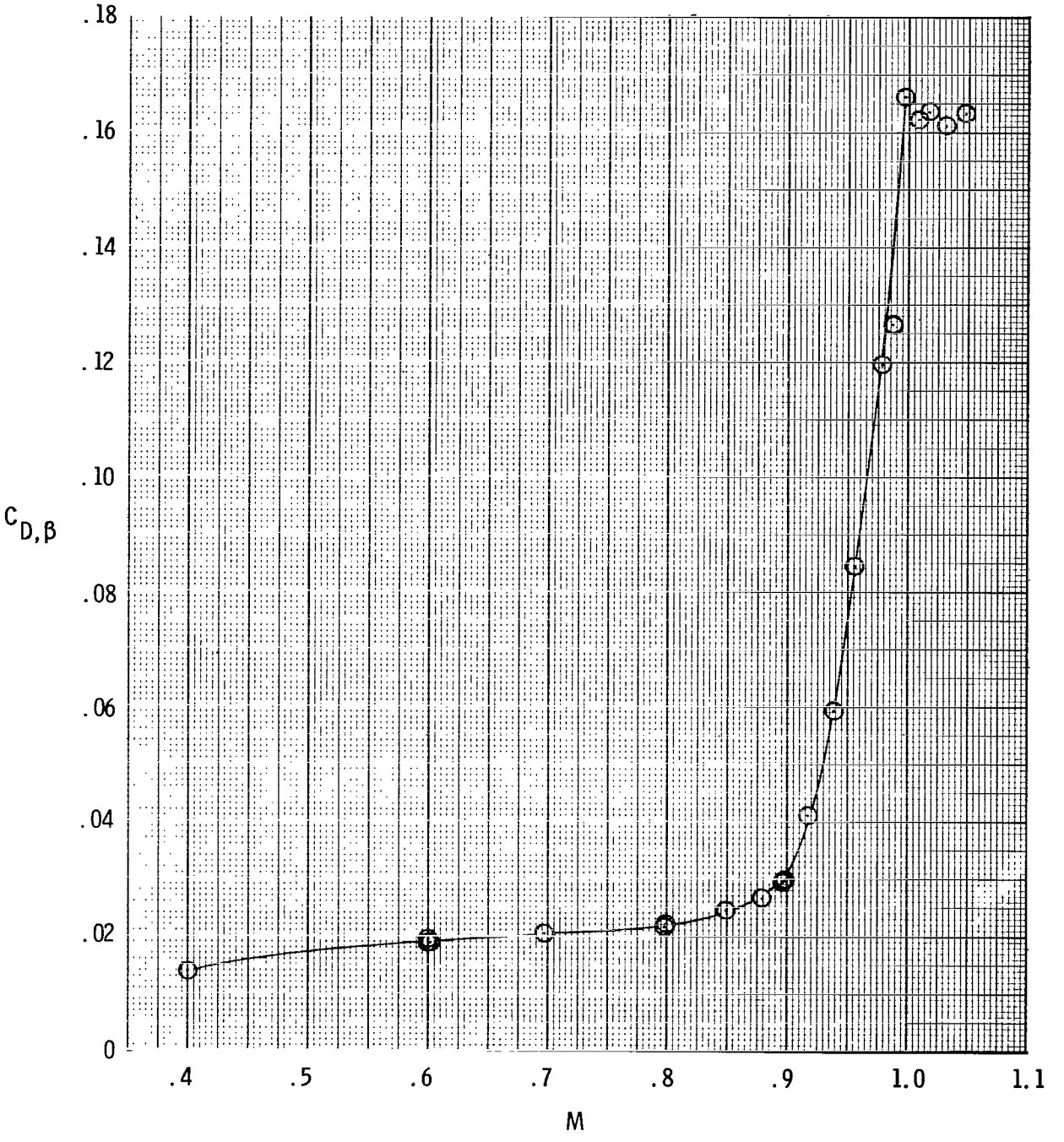

(b) $L/d_m = 16.0$, $l/d_m = 0.80$ circular-arc.

Figure 12.- Continued.

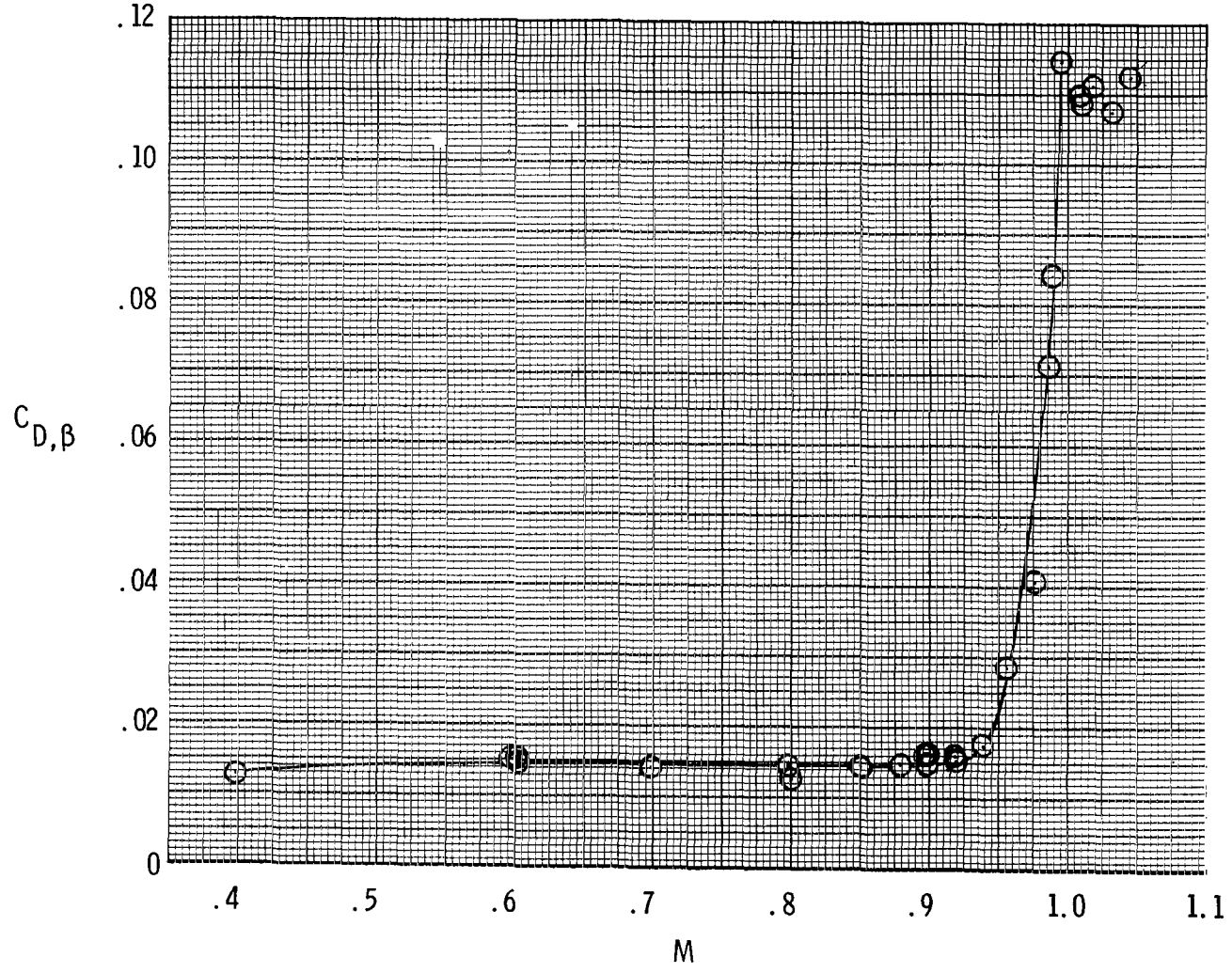

(c) $L/d_m = 8.0$, $l/d_m = 1.77$ circular-arc.

Figure 12.- Continued.

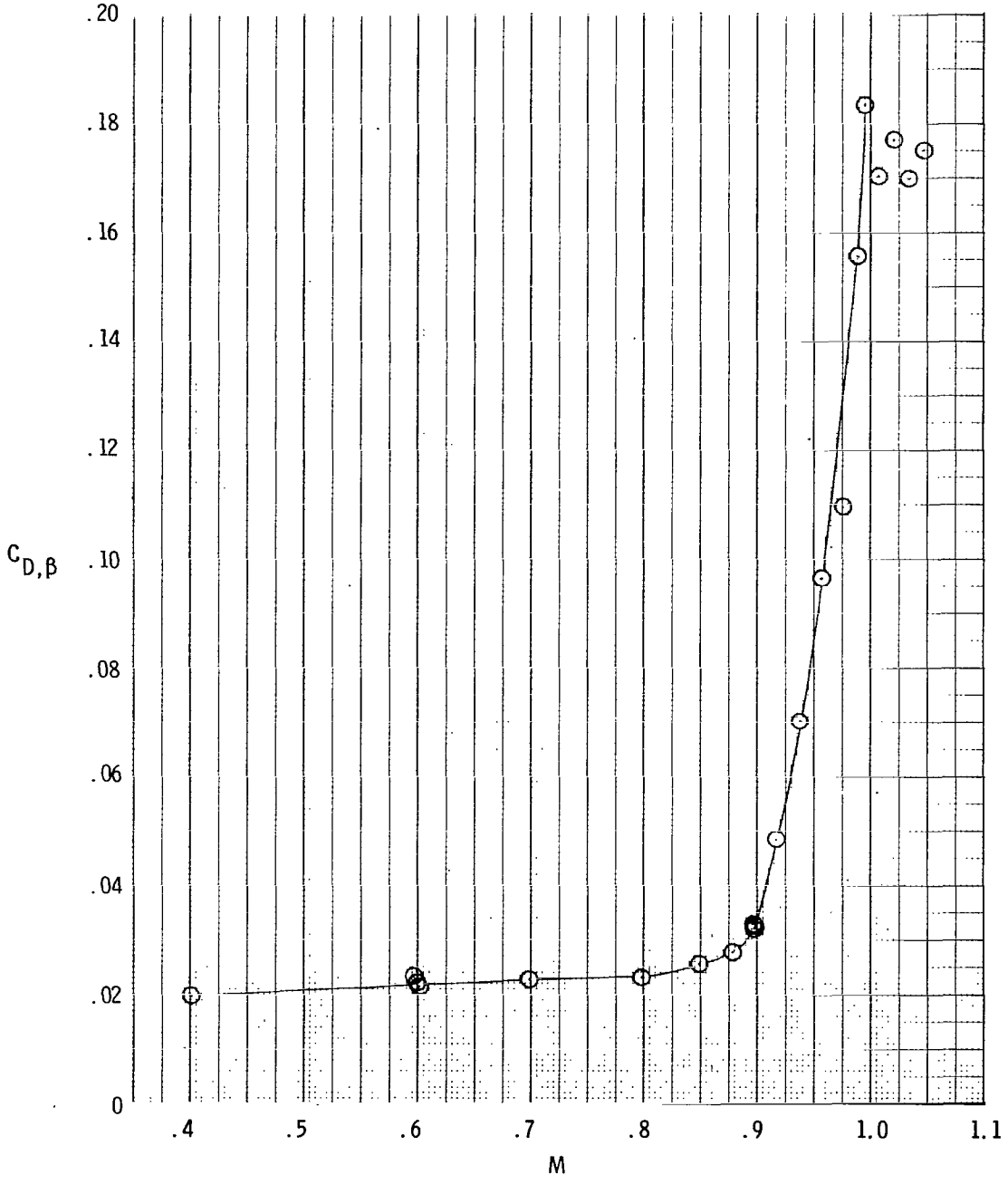

(d) $L/d_m = 8.0$, $l/d_m = 0.96$ circular-arc—conic.

Figure 12.- Continued.

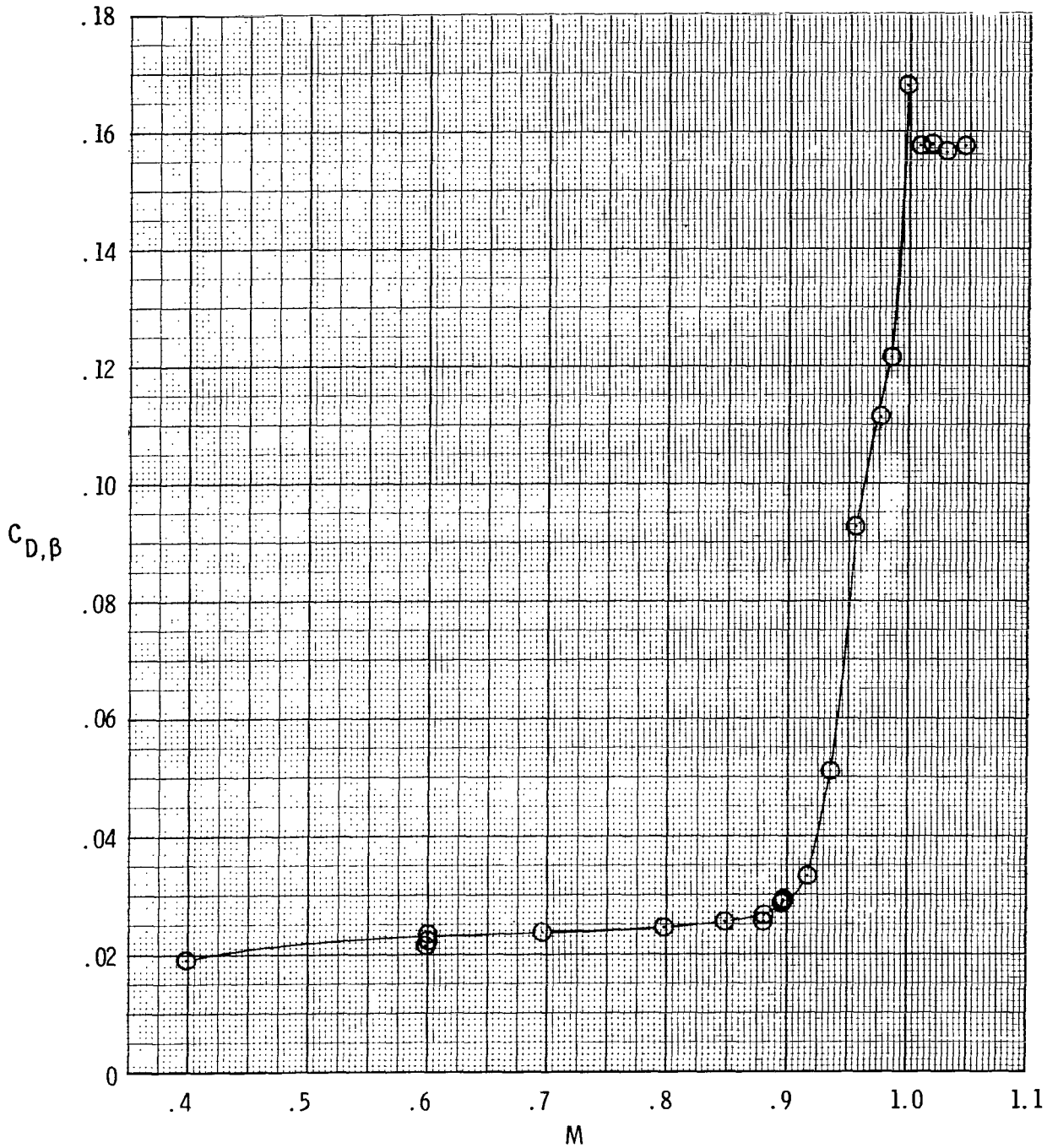

(e) $L/d_m = 16.0$, $l/d_m = 0.96$ circular-arc—conic.

Figure 12.- Continued.

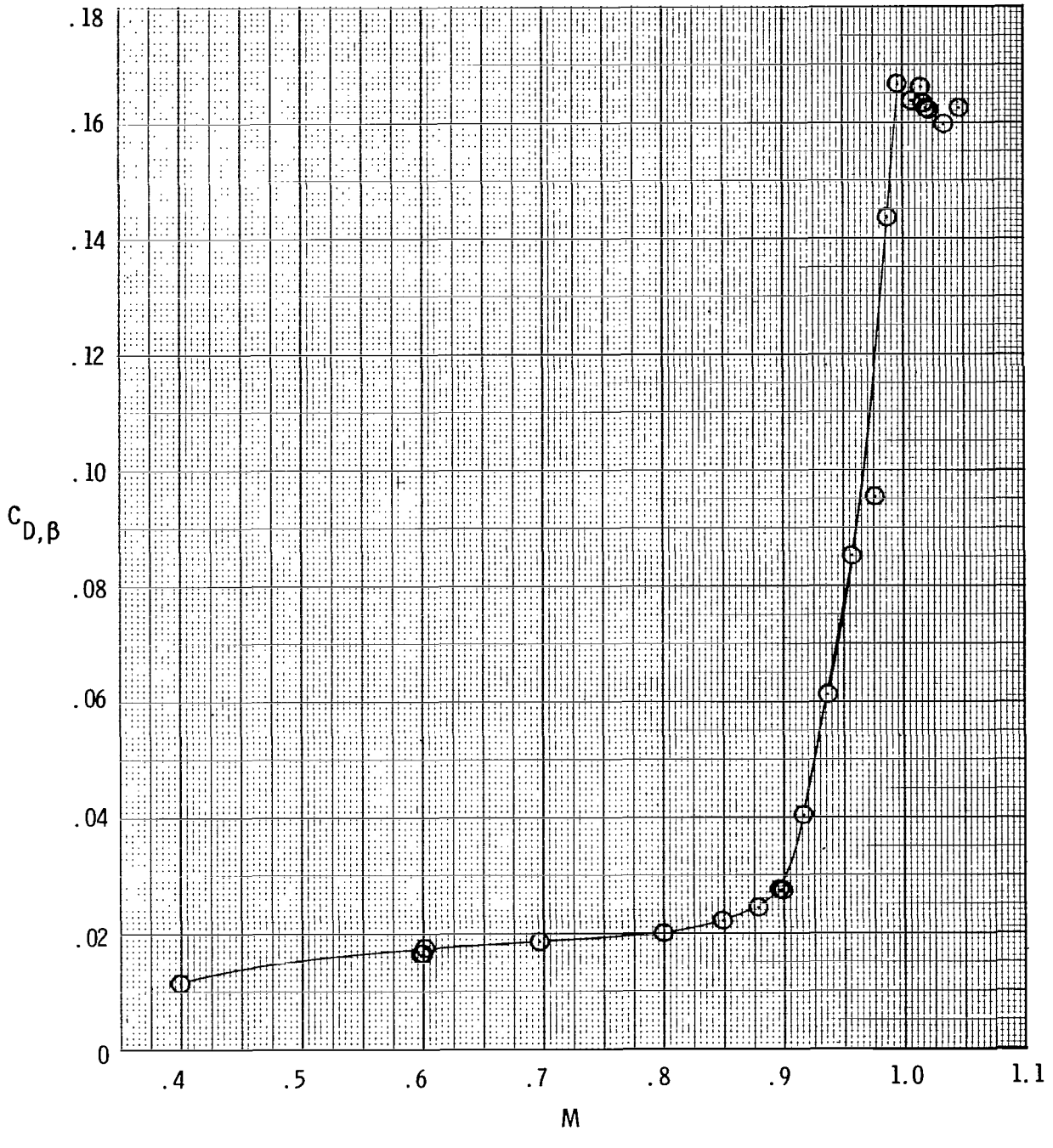

(f) $L/d_m = 8.0$, $l/d_m = 0.95$ contoured.

Figure 12.- Concluded.

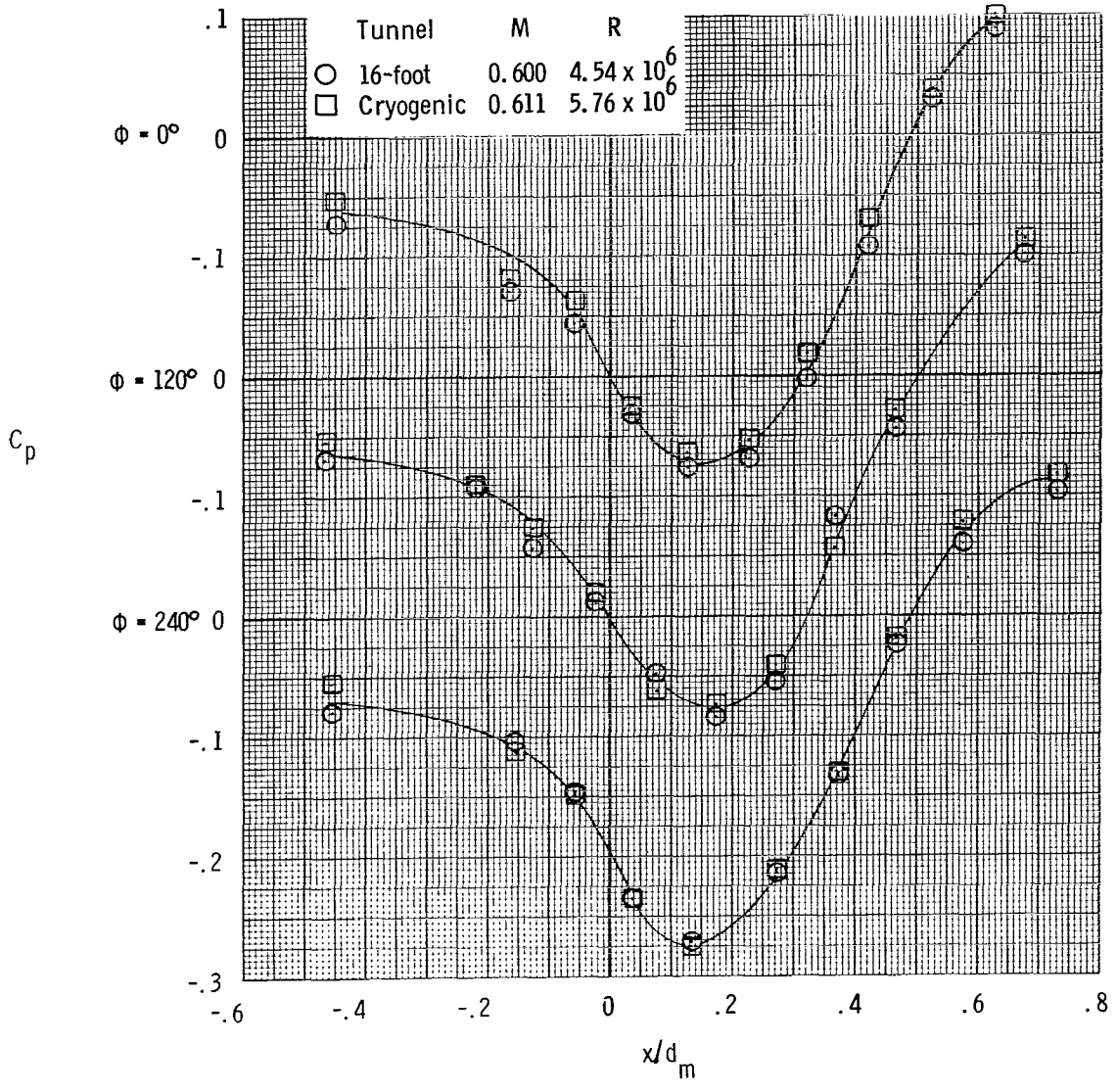

(a) M = 0.6.

Figure 13.- Boattail pressure coefficient distributions for the $L/d_m = 16.0$, $l/d_m = 0.80$ circular-arc boattail obtained in both the Langley 16-foot transonic and 0.3-meter transonic cryogenic tunnels at about the same Reynolds number.

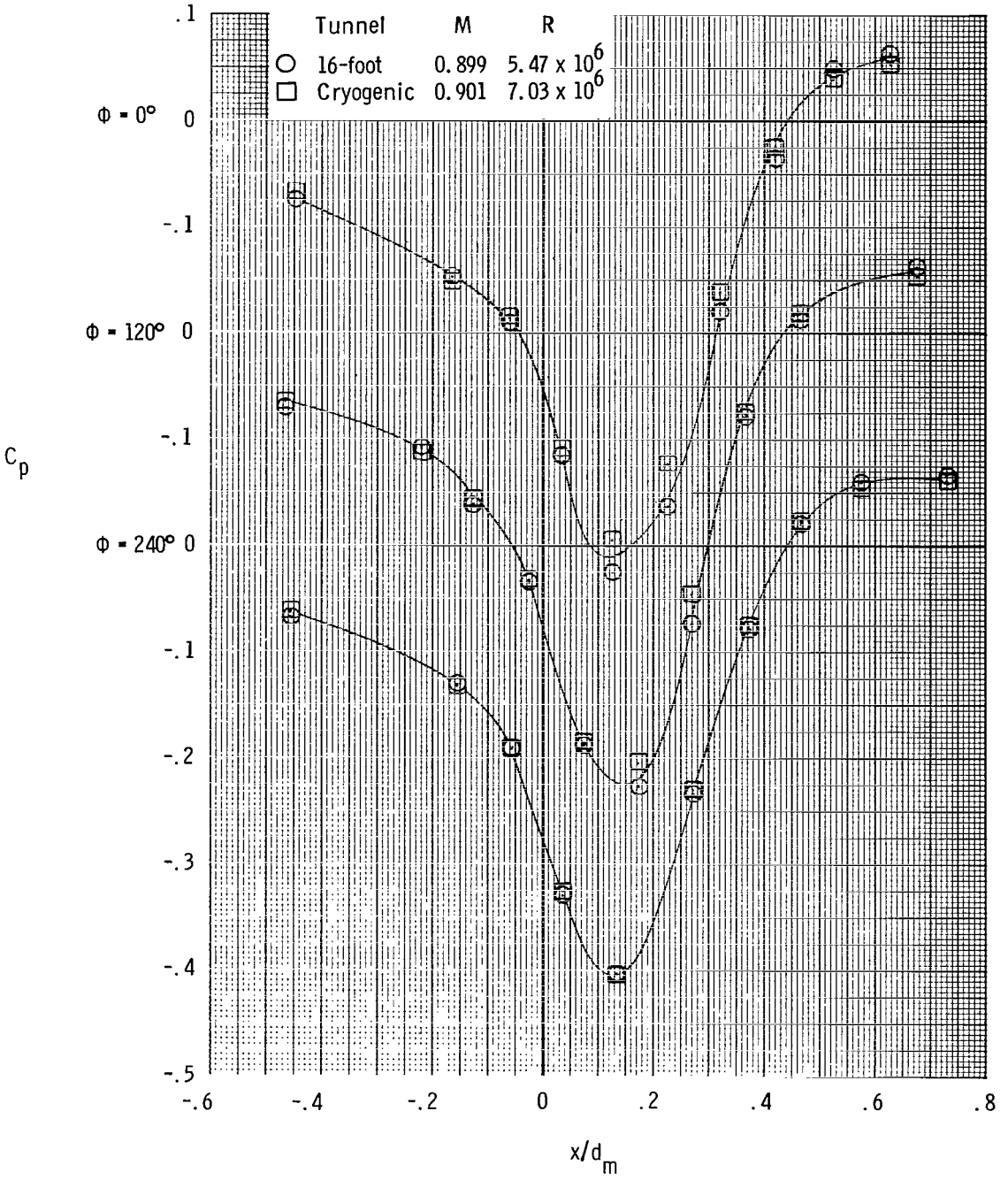

(b) M = 0.9.

Figure 13.- Concluded.

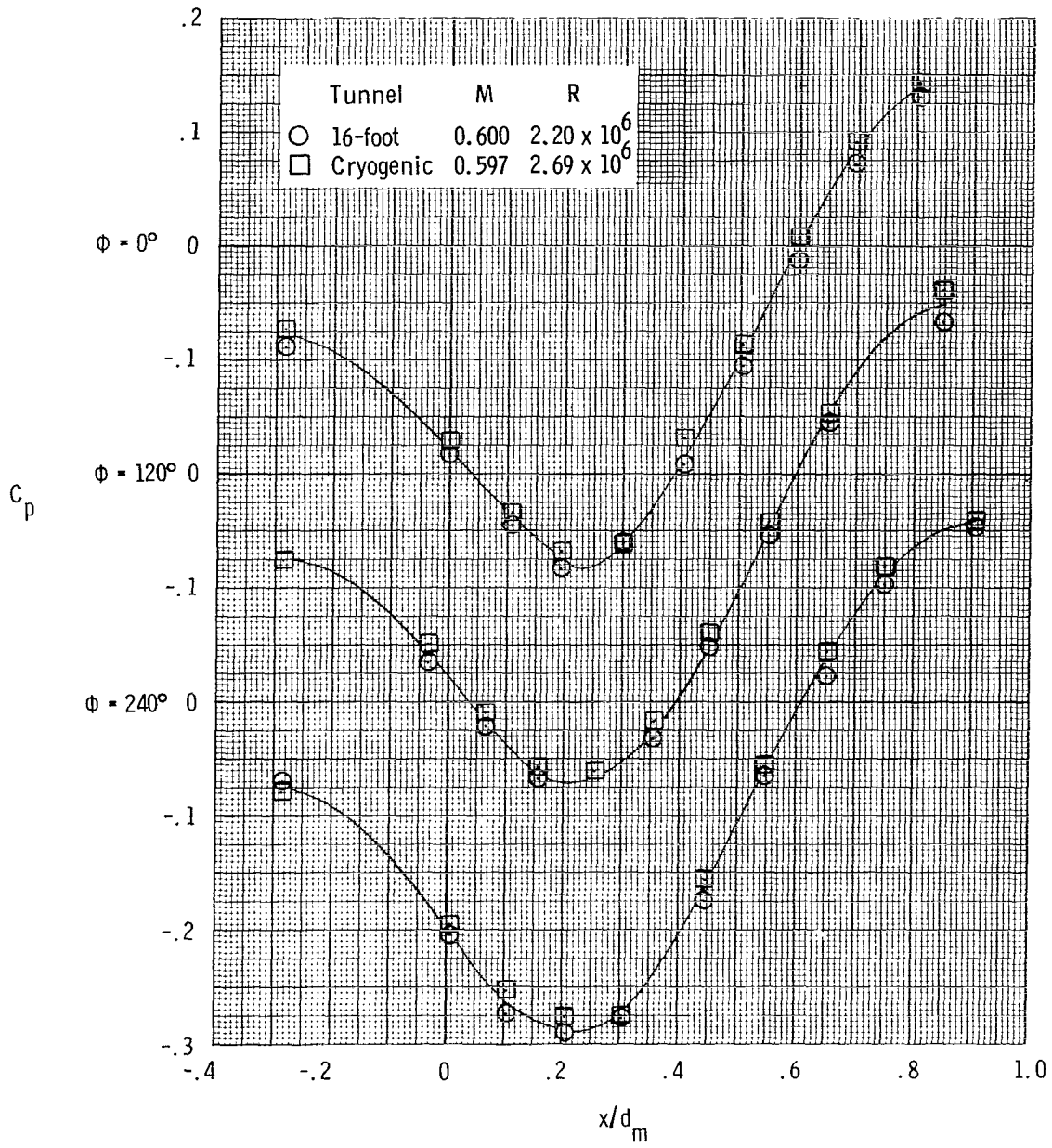

(a) M = 0.6.

Figure 14.- Boattail pressure coefficient distributions for the $L/d_m = 8.0$, $l/d_m = 0.96$ circular-arc—conic boattail obtained in both the Langley 16-foot transonic and 0.3-meter transonic cryogenic tunnels at about the same Reynolds number.

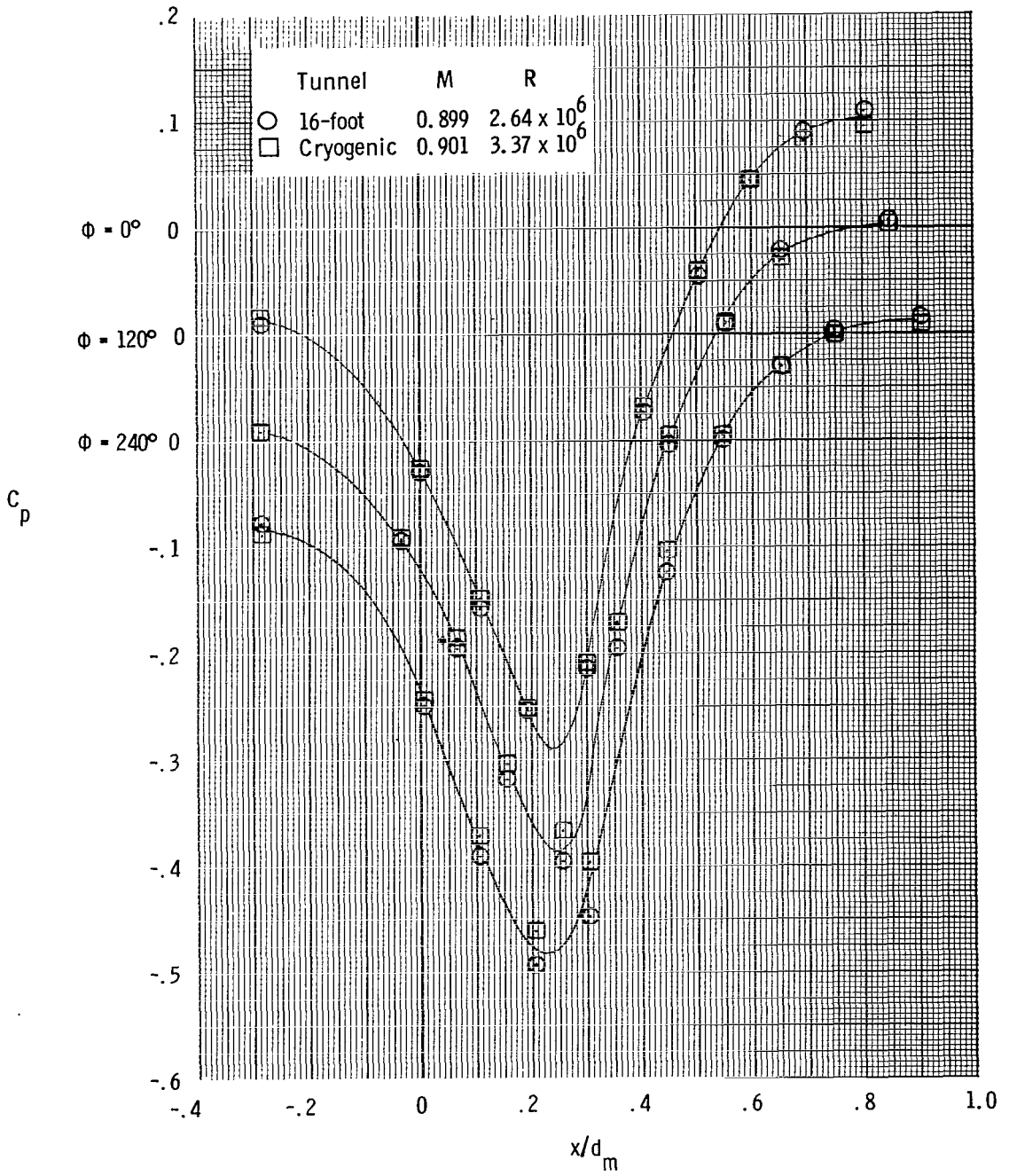

(b) M = 0.9.

Figure 14.- Concluded.

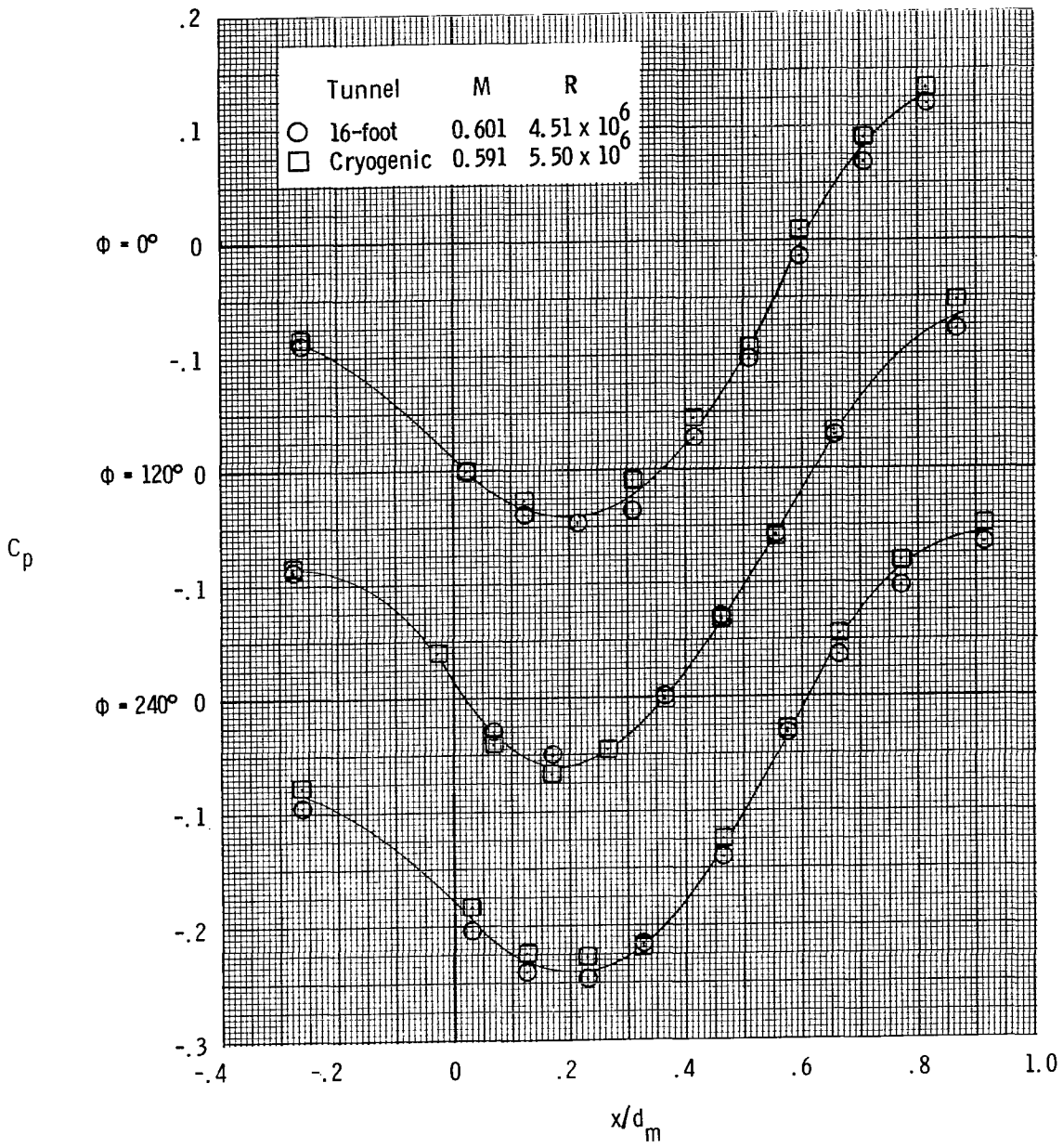

(a) M = 0.6.

Figure 15.- Boattail pressure coefficient distributions for the $L/d_m = 16.0$, $l/d_m = 0.96$ circular-arc—conic boattail obtained in both the Langley 16-foot transonic and 0.3-meter transonic cryogenic tunnels at about the same Reynolds number.

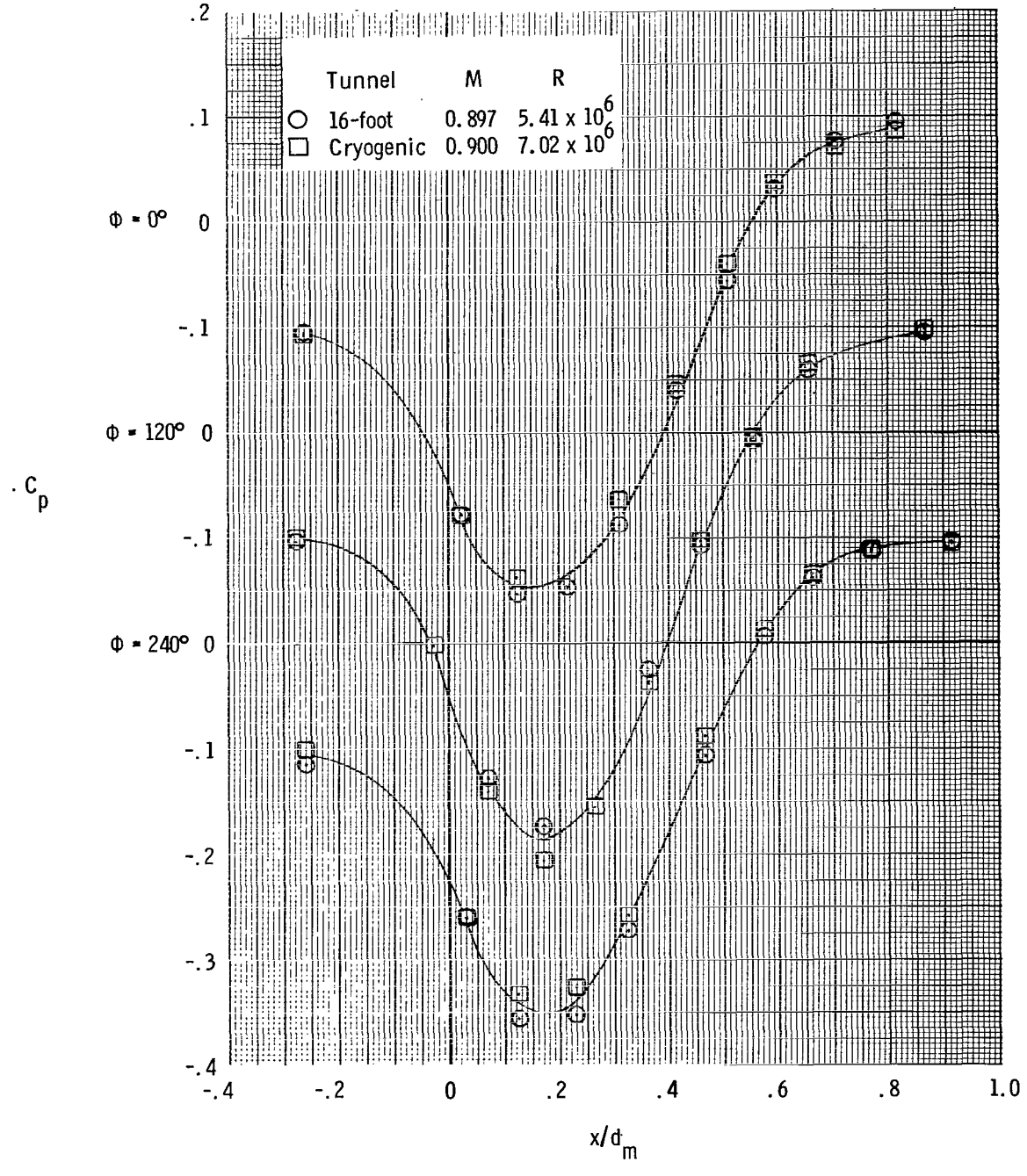

(b) M = 0.9.

Figure 15.- Concluded.

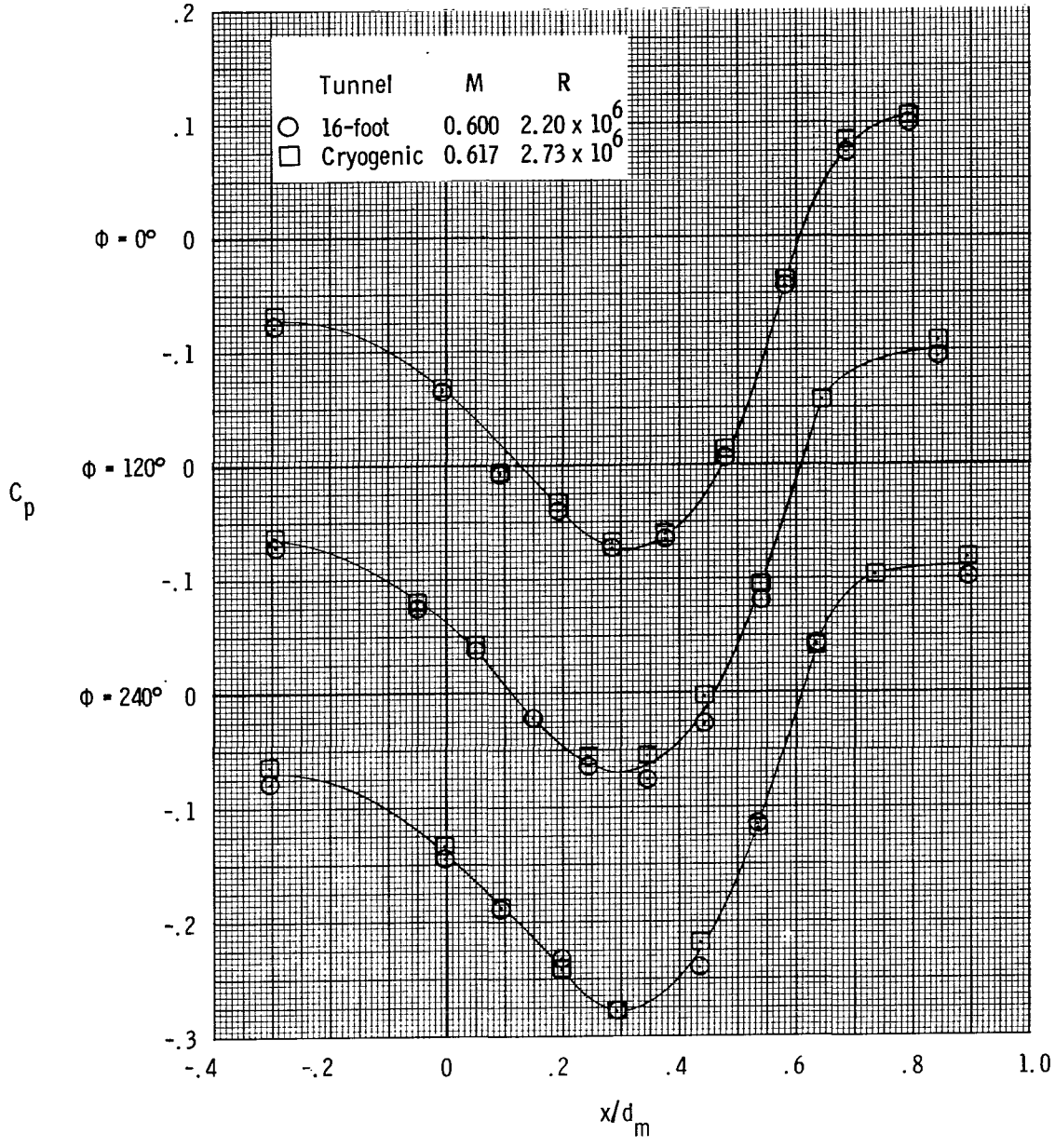

(a) M = 0.6.

Figure 16.- Boattail pressure coefficient distributions for the $L/d_m = 8.0$, $l/d_m = 0.95$ contoured boattail obtained in both the Langley 16-foot transonic and 0.3-meter transonic cryogenic tunnels at about the same Reynolds number.

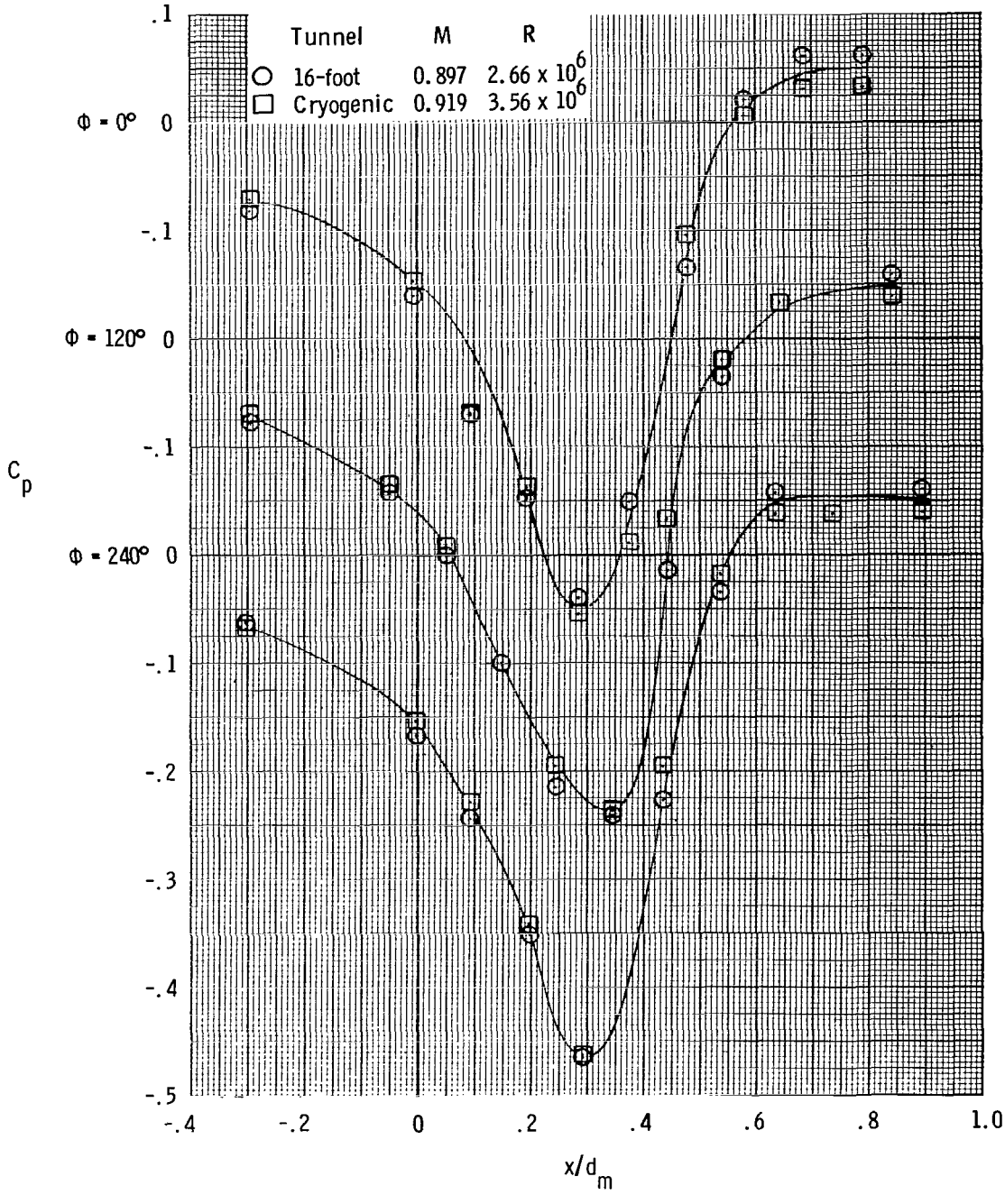

(b) M = 0.9.

Figure 16.- Concluded.

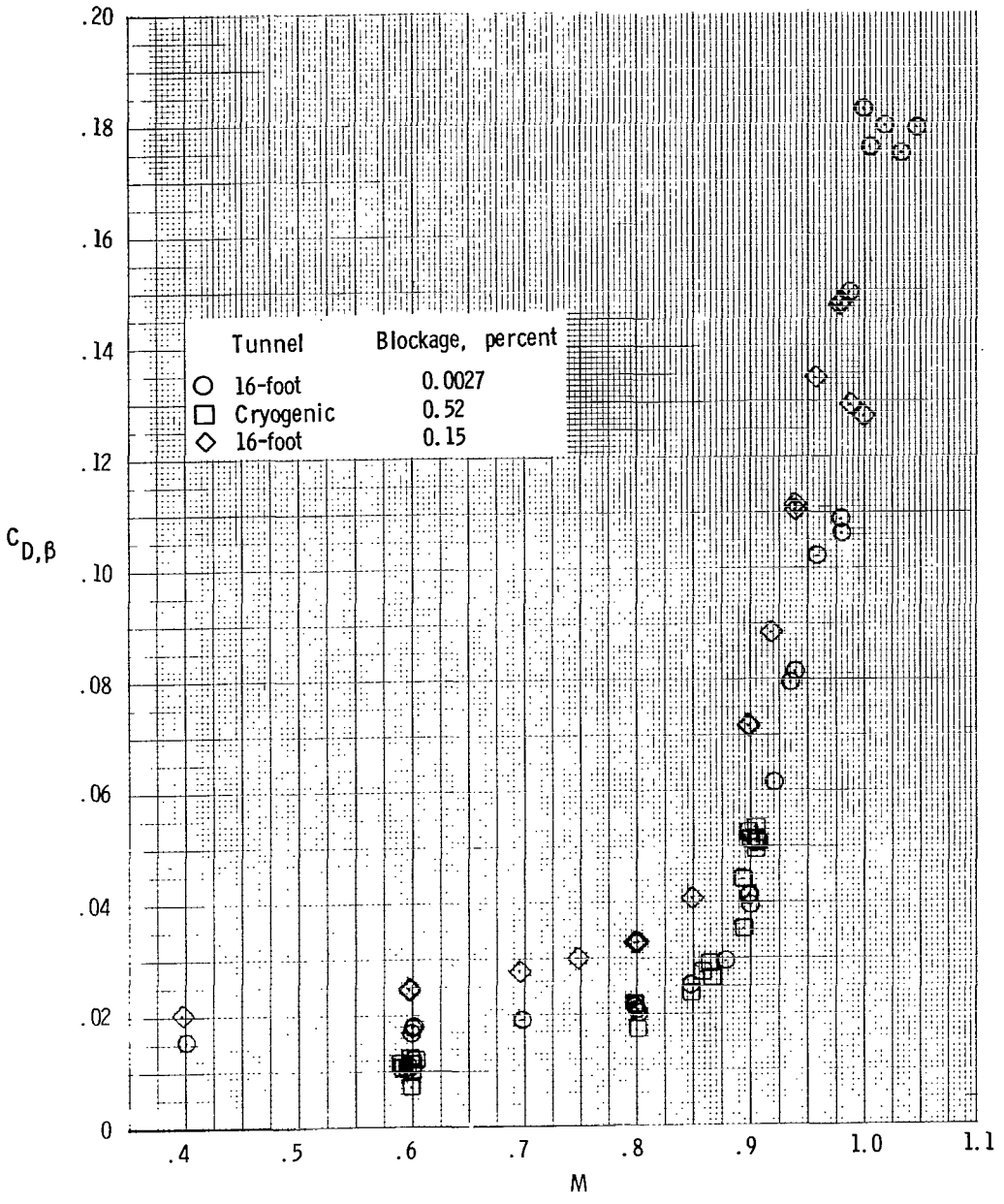

(a) $L/d_m = 8.0$, $l/d_m = 0.80$ circular-arc.

Figure 17.- Boattail pressure drag coefficients for the various boattails obtained in both the Langley 16-foot transonic and 0.3-meter transonic cryogenic tunnels.

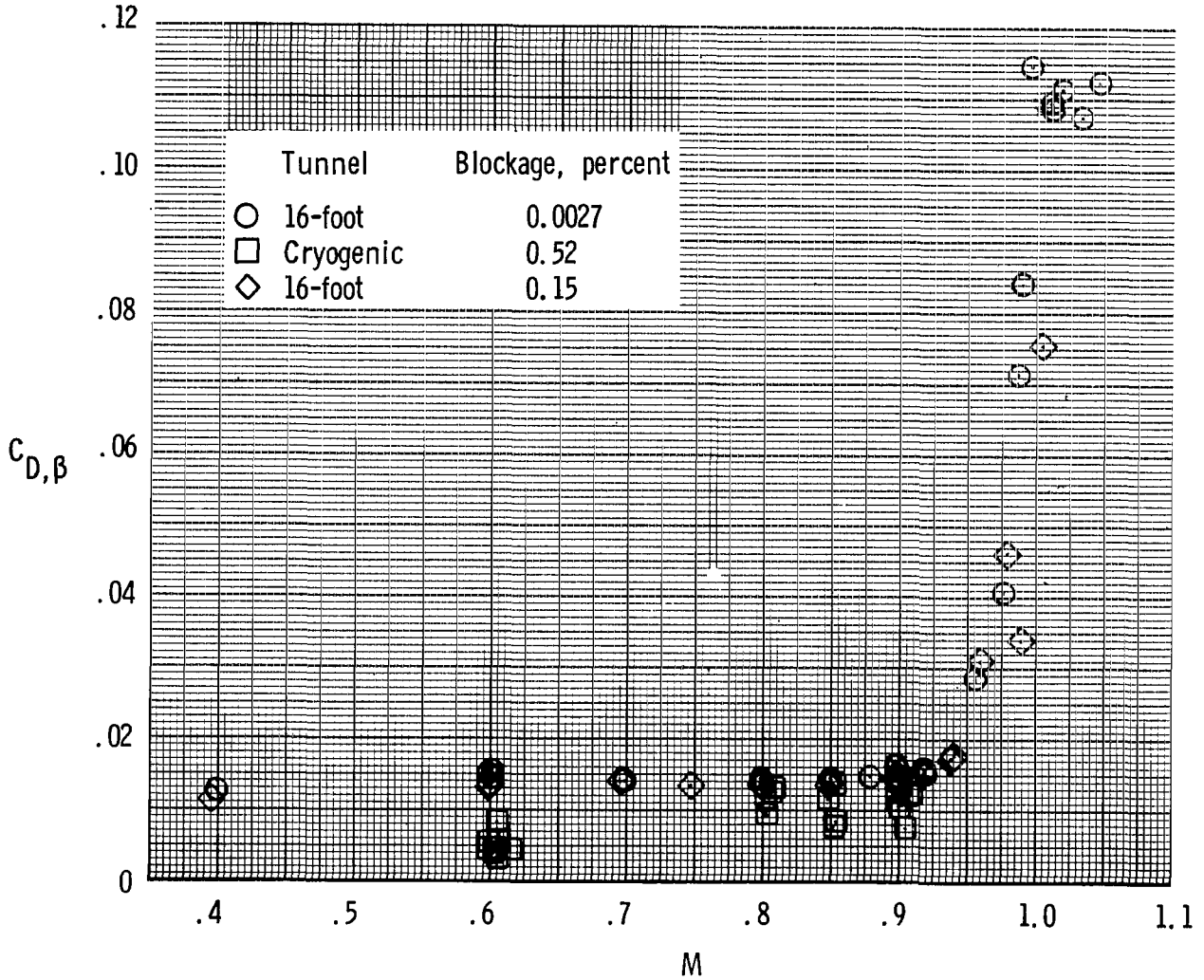

(b) $L/d_m = 8.0$, $l/d_m = 1.77$ circular-arc.

Figure 17.- Continued.

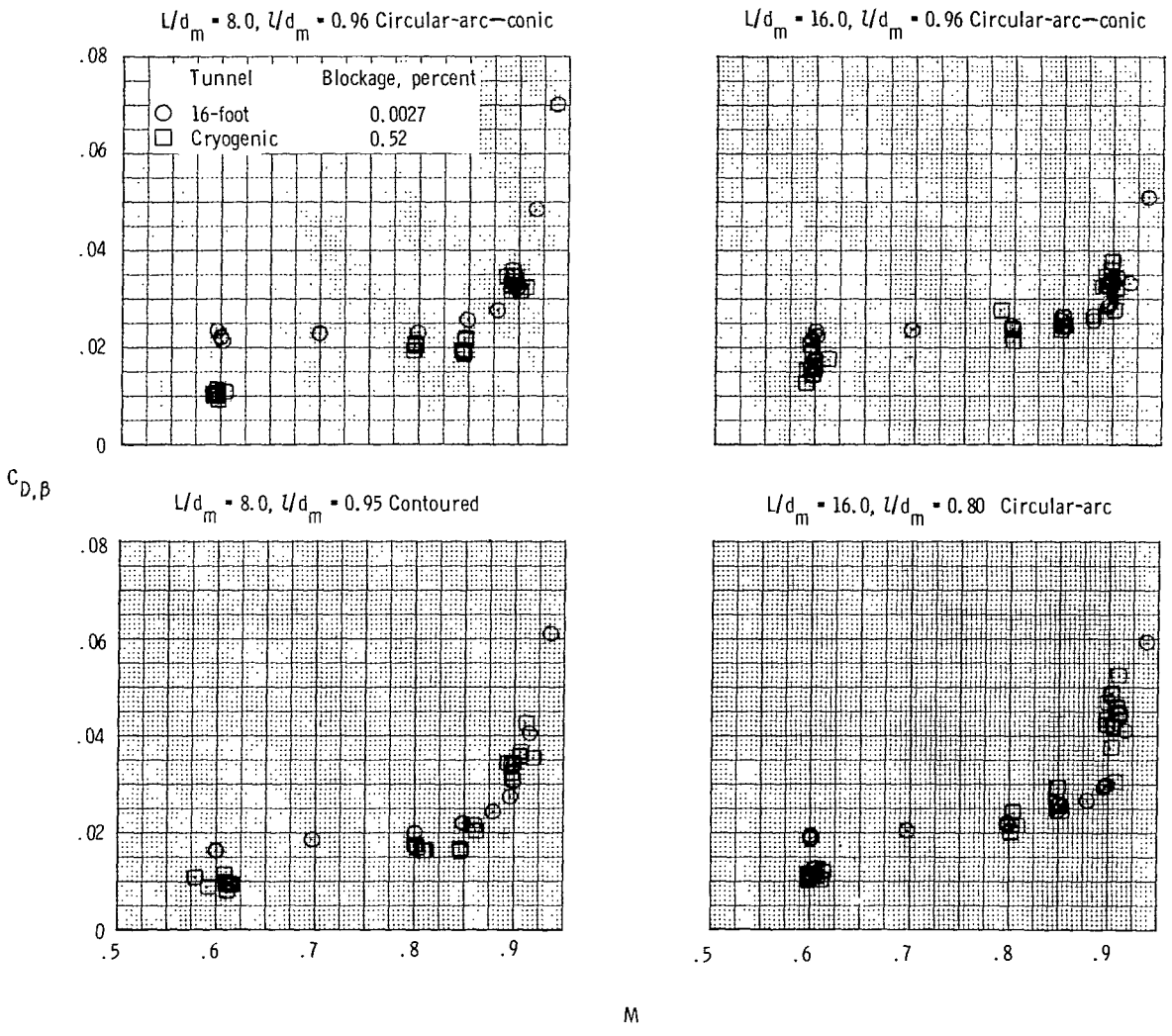

(c) Other configurations.

Figure 17.- Concluded.

"The aeronautical and space activities of the United States shall be conducted so as to contribute . . . to the expansion of human knowledge of phenomena in the atmosphere and space. The Administration shall provide for the widest practicable and appropriate dissemination of information concerning its activities and the results thereof."

—NATIONAL AERONAUTICS AND SPACE ACT OF 1958

NASA SCIENTIFIC AND TECHNICAL PUBLICATIONS

TECHNICAL REPORTS: Scientific and technical information considered important, complete, and a lasting contribution to existing knowledge.

TECHNICAL NOTES: Information less broad in scope but nevertheless of importance as a contribution to existing knowledge.

TECHNICAL MEMORANDUMS: Information receiving limited distribution because of preliminary data, security classification, or other reasons. Also includes conference proceedings with either limited or unlimited distribution.

CONTRACTOR REPORTS: Scientific and technical information generated under a NASA contract or grant and considered an important contribution to existing knowledge.

TECHNICAL TRANSLATIONS: Information published in a foreign language considered to merit NASA distribution in English.

SPECIAL PUBLICATIONS: Information derived from or of value to NASA activities. Publications include final reports of major projects, monographs, data compilations, handbooks, sourcebooks, and special bibliographies.

TECHNOLOGY UTILIZATION PUBLICATIONS: Information on technology used by NASA that may be of particular interest in commercial and other non-aerospace applications. Publications include Tech Briefs, Technology Utilization Reports and Technology Surveys.

Details on the availability of these publications may be obtained from:

SCIENTIFIC AND TECHNICAL INFORMATION OFFICE

NATIONAL AERONAUTICS AND SPACE ADMINISTRATION

Washington, D.C. 20546